

Faculty of Science, Charles University in Prague  
Department of Biochemistry

Diploma Thesis

**Study of the Active Site of  
Glutamate Carboxypeptidase II**

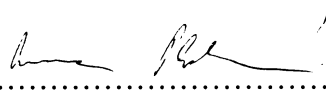
Anna Plechanovová

Thesis supervisor: Doc. RNDr. Jan Konvalinka, Csc.

Prague 2006

Prohlašuji, že jsem tuto diplomovou práci vypracovala samostatně pod vedením školitele  
Doc. RNDr. Jana Konvalinky, Csc. a že jsem všechny použité prameny řádně citovala.

V Praze, dne 4.5.2006



.....

# Acknowledgements

First of all, I would like to thank my supervisor Jan Konvalinka for his kind supervision and support. My acknowledgements also belong to Petra Mlčochová and Cyril Bařinka for their advice and invaluable help with the project.

I would also like to thank all the other present and former members of Jan Konvalinka's laboratory, namely Klárka Hlouchová, Pavel Šácha, Mirka Rovenská, Jana Starková, Jana Jirásková, Kvido Střišovský, Hillary Hoffman, Jana Václavíková, Klárka Šašková, Milan Kožíšek, Jana Pokorná, Vašek Navrátil and Honza Tykvart for creating friendly atmosphere in the lab.

Last but not least, I would like to thank my family and friends for their support during my studies.

# Contents

<b>1. Introduction</b> .....	1
<b>2. Theoretical Part</b> .....	2
2.1. Glutamate Carboxypeptidase II.....	2
2.1.1. Short Overview of the Nervous System.....	3
2.1.1.1 L-Glutamate as a Neurotransmitter .....	5
2.1.1.1.1. Glutamate-mediated Excitotoxicity .....	6
2.1.1.1.2. NAAG as a Neurotransmitter.....	7
2.1.2 GCPII Expression and Function.....	9
2.1.2.1 Nervous System .....	9
2.1.2.1.1 GCPII and Neurological Disorders .....	10
2.1.2.2. Prostate .....	12
2.1.2.2.1. GCPII and Prostate Cancer .....	13
2.1.2.3. Small Intestine.....	14
2.1.2.4. Other Tissues.....	14
2.1.3. Structure of GCPII .....	14
2.1.3.1. Active site of GCPII.....	16
2.1.3.2. Inhibitors .....	19
2.1.3.3. Site-directed mutagenesis studies of the GCPII active site.....	20
<b>3. Objectives</b> .....	23
<b>4. Materials and Methods</b> .....	24
4.1. Materials and Instruments .....	24
4.1.1. Materials.....	24
4.1.2. Instruments .....	26
4.2. Methods.....	27
4.2.1. Site-Directed Mutagenesis .....	27
4.2.2. Transformation of <i>E. coli</i> Cells.....	28
4.2.3. Midipreparation of Plasmid DNA (Midiprep) .....	29
4.2.4. Determination of DNA Concentration .....	30
4.2.5. DNA Sequencing .....	30
4.2.6. Maxipreparation of Plasmid DNA (Maxiprep).....	31
4.2.7. Purification of Plasmid DNA with QIAGEN Plasmid Midi Kit.....	33
4.2.8. Agarose Gel Electrophoresis.....	33
4.2.9. Stable Transfection of Drosophila S2 Cells Using Calcium Phosphate .....	34
4.2.10. Trypan Blue Exclusion Assay of Cell Viability.....	35
4.2.11. Expression of Mutant Forms of Recombinant GCPII.....	35
4.2.12. Purification of Mutant Forms of Recombinant GCPII.....	36
4.2.12.1. Dialysis.....	36
4.2.12.2. QAE-Sephadex Batch Chromatography .....	36
4.2.12.3. Source 15S Column Chromatography .....	38
4.2.12.4. Lentil Lectin Chromatography .....	38
4.2.12.5. Gel Permeation Chromatography.....	38
4.2.12.6. Chromatofocusing.....	39
4.2.13. Determination of Protein Concentration .....	39
4.2.14. Sodium Dodecyl Sulfate-Polyacrylamide Gel Electrophoresis (SDS-PAGE)..	40
4.2.15. Silver Staining.....	40
4.2.16. Western Blotting .....	41

4.2.16.1. Protein Quantification from Western Blot .....	42
4.2.17. Hanging Drop Vapour Diffusion Crystallization.....	43
4.2.18. GCPII Enzymatic Activity Assays.....	43
4.2.18.1. Radiometric Measurement of NAAG-hydrolyzing Activity.....	43
4.2.18.2. HPLC Assay of GCPII Enzymatic Activities .....	44
4.2.18.2.1. Derivatization Reaction with FDAA.....	46
<b>5. Results</b> .....	47
5.1. Active-site Mutants .....	47
5.1.1. Site-directed Mutagenesis .....	48
5.1.2. Expression of Mutant Forms of rhGCPII in Drosophila S2 Cells .....	51
5.1.3. Expression and Activity Testing .....	51
5.1.4. Large Scale Production and Purification.....	53
5.1.5. Crystallization Experiments with Mutant E424A .....	56
5.1.6. Kinetic Characterization of Mutant Proteins.....	56
5.1.7. Inhibition by 2-PMPA.....	60
5.2. Novel Dipeptidic Substrates.....	62
5.2.1. Kinetic Characterization of Novel Dipeptidic Substrates .....	64
5.2.2. The Role of Lys699 in the GCPII Specificity for Glutamate-containing Substrates .....	67
<b>6. Discussion</b> .....	68
6.1. Active-site Mutants .....	68
6.2. Novel Dipeptidic Substrates.....	71
<b>7. Conclusions</b> .....	73
<b>8. List of Abbreviations</b> .....	74
<b>9. References</b> .....	76

# 1. Introduction

Human glutamate carboxypeptidase II (GCPII, E.C. 3.4.17.21) is a transmembrane co-catalytic zinc metallopeptidase expressed in various tissues, brain, prostate and small intestine. In the nervous system, GCPII terminates the action of the most abundant peptide neurotransmitter N-acetyl-L-aspartyl-L-glutamate (NAAG), yielding free glutamate into the extracellular space. Inhibition of this activity was shown to be neuroprotective in animal models of several neurological disorders which are associated with elevated levels of glutamate (e.g. stroke, amyotrophic lateral sclerosis and neuropathic pain). GCPII is thus viewed as a promising target for treatment of these pathological conditions. The function of GCPII in prostate is still unknown. However, GCPII is up-regulated in prostate cancer and therefore is used as a prostate cancer marker. In small intestine, GCPII participates in absorption of dietary folates.

Recently, the three-dimensional crystal structure of extracellular part of GCPII in complex with glutamate, the product of the hydrolytic reaction, was solved by Cyril Bařinka and Jeroen Mesters. The structure revealed amino acid residues interacting with the bound product, as well as residues located nearby and presumably also playing important role in substrate hydrolysis. In the work reported here, we used site-directed mutagenesis to assess the influence of these active site residues on substrate binding/cleavage.

Substrate specificity and crystallographic studies suggested that hydrophobic interactions might play a role in positioning the C-terminal residue of the substrate in the GCPII active site. To study these interactions in more detail, we kinetically characterized a series of novel dipeptidic substrates of GCPII harbouring non-naturally occurring amino acids with aliphatic side chains in the C-terminal position of the substrate. Since most of the reported potent inhibitors of GCPII are highly polar compounds, studies of hydrophobic interactions in the GCPII active site might facilitate design of specific GCPII inhibitors with increased hydrophobicity and thus with better pharmacokinetic properties.

## 2. Theoretical Part

### 2.1. Glutamate Carboxypeptidase II

Glutamate carboxypeptidase II (GCPII, E.C. 3.4.17.21) is a membrane-bound metallopeptidase expressed predominantly in nervous system, prostate, small intestine and kidney. Due to the wide expression in various tissues, GCPII was initially studied independently as three different proteins, which also lead to several names being given to it. While in the brain, GCPII was recognized as a dipeptidase and termed N-acetylated- $\alpha$ -linked acidic dipeptidase (NAALADase) [1], in the prostate, it was originally identified as an antigen of 7E11-C5 monoclonal murine antibody and since the expression of this antigen was thought to be prostate-specific at that time, it was designated prostate-specific membrane antigen (PSMA) [2]. Finally, the third name used in scientific literature for GCPII is folate hydrolase. To make the situation at least a bit less confusing the Nomenclature Committee of the International Union of Biochemistry and Molecular Biology recommended to use the name glutamate carboxypeptidase II [3].

From the enzymological point of view, GCPII is now known to possess two physiologically relevant enzymatic activities: it hydrolyzes a peptide neurotransmitter N-acetyl-L-aspartyl-L-glutamate (NAAG) to N-acetylaspartate and glutamate [1] and it also cleaves off  $\gamma$ -linked glutamates from folylpoly- $\gamma$ -glutamates [4] (Fig. 1, page 3). The former activity is believed to play role in regulation of neurotransmission in both central and peripheral nervous system, while the latter is involved in the absorption of dietary folates in small intestine.

In the next paragraphs I will try to summarize what has been found out about this enzyme during almost twenty years of study since 1987, when it was described for the first time [1;2], and why it is still being studied. In the first part of this chapter I will describe the expression and the function (unfortunately, mostly unknown) of GCPII in various tissues and since I will focus mainly on the nervous system and the role GCPII and its substrate NAAG are proposed to play there, a short overview of the nervous system and neurotransmission is included in the beginning. The subject of this diploma thesis is mainly the active site of GCPII, therefore the second part of the chapter is devoted to the rather boring description of the GCPII structure (but don't worry, there are a lot of colourful pictures, too).

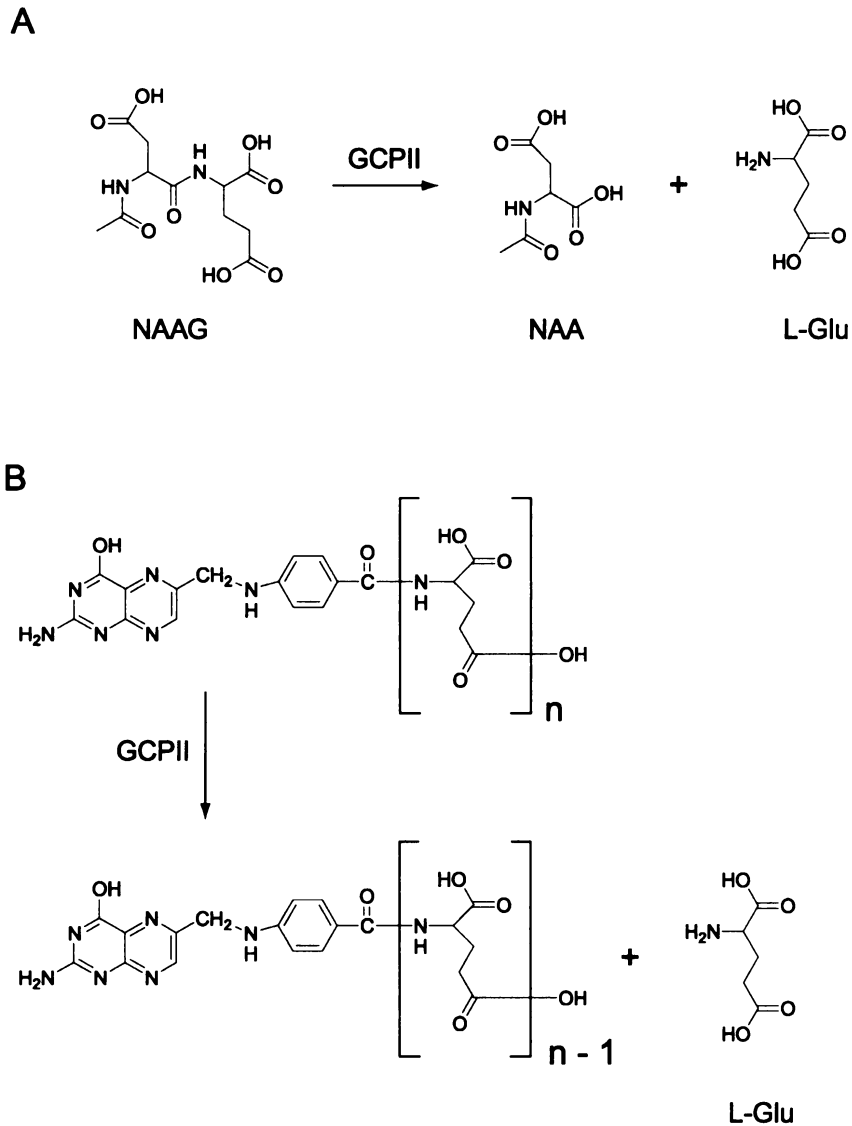


**Fig. 1 Enzymatic activities of GCPII.**

GCPII hydrolyzes the most abundant peptide neurotransmitter N-acetylglutamate (A) and it also cleaves off  $\gamma$ -linked glutamates from poly-poly- $\gamma$ -glutamates (B).

### 2.1.1. Short Overview of the Nervous System

The cells of the nervous system can be divided into two broad categories: nerve cells (or neurons) and a variety of supporting cells (or glial cells). Neurons are specialised in conducting electrical impulses over long distances and through their interconnections via synapses into intricate ensembles called circuits, they mediate all the complex functions of nervous system, such as sensory processes, perception and behaviour [5].



Although there are many various morphological types of nerve cells, a typical neuron has a cell body containing nucleus and organelles from which dendritic processes (or dendrites) arise. The dendrites together with the neuronal body provide the major site for synaptic terminals made by the axonal endings of other nerve cells. The input signals from other neurons received from all the synapses on the dendrites and the cell body are integrated at the origin of axon, a unique extension from the neuronal body that is specialised for signal conduction to the next site of synaptic interaction. The mechanism by which the information is carried along the axon is called action potential. The action potential is a self-regenerating wave of electrical activity that propagates to the terminus of the axon where the signal is passed on the next nerve cells in the pathway by a process called synaptic transmission [6].

Most of the synapses in the nervous system are chemical ones. This means that electrical signal cannot spread directly from one neuron to the other, but neurons communicate with one another via secretion of chemical compounds called neurotransmitters. When the action potential reaches the axon terminal, it causes release of molecules of neurotransmitters from synaptic vesicles into the synaptic cleft, a narrow extracellular space separating presynaptic and postsynaptic neurons. The released neurotransmitters modify the electrical properties of the target cell by binding to specific receptors in its membrane. The neurotransmitter must then be swiftly removed from the synaptic cleft. This is accomplished mainly by diffusion of transmitter from the synaptic cleft in combination with reuptake back into presynaptic terminal or into surrounding glial cells. Some neurotransmitters are degraded by specific enzymes [6].

The second category of cells constituting the nervous system are supporting cells referred to as neuroglial cells, or simply glial cells. Although these cell types are not capable of electrical signaling, which is the function of neurons, they are indispensable part of central nervous system with their mainly supportive functions ranging from homeostasis maintenance to phagocytosis of debris. There are four types of neuroglial cells: astrocytes, oligodendrocytes, microglia and ependymal cells. **Astrocytes** enwrap synapses and the bodies of some neurons and interact with neurons in various metabolic and transport processes, e.g. the reuptake of neurotransmitter glutamate. They are also believed to be responsible for the regulation of local ionic and pH balances and might be involved in the blood-brain barrier system. **Oligodendrocytes** as myelin-producing cells form myelin sheaths around axons and thus facilitate the spread of action potential along the axon.

**Microglia** share many properties with tissue macrophages. They are primarily scavenger cells that remove cellular debris from sites of injury or normal cell turnover and they play role in inflammatory responses. **Ependymal cells** line brain ventricles and spinal cord central canal [6].

### 2.1.1.1 L-Glutamate as a Neurotransmitter

L-glutamate is generally acknowledged to be an excitatory amino acid neurotransmitter in a range of organisms from *Caenorhabditis elegans* to mammals. Nearly all excitatory neurons in the central nervous system are glutamatergic [5;6] (Fig. 2).

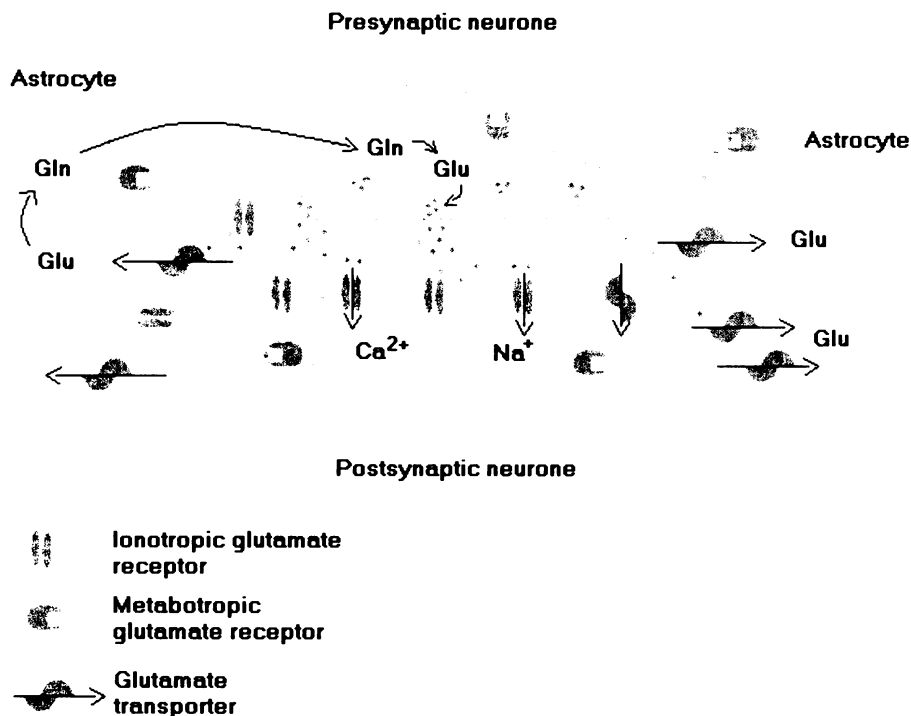


**Fig. 2 Glutamatergic synapse**

Glutamate is a major excitatory neurotransmitter in the nervous system. Following its release from the presynaptic neuron, it activates a variety of ionotropic as well as metabotropic receptors. A large fraction of released glutamate is taken up into glial cells, where it is converted into glutamine. Glutamine then cycles back to nerve cell terminals, where it participates in the replenishment of the stores of glutamate.

Following glutamate release from presynaptic axonal terminals, glutamate binds to a variety of glutamate receptors (GluRs), which can be found on both presynaptic and postsynaptic neurons and also on glial cells. These receptors are categorized into two major classes: metabotropic glutamate receptors (mGluRs) and ionotropic glutamate

receptors (iGluRs) [5;7]. Metabotropic glutamate receptors are coupled to G-proteins and regulate the production of intracellular second messengers. mGluRs are further divided into three subgroups (group I-III) on the basis of their amino acids sequence homology and pharmacological properties. Group I mGluRs are coupled via G-proteins to activation of phospholipase C, whereas activation of group II a III mGluRs leads to inhibition of adenylate cyclase and decrease of cAMP [8-10]. Ionotropic glutamate receptors are ligand-gated cation channels. They are classified into three major types, which were named after exogenous agonists that were originally identified to activate them selectively: N-methyl-D-aspartate (NMDA), DL- $\alpha$ -amino-3-hydroxy-5-methyl-4-isoxasolepropionate (AMPA) and kainate (KA) receptors [8;9].

Once released into the synaptic cleft, glutamate is swiftly removed from the extracellular space by reuptake via specific excitatory amino acid transporters into both neurons and astrocytes, the astrocyte-mediated clearance of glutamate being the prevalent one [11].

#### **2.1.1.1.1. Glutamate-mediated Excitotoxicity**

Besides its indispensable function in excitatory neurotransmission that mediates normal information processing and neuronal plasticity, glutamate also plays an especially important role in many pathophysiological conditions because elevated concentrations of extracellular glutamate (released, for example, as a result of neural injury or ischemia) are toxic to neurons. In normal conditions, the concentration of glutamate released into the synaptic cleft rises to high levels (approximately 1mM), but remains at this level for only a few milliseconds and then drops back to basal level. However, when abnormally high concentrations of extracellular glutamate remain in the synaptic cleft for longer period of time, the overstimulation of glutamate receptors triggers processes that may lead to the death of neurons. This phenomenon is called excitotoxicity [5;12].

Excitotoxicity was shown to be involved in several neuropathological conditions, including ischemia, traumatic brain injury, amyotrophic lateral sclerosis (ALS), Alzheimer disease and inflammatory and neuropathic pain [12-14]. Excitotoxicity is an impotent cause of neuronal death after stroke. An interrupted blood supply to the brain causes deprivation of oxygen and glucose that are utilised as a source of energy. Impaired energy causes depolarization of neuronal membranes and subsequent activation of voltage-

dependent  $\text{Ca}^{2+}$  channels at presynaptic terminals, which leads to the release of glutamate into the synaptic cleft. The reuptake of glutamate into neurons and astrocytes by glutamate transporters is also energy-dependent, thus glutamate accumulates in the extracellular space [15]. Consequent over-activation of postsynaptic ionotropic glutamate receptors causes excessive influx of  $\text{Ca}^{2+}$  and  $\text{Na}^+$  cations into the postsynaptic nerve cells and their depolarization.  $\text{Ca}^{2+}$  overload can trigger many downstream neurotoxic cascades, such as the uncoupling of mitochondrial electron transfer from ATP synthesis and overstimulation of variety of enzymes, including calpains, protein kinases, nitric oxide synthase and endonucleases [16]. All these processes can eventually lead to nerve cell death and glutamate is the mediator which spreads the depolarization and associated neurotoxicity to the previously healthy neurons in the vicinity of the stroke-stricken site [12] (Fig. 3).

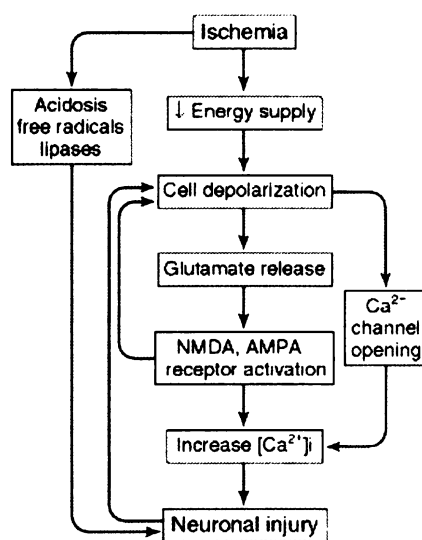


**Fig. 3 Potential paths leading to neuronal injury caused by ischemia.**

Taken over from [6].

As mentioned above, glutamate-mediated excitotoxicity is associated not only with stroke, but also with many other neurological disorders. So, drugs targeting neurotoxic effects of elevated levels of extracellular glutamate are, quite naturally, being sought. One obvious way how to prevent the consequences of excessive glutamate signalling is blocking  $\text{Ca}^{2+}$  influx into the postsynaptic neurons. Since this influx is mediated mainly by NMDA receptors, selective NMDA receptor antagonists were suggested as potential drugs [17]. However, clinical trials of these agents have unfortunately not led to much improvement in the outcome of stroke or produced intolerable side effects [18;19].

### 2.1.1.2. NAAG as a Neurotransmitter

N-acetyl-L-aspartyl-L-glutamate (NAAG) was discovered in the mammalian nervous system in the mid-1960s, but its function as a neurotransmitter was not recognised until twenty years later. Since that time, it was shown that NAAG meets all the established

criteria for a neurotransmitter: i) it's concentrated in neurons and in synaptic vesicles, ii) it's released from axon terminals in a calcium dependent manner following initiation of action potentials and iii) it is degraded by at least two specific membrane-bound peptidases, glutamate carboxypeptidase II (GCP II) and glutamate carboxypeptidase III (GCP III) [20;21].

NAAG is distributed widely in central and peripheral nervous system of mammals and is probably the most abundant neuropeptide with its concentrations in the brain and spinal cord reaching high micromolar to low millimolar range. NAAG is present in neurons that use variety of neurotransmitters, including glutamate, GABA, serotonin, dopamine, norepinephrine and acetylcholine [22-24]. This co-distribution of NAAG with other transmitters suggests that NAAG has a modulatory role in various neuronal circuits.

Equilibrium binding studies have shown that NAAG binds to NMDA receptors, but not to AMPA or kainate receptors [25]. NAAG has also been reported to activate NMDA receptors in some systems, such as rat olfactory bulb neurons [26] or mouse spinal cord neurons [27], nevertheless NAAG was far less potent activator of these receptors than glutamate. In contrast, no activation of NMDA receptors by NAAG was observed in neurons from cat dorsal lateral geniculate nucleus [28]. These contradictory observations might be explained by differences in subunit composition of NMDA receptors expressed by different cell types. NAAG was also observed to decrease excitatory responses related to activation of NMDA receptors [29;30] and it was proposed that NAAG may act as a mixed agonist/antagonist at NMDA receptors [20]. To make the problem even more complicated Losi et al. have recently reported that NAAG does not antagonise NMDA receptors in cerebellar granule neurons [31], whereas Bergeron et al. have shown that NAAG reduces NMDA receptor-mediated current in CA1 hippocampal pyramidal neurons [32].

Besides its not yet clear effect on NMDA receptors, NAAG was shown to selectively activate mGluR3 with potency approaching that of glutamate [33-35]. mGluR3 receptors belong to the group II mGluRs. These metabotropic glutamate receptors are expressed in both presynaptic and postsynaptic neurons, as well as in glial cells. Activation of presynaptic mGluR3 leads to decrease in release of primary neurotransmitters, including glutamate and GABA [36;37], whereas activation of glial mGluR3 causes secretion of transforming growth factors- $\beta$  (TGF- $\beta$ ) from astrocytes, which has a neuroprotective effect on neurons [38;39].

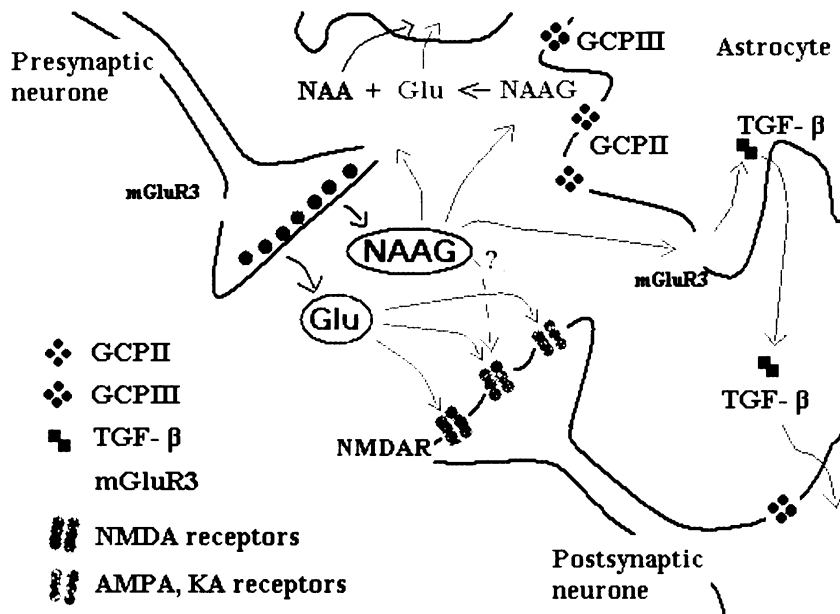


**Fig. 4 A model of the proposed role of NAAG in a glutamatergic synapse.**

When released from the presynaptic neuron, NAAG can activate mGluR3 receptors on both the presynaptic neuron and glial cells. While the activation of presynaptic mGluR3 decreases the release of the primary neurotransmitter glutamate, the activation of glial mGluR3 leads to the secretion of neuroprotective TGF- $\beta$ . The action of NAAG is terminated by GCPII and probably also by GCPIII.

The above-mentioned findings suggest that endogenous NAAG might be neuroprotective in conditions when excessive glutamate is neurotoxic by at least two distinct mechanisms: i) activation of presynaptic mGluR3 decreases further release of glutamate from presynaptic neurons and ii) activation of glial mGluR3 leads to secretion of neuroprotective TGF- $\beta$ . Furthermore, NAAG might partially antagonise some subtypes of NMDA receptors and thus attenuate the overactivation of postsynaptic neurons caused by excessive glutamate [20] (Fig. 4)

## 2.1.2 GCPII Expression and Function

### 2.1.2.1 Nervous System

Glutamate carboxypeptidase II (GCPII), in connection with nervous system also known as N-acetylated- $\alpha$ -linked-acidic dipeptidase (NAALADase), is a membrane-bound protein expressed in glial cells, more specifically in astrocytes [40;41]. GCPII is capable of

hydrolyzing the peptide neurotransmitter N-acetyl-L-aspartyl-L-glutamate (NAAG) and since astrocytes are known to enwrap synapses, the most probable role for GCPII in nervous system is to terminate the action of NAAG released from presynaptic neurons by cleaving it. The reaction products, i.e. N-acetylaspartate (NAA) and glutamate, are then released into the extracellular space.

NAAG-hydrolyzing activity was first observed by Riveros and Orrego in rat brain cortex slices [42]. In 1987, Robinson et al. enzymatically characterized this activity in rat brain cell membranes [1]. Later on, NAAG-hydrolyzing peptidase was purified from rat brains and antibodies were produced against it [43] and the enzyme was termed NAALADase. cDNA for the rat NAALADase was shown to be homologous to human prostate-specific membrane antigen (PSMA) cDNA and consequently, PSMA was demonstrated to have NAAG-hydrolyzing activity [44]. In 1998, Luthi-Carter et al. finally showed that human PSMA and human brain NAALADase are in fact protein products of the same gene [45] and this enzyme was designated glutamate carboxypeptidase II (GCPII).

GCPII is not the only enzyme capable of cleaving NAAG. In 1999, Pangalos et al. reported cloning of second human enzyme with NAAG-hydrolyzing activity [46] and the enzyme was later on designated glutamate carboxypeptidase III (GCPIII). GCPIII mRNA was detected in ovary and testis as well as within discrete areas of brain [46]. The presence of GCPIII in the brain was also proposed by Bacich et al. who deleted gene encoding GCPII in mice, yet observed residual NAAG-hydrolyzing activity in the brains of these mice [47]. Klárka Hlouchová from our laboratory cloned, expressed and purified recombinant human GCPIII and showed that GCPIII cleaved NAAG with kinetic parameters similar to those of GCPII. Moreover, GCPIII is inhibited by GCPII-specific inhibitors [48]. Taken together, these data indicate that there are most probably at least two enzymes capable of cleaving NAAG in human brain.

#### **2.1.2.1.1 GCPII and Neurological Disorders**

As mentioned above, excitotoxic neuronal damage is involved in several neurological disorders, including ischemia, traumatic brain injury, ALS, Alzheimer disease, inflammatory and neuropathic pain and schizophrenia. It was proposed that endogenous NAAG might attenuate adverse effects of excessive glutamatergic

neurotransmission and thus, inhibition of NAAG-hydrolyzing activity might be protective in neuropathological conditions which are associated with glutamate-mediated excitotoxicity.

Several potent GCPII inhibitors were synthesized and characterized so far, which provided an opportunity to test the above-mentioned hypothesis. Indeed, GCPII inhibition was shown to be neuroprotective in animal models of several neurological disorders (reviewed in [21]).

A series of studies was published on GCPII inhibition in models of stroke. It was shown that 2-(phosphonomethyl)pentanedioic acid (2-PMPA), a potent and selective GCPII inhibitor, protected against ischemic injury in a neuronal culture model of stroke, as well as in a rat model of ischemia [49;50]. In the rat model the administration of 2-PMPA caused increase in NAAG levels and attenuated ischemia-induced rise in extracellular glutamate [49], both these effects can contribute to the overall neuroprotection observed in this study. Another GCPII inhibitor, termed GPI5232, also decreased brain injury in the rat model of stroke and this effect was significant even when the inhibitor was administered 2 hours after the ischemic injury [51]. The neuroprotective effect of GCPII inhibition observed in models of stroke is proposed to be mediated by increased levels of NAAG and consequent increased activation of both presynaptic and glial mGluR3 receptors. As mentioned above, activation of presynaptic mGluR3 and glial mGluR3 receptors may contribute to neuroprotection by reducing glutamate release from presynaptic neurons and stimulating the release of neuroprotective TGF- $\beta$ , respectively [21]. Finally, NAAG itself may serve as a significant source of extracellular glutamate and thus inhibition of NAAG-hydrolyzing activity is likely to decrease the levels of extracellular glutamate.

GCPII inhibition was shown to be beneficial not only in the models of stroke, but also in models of several other neurological disorders. Yamamoto et al. showed that GCPII inhibition reduced the perception of pain in rat models of both inflammatory and neuropathic pain [52-54]. GCPII inhibition was also beneficial in a rat model of diabetic neuropathy [55], as well as in a cell culture model of this disease [56]. GCPII inhibition was also tested in transgenic mice expressing a mutant form of superoxide dismutase 1 gene, an animal model for human familial amyotrophic lateral sclerosis (ALS). The onset of the disease was significantly delayed in mice treated with 2-MPPA, a GCPII inhibitor with enhanced oral bioavailability, while the mean life span of these mice was prolonged by 15% [57].



### 2.1.2.2. Prostate

Besides nervous system, GCPII is also expressed in several other tissues, including prostate. GCPII was first identified in prostate in 1987 owing to its binding to monoclonal murine antibody 7E11-C5 [2], which was obtained after immunization with partially purified membranes of LNCaP cells, a cell line isolated from human prostatic cancer. This antibody was observed to bind specifically to membranes of prostatic epithelium, thus the expression of the 7E11-C5 antigen was first thought to be prostate-specific and therefore the antigen was named prostate-specific membrane antigen (PSMA). However, further studies of PSMA expression on both mRNA [58-60] and protein [58;61-63] level showed that PSMA is not a prostate-specific protein as originally thought. In 1993, Israeli et al. cloned cDNA coding for PSMA from LNCaP cDNA library [64] and in 1996, Carter et al. showed that PSMA possessed NAAG-hydrolyzing activity [44]. Later that year, Pinto et al. reported that, besides the NAAG-hydrolyzing activity, PSMA also had folate hydrolase activity [4]. Further studies confirmed that NAALADase from human brain and PSMA are protein products of the same gene [45].

The physiological role of GCPII in prostate is unfortunately still unknown. It was shown that GCPII possessed several characteristics of membrane receptors, including homodimer formation [65-67] and endocytosis via clathrin-coated pits [68]. GCPII also shares modest homology with transferrin receptor [69]. Like a variety of other transmembrane receptors, transferrin receptor undergoes internalization upon binding to its ligand, iron-loaded transferrin. Transferrin receptor with bound transferrin is then trafficked through the endocytic system where the iron is released from transferrin and transferrin receptor with bound apo-transferrin returns back to the plasma membrane. Transferrin receptor thus mediates uptake of iron into cells [70]. Liu et al. showed that, similar to the transferrin receptor, GCPII internalized via clathrin-coated pits in LNCaP cells and that antibodies against extracellular part of GCPII increased the rate of the internalization [68]. GCPII was also reported to possess novel internalization motif MWNLL in its cytoplasmic tail [71]. Furthermore, GCPII cytoplasmic domain was found to interact with filamin A in a yeast two-hybrid assay [72]. These findings support popular hypothesis that GCPII might function as a receptor for yet unidentified ligand [68;73;74].

Besides its unknown function in normal prostate, GCPII probably plays some role in prostate cancer. Immunohistochemical studies demonstrated that GCPII levels were

elevated in primary prostate cancer and metastatic disease and the expression correlated with tumour aggressiveness [75-78].

#### **2.1.2.2.1. GCPII and Prostate Cancer**

Even though almost nothing is known about physiological role of GCPII in normal prostate or in prostate carcinoma, the fact that GCPII expression is upregulated in prostate cancer offers an opportunity for GCPII-targeted imaging as well as treatment of prostate cancer. At present, GCPII is exploited for detection and *in vivo* imaging of GCPII-expressing tumour cells using <sup>111</sup>In-labeled monoclonal antibody 7E11-C5, marketed under the brand name ProstaScint (Cytogen Corporation, Princeton, New Jersey) [79-81]. The major drawback of this antibody is that it recognizes intracellular epitope of GCPII [82], thus only dead or dying cells can be detected. The second-generation anti-GCPII monoclonal antibodies that bind to extracellular domain of GCPII are now in clinical trials [83].

In addition to imaging strategies, anti-GCPII monoclonal antibodies are also assessed for therapeutical purposes, mainly for the treatment of metastatic prostate cancer. Clinical trials using these antibodies conjugated either to radionuclides or to cytotoxic agents are now under way [84;85]. Even though GCPII is not entirely prostate-specific, the GCPII expression seen in prostate cancer cells is significantly higher than that in other tissues, therefore cytotoxic anti-GCPII antibodies are expected to primarily affect prostate cancer and spare healthy tissues.

Immunotherapy using patient's own dendritic cells represents another approach to the treatment of prostate cancer [86;87]. Dendritic cells are antigen-presenting cells capable of stimulating T-cell proliferation and cytotoxicity. These cells, isolated from patients and *in vitro* pulsed with GCPII-derived peptides, were shown to generate immune response and improvement in 30% of patients in phase II clinical trial. The results suggest that this therapy might be an alternative for prostate cancer patients whose disease no longer responds to conventional therapy [88;89].

### 2.1.2.3. Small Intestine

Studies of GCPII localization in human body showed that GCPII is also expressed in the proximal small intestine [61-63]. In addition to brain, small intestine is the only other site of GCPII expression where the function of the enzyme is known. In small intestine, GCPII cleaves off  $\gamma$ -linked glutamates from folylpoly- $\gamma$ -glutamates and thus participates in the absorption of dietary folates [4;90]. Folates in food are a heterogeneous mixture of folylpoly- $\gamma$ -glutamates and as such, they can not be taken into the cells by folate transporters. Only when the poly- $\gamma$ -glutamates are removed, folic acid can be transported across the intestinal wall.

### 2.1.2.4. Other Tissues

Besides the above-mentioned sites of GCPII expression, GCPII has also been observed in kidney [91;92], salivary gland [63], ovary [93] and breast [93]. However, the function of GCPII in these tissues remains unclear.

Interestingly, GCPII was also found to be expressed in tumor-associated neovasculature of most of the solid tumors examined, yet is absent in normal vasculature [61;91;92]. This finding might extend the possible use of GCPII-targeted anticancer drugs also to solid tumors of nonprostatic origin.

### 2.1.3. Structure of GCPII

Human GCPII is a 750-residue type II membrane glycoprotein with a short N-terminal cytoplasmic tail (amino acids 1-18), a transmembrane domain (amino acids 19-43) and a large extracellular domain (amino acids 44-750), where the active site of the enzyme is situated. The intracellular segment encompasses an internalization motif and it was also shown to interact with filamin A [71;72].

Long before the three-dimensional structure of GCPII was determined, Rawlings and Barrett analyzed the amino acid sequence of GCPII and on the basis of sequence comparison with aminopeptidases from *Aeromonas proteolytica*, *Streptomyces griseus* and *Saccharomyces cerevisiae* classified GCPII as a member of peptidase family M28 [94]. This peptidase family comprises metallopeptidases with two co-catalytic zinc ions in the

active site which are necessary for the enzymatic activity. A common feature of members of the family is the binding mode of the active site zinc atoms. Each metal ion is tetrahedrally coordinated by a carboxylate group of either Glu or Asp residue, by an imidazole nitrogen of His residue and, in addition, a carboxylate group of an Asp residue and an activated water molecule serve as bridging ligands, binding both the zinc atoms. For GCPII, these zinc ligands were proposed to be His377, Asp453, Glu425 and His553, with Asp387 functioning as the bridging ligand [94].

Besides the sequence similarities with co-catalytic zinc aminopeptidases, GCPII is homologous with transferrin receptor (sequences of extracellular parts are 28% identical). Transferrin receptor is also a type II membrane glycoprotein, but the putative zinc ligands are mutated in transferrin receptor and it lacks peptidase activity [69].

Recently, crystal structures of GCPII extracellular domain have been presented by two independent groups. While Davis et al. reported GCPII structure with unoccupied substrate-binding site at 3.5 Å resolution [65], Cyril Bařinka from our laboratory in collaboration with Jeroen Mesters from the laboratory of Rolf Hilgenfeld determined three

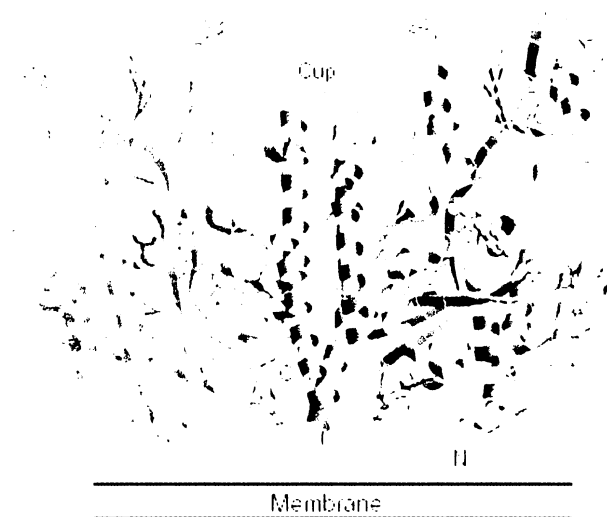


**Fig. 5 Ribbon diagram of the crystal structure of the GCPII extracellular domain.**

Butterfly-like three-dimensional structure of a homodimer of GCPII is shown, with one monomer coloured in grey, while the other is coloured according to organization into domains (protease domain – blue; apical domain – yellow; C-terminal domain – brown). The bound inhibitor and the active site zinc ions are shown as beige and green spheres, respectively. Calcium cation is depicted as a red sphere and chloride anion as a yellow sphere. Taken over from [66].

crystal structures of GCPII in complex with both potent and weak inhibitors and with glutamate, the product of the enzyme's hydrolytic reaction, at 2.0, 2.4 and 2.2 Å resolution, respectively [66]. The three-dimensional structures revealed a homodimer of GCPII with the overall butterfly-like shape similar to that of transferrin receptor. The extracellular part of GCPII folds into three domains: the protease domain, the apical domain and the C-terminal domain and the active site is formed by amino acid residues from all these three domains (Fig. 5, page 15). In addition to the two active site zinc ions, two other ions were found to be bound in the structure: a chloride anion and a calcium cation. Whereas the chloride ion, located near the active site, presumably plays role in substrate binding, the calcium ion is situated too far from the active site to be involved in the catalytic activity. More likely, it helps to stabilize the structure and probably is important for the dimerization [66].

GCPII is a glycoprotein with ten potential N-linked glycosylation sites, all of which were shown to be occupied by sugar moieties [95]. Moreover, glycosylation is necessary for proper folding and enzymatic activity of GCPII [95;96]. One of the carbohydrate chains, attached to Asn638, was proposed to be involved in the homodimer formation [65;66] and since dimerization was reported to be required for GCPII hydrolytic activity [67], this sugar moiety might significantly affect GCPII activity even though it is located far from the active site. This hypothesis is supported by site-directed mutagenesis studies, in which the deletion of this particular glycosylation site resulted in dramatic decrease of enzymatic activity [95;96].

### **2.1.3.1. Active site of GCPII**

As mentioned above, based on the sequence alignments with co-catalytic zinc aminopeptidases, GCPII was also classified as a co-catalytic zinc metallopeptidase and the putative zinc-binding residues were proposed to be His377 and Asp453 for Zn1 and Glu425 and His553 for Zn2, with Asp387 bridging both metal ions [94]. Indeed, the three-dimensional crystal structure revealed two zinc ions in the active site and also confirmed the assignment of zinc ligands [65;66]. In addition to these residues, the zinc ions are bridged by a water molecule/hydroxide anion and nearby resides a glutamic acid residue (Glu424) which forms a hydrogen bond with the bridging water molecule (Fig. 6, page 17). According to the proposed catalytic mechanism for cleavage of NAAG, Glu424 functions

as a general acid/base during the catalytic hydrolysis by abstracting a proton from the bridging water molecule. After the proton abstraction, the generated hydroxide anion attacks the carbonyl group of aspartyl residue of NAAG and Glu424 further facilitates cleavage of the peptide bond by transferring the proton to the leaving amino group of C-terminal glutamate residue [66]. This catalytic mechanism is similar to that proposed for *Aeromonas proteolytica* aminopeptidase and other co-catalytic zinc metallopeptidases [97].

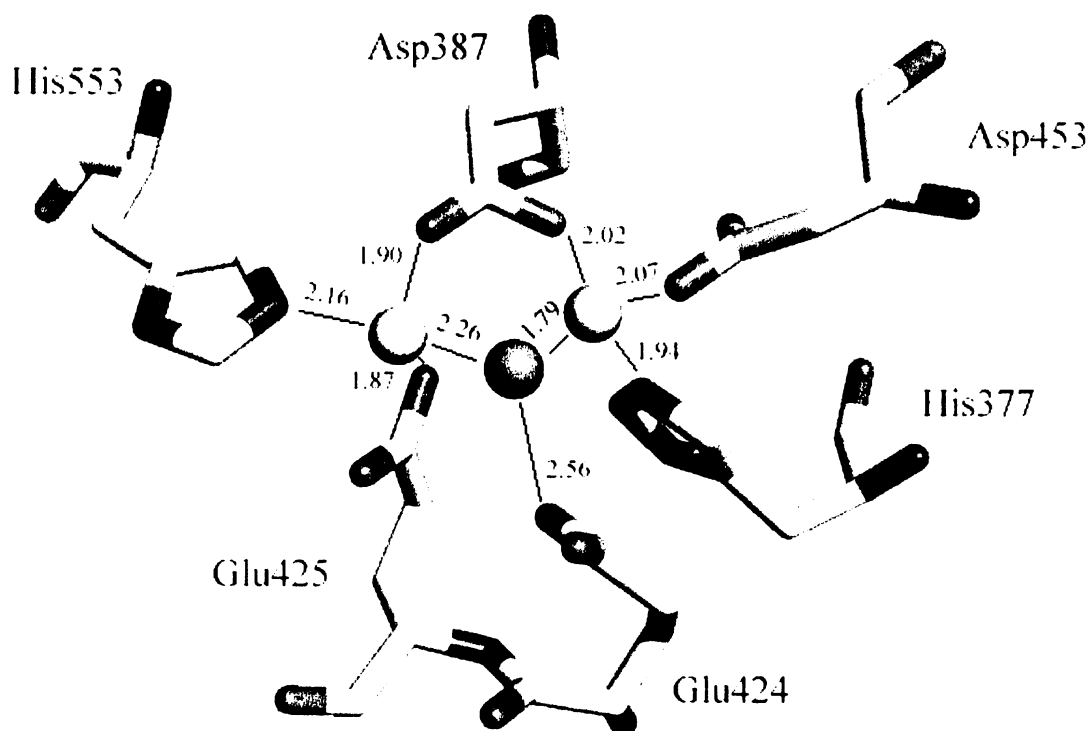


**Fig. 6 The active site of GCPII**

GCPII, as a co-catalytic metallopeptidase, has two zinc ions in the active site (shown as yellow spheres). One of the zinc ions is coordinated by His377 and Asp453, while the other is ligated to His553 and Glu425. In addition, the two metal ions are bridged by Asp387 and a water molecule (indicated as a blue sphere), which, in turn, is hydrogen-bonded to Glu424, the proposed catalytic amino acid residue. Bonding distances are shown in Å. The picture (from the crystal structure of the GCPII-glutamate complex [66], PDB code 2C6G) was generated using PyMOL [98].

The crystal structure of GCPII in complex with glutamate, one of the products of hydrolytic reaction, revealed amino acid residues important for substrate recognition. The C-terminal  $\alpha$ -carboxylate group of glutamate forms a salt bridge with Arg210 and accepts hydrogen bonds from two tyrosine residues (Tyr552 and Tyr700). The free amino group of bound glutamate interacts with  $\gamma$ -carboxylate group of Glu424 and with carbonyl oxygen of Gly518. The side chain of glutamate is positioned via a salt bridge with Lys699 and a

hydrogen bond with side chain amide of Asn257 (Fig. 7, panel A) [66]. The N-Ac-aspartyl portion of NAAG is not bound in the active site, therefore amino acid residues binding this part of substrate can only be proposed from the structure. Such residues that are likely to be involved in interactions with N-Ac-Asp include, among others, three arginines (Arg463, Arg534 and Arg536) and Asn519.

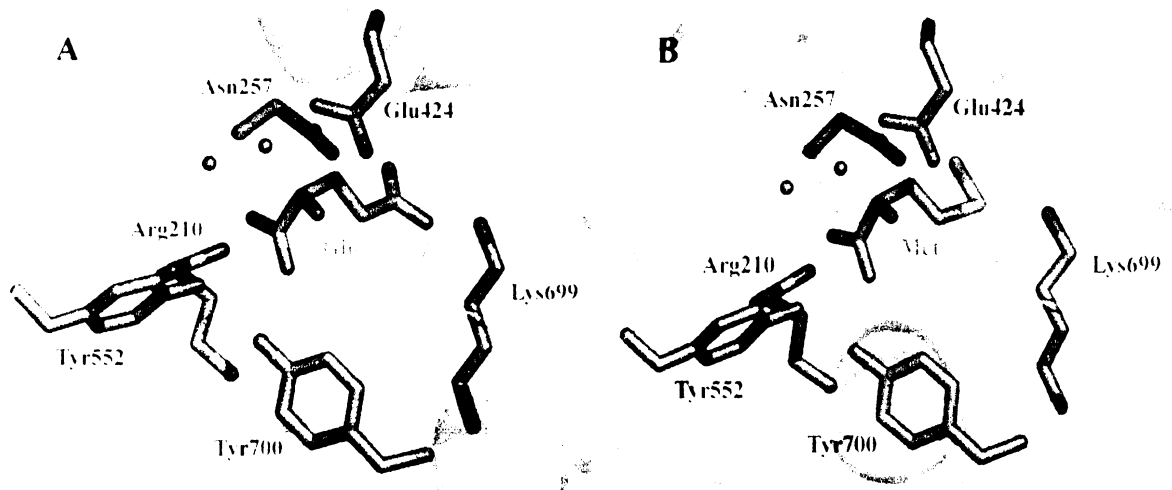


**Fig. 7 Find ten differences.**

The view of the GCPII active site with bound glutamate (panel A) or methionine (panel B). Both glutamate and methionine (coloured in green) are products of the GCPII hydrolytic reactions and their mode of binding into the active site is very similar. While  $\alpha$ -carboxylate groups of both amino acids interact with Arg210, Tyr552 and Tyr700, free amino groups are hydrogen-bonded to Glu424. The side chain of the bound glutamate is positioned via interactions with Lys699 and Asn257 (A). Interestingly, the side chain of the methionine adopts similar conformation, even though it lacks negative charge and consequently can not engage in the same interactions as glutamate (B). The active site zinc ions are shown as violet spheres.

The picture was generated using PyMOL [98].

N-Ac-Asp-Glu (NAAG) is not the only dipeptidic substrate cleaved by GCPII. Substrate specificity studies, carried out in our laboratory using dipeptidic libraries N-Ac-X-Glu and N-Ac-Asp-X (where X stands for any naturally occurring amino acid), revealed that also N-Ac-Glu-Glu, N-Ac-Ala-Glu, N-Ac-Asp-Met and N-Ac-Asp-Ala were efficiently hydrolyzed by GCPII ([99] and unpublished observation). In contrast with the naturally occurring substrates of GCPII, all of which have negatively charged glutamate in the C-terminal position of the substrate, two of these newly identified GCPII substrates, i.e. N-Ac-Asp-Met and N-Ac-Asp-Ala, harbour amino acids with hydrophobic side chains in the C-terminal position. Thus, in addition to hydrogen bonds and salt bridges that position the glutamate-containing substrates in the active site, also hydrophobic interactions are

likely to be involved in binding of the C-terminal residue side chain. The crystal structure of GCPII in complex with methionine at 2.4 Å resolution, solved by Cyril Bařinka (Bařinka et al., manuscript in preparation), revealed that the binding mode of methionine in the active site of GCPII is very similar to that of glutamate and even the side chains of Lys699 and Asn257, which interact with  $\gamma$ -carboxylate group of glutamate in the GCPII-glutamate complex, have nearly identical conformations in the complex with methionine as in that with glutamate (Fig. 7, panel B, page 18).

### 2.1.3.2. Inhibitors

As mentioned above, GCPII is regarded as a promising target for treatment of various neurological disorders which are associated with dysregulation of glutamatergic neurotransmission. Moreover, GCPII inhibition was shown to be neuroprotective in animal models of several of these disorders. Therefore, one of the obvious aims of structural studies of GCPII is to provide insight into the active site and thus facilitate the design of specific and potent inhibitors with good pharmacokinetic properties.

The compounds that were first observed to inhibit GCPII included polyvalent oxoanions such as phosphate and sulphate and divalent metal ion chelators (e.g. EDTA and EGTA) [1]. GCPII was also reported to be inhibited by quisqualic acid and  $\beta$ -NAAG, an analog of NAAG, with  $K_i$  values of 1.9  $\mu$ M and 0.7  $\mu$ M, respectively [1;100]. However, all these compounds by far lacked the potency and specificity of 2-(phosphonomethyl)pentanedioic acid (2-PMPA), the first efficient GCPII inhibitor reported in 1996 ( $K_i = 0.3$  nM) [101]. Since then, several other potent GCPII inhibitors, derived from the structure of 2-PMPA, were synthesized [102] (Fig. 8, page 20). In addition to compounds bearing phosphonate or phosphinate groups as active site zinc ions chelators, other zinc-binding groups were also tested for their ability to inhibit GCPII. 2-(3-mercaptopropyl)pentanedioic acid (2-MPPA), a representative of thiol-based inhibitors, was identified as not only potent but also as the first orally bioavailable GCPII inhibitor [103]. Compounds with hydroxamate group as a zinc-binding group were also tested, but showed to be less potent GCPII inhibitors than the phosphonate- and thiol-based ones [104]. Besides the above-mentioned inhibitors, urea-based compounds were also reported to efficiently inhibit GCPII [105;106].



The crystal structures reported by Mesters et al. showed the binding mode of GPI-18431, a derivative of 2-PMPA and a potent GCPII inhibitor, as well as the binding mode of phosphate, a weak inhibitor of GCPII. While phosphate only ligates the active site zinc ions, GPI-18431, in addition to that, also interacts with the substrate-binding site, thus achieving much better potency and specificity as a GCPII inhibitor [66].

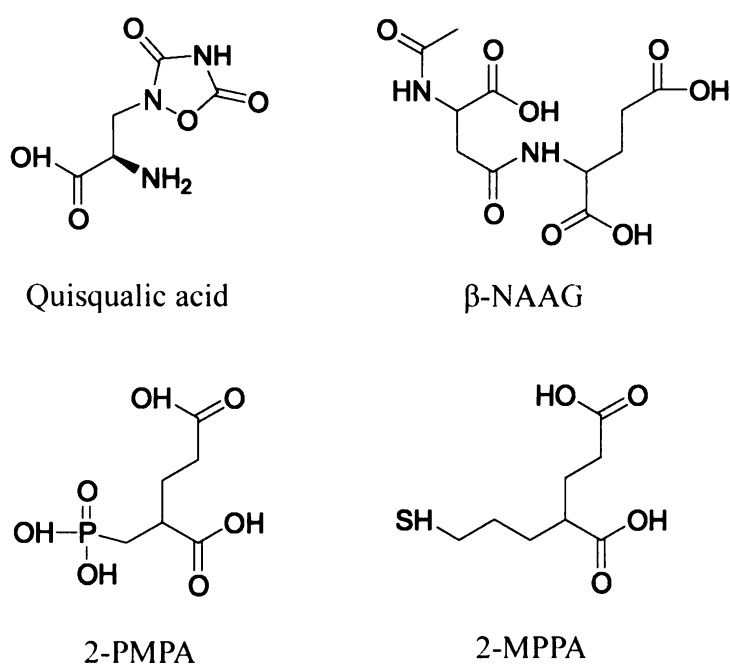


**Fig. 8 Inhibitors of GCPII.**

Quisqualic acid (2-amino-3-(3,5-dioxo-[1,2,4]oxadiazolidin-2-yl)-propionic acid;  $K_i = 1.9 \mu\text{M}$ ) and  $\beta$ -NAAG ( $K_i = 700 \text{ nM}$ ) are representatives of the first GCPII inhibitors reported [1;100]. 2-PMPA (2-(phosphonomethyl)pentanedioic acid;  $K_i = 0.3 \text{ nM}$ ) and its thiol-based derivative, 2-MPPA (2-(3-mercaptopropyl)-pentanedioic acid;  $\text{IC}_{50} = 90 \text{ nM}$ ), belong to the most potent GCPII inhibitors known at present. Moreover, 2-MPPA, thanks to the replacement of charged phosphonate group of 2-PMPA by a thiol group, is orally bioavailable [103].

### 2.1.3.3. Site-directed mutagenesis studies of the GCPII active site

Before the X-ray crystal structure of GCPII was solved, the active site residues of GCPII were proposed based on the homology of the protease domain of GCPII with *Aeromonas proteolytica* and *Streptomyces griseus* aminopeptidases [94;107], the structures of which were reported in 1994 and 1997, respectively [108;109]. The assignment of zinc-binding ligands turned out to be in complete agreement with what was later observed in the

crystal structure. However, since the *Aeromonas* and *Streptomyces* aminopeptidases have different substrate specificities than GCPII, the prediction of substrate-binding residues showed to be less accurate.

Speno et al. used site-directed mutagenesis approach to test this assignment of both zinc-binding and substrate-binding residues [107]. Mutation of zinc ligands lead to dramatic decrease in enzymatic activity, although mutant proteins were expressed, as demonstrated by immunoblot analysis. In contrast, single substitutions to putative substrate-binding residues showed to be less perturbing and kinetic parameters of NAAG hydrolysis were obtained for most of the mutant proteins. The largest increase in  $K_M$  values was observed for mutations of Arg463 and Arg536 that did not preserve the positive charge of these residues. This is consistent with the crystal structure reported by Mesters et al., who proposed that these two arginines are likely to be involved in the binding of the N-acetyl-aspartyl portion of NAAG [66]. In addition, mutation of Asn519, which was also proposed to form the binding site for N-acetyl-aspartyl, resulted in large decrease of enzymatic activity, such that kinetic parameters could not be measured. None of the residues observed to interact with glutamate in the crystal structure was targeted for substitution in the Speno's study, except for Tyr552, the mutation of which lead mainly to decrease in  $V_{max}$  value. Moreover, Glu424, the proposed catalytic amino acid, was mutated to glutamine, which also resulted in reduced  $V_{max}$  value [107] (Fig. 9, page 22).

The site-directed mutagenesis approach has also been used by Petra Mlčochová from our laboratory to study the active site of GCPII [110]. The choice of putative substrate-binding residues targeted for mutagenesis in this study was based on the model of GCPII created by Daruka Mahadevan (University of Arizona Cancer Center, Tucson) and Jose W. Saldanha (National Institute for Medical Research, London). Similar to Speno's work, none of the glutamate-binding residues was predicted to play role in substrate binding, besides Tyr552. In agreement with the previous study, the mutation of this tyrosine was shown to affect primarily  $k_{cat}$  value. However, the results of substitutions to the arginine residues that are proposed to interact with the N-acetyl-aspartyl portion of NAAG differ between the two studies. While Speno et al. reported increase in  $K_M$  values for mutations R463I and R536E, the results from our laboratory indicated decrease in  $k_{cat}$  for mutations R534L and R536L. Dramatic fall in  $k_{cat}$  value was also observed for substitution of Asn519 to valine [110] (Fig. 9, page 22).

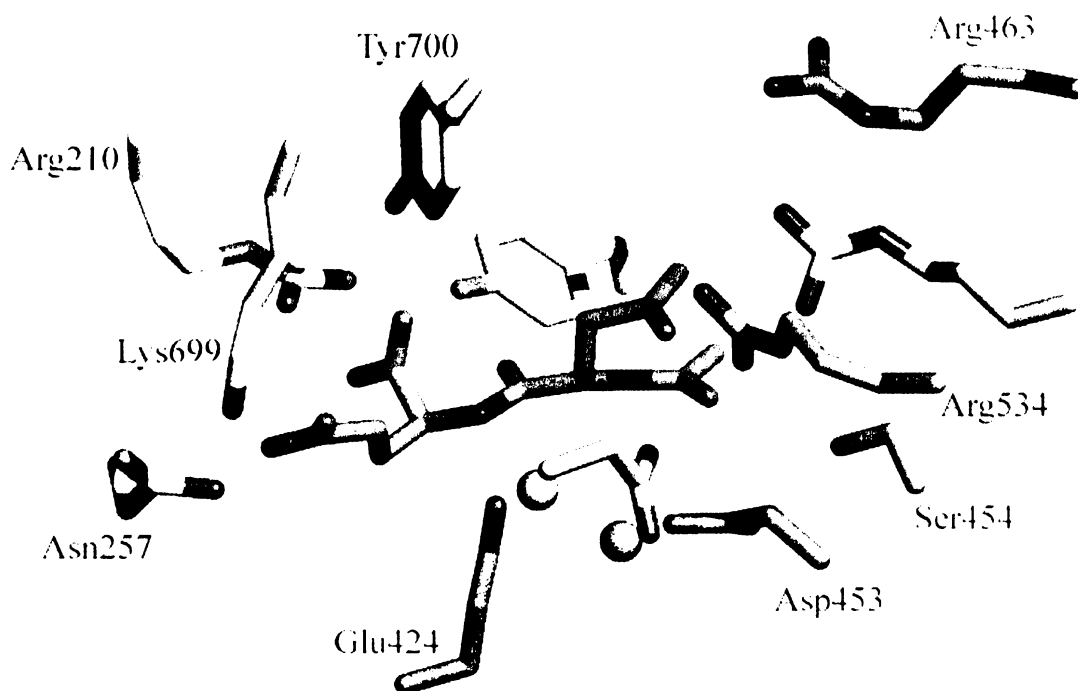


**Fig. 9 Computer model of the GCPII active site with bound NAAG.**

Amino acid residues mutated in the aforementioned mutational studies are highlighted as follows: residues mutated in Speno's study are shown in blue, residues mutated by Petra Mlčochová in our laboratory are shown in brown and residues substituted in both these studies are in yellow [107;110]. NAAG in the GCPII active site is coloured green and zinc ions are depicted as orange spheres. Finally, residues interacting with the C-terminal glutamate of NAAG are coloured grey. For clarity, not all the residues targeted for mutagenesis are shown.

The three-dimensional model of GCPII with bound NAAG was constructed by Lubomír Rulíšek, based on the crystal structure of GCPII in complex with inhibitor GPI-18431 [66]. The picture was generated using PyMOL [98].

### 3. Objectives

- 1) analyze the GCPII active site using the site-directed mutagenesis approach
  - mutate amino acid residues of recombinant human GCPII (rhGCPII) implicated in substrate binding/catalysis
  - express, purify and kinetically characterize the mutant forms of rhGCPII
  - prepare an inactive mutant of rhGCPII and cocrystallize it with a substrate
  
- 2) study hydrophobic interactions in the GCPII active site
  - kinetically characterize hydrolysis of a series of novel dipeptidic substrates of rhGCPII harbouring non-naturally occurring amino acids with hydrophobic side chains at the C-terminus

## 4. Materials and Methods

### 4.1. Materials and Instruments

#### 4.1.1. Materials

##### **Bio-Rad (Hercules, USA)**

AG 1X8-resin, agarose, Protein Assay Kit.

##### **Fluka (Buchs, Switzerland)**

acetonitrile, acrylamide, (R,S)-2-aminoheptanoic acid, (R,S)-2-aminooctanoic acid, (R,S)-2-aminononanoic acid, N,N'-methylenebisacrylamide, N,N,N',N'-tetramethylethylenediamine,

##### **Gibco (Rockville, USA)**

Defined Lipid Concentrate, fetal bovine serum, L-glutamine, SF900 II medium, Yeastolate Ultrafiltrate

##### **Invitrogen (San Diego, USA)**

Calcium Phosphate Transfection Kit, Hygromycin B, *Drosophila* Schneider's S2 cells, pCoHYGRO vector, pMT/BiP/V5-His A vector

##### **Lachema (Brno, Czech Republic)**

acetic acid, acetone, ethanol, formaldehyde, formic acid, hydrochloric acid, isopropanol, methanol, silver nitrate, sodium acetate, sodium carbonate, sodium hydroxide, sodium thiosulfate, trichloroacetic acid

##### **Léčiva (Prague, Czech Republic)**

ampicillin

##### **Merck (New Jersey, USA)**

dimethylsulfoxide, sodium dodecylsulfate

##### **Millipore (Billerica, USA)**

Centriprep YM-50, Microcon YM-10, 0.22  $\mu$ m filters

##### **New England Biolabs (Beverly, USA)**

restriction endonucleases

##### **Nextal Biotechnologies (Montreal, Canada)**

crystallization plates

**Packard (Meriden, USA)**

Ultima Gold Scintillation Cocktail

**Perkin Elmer Corporation (Foster City, USA)**

ABI Prism BigDye Terminator Cycle Sequencing Ready Reaction Kit v3.1

**Perkin Elmer (Wellesley, USA)**

<sup>3</sup>H-NAAG (50 Ci/mmol)

**Pharmacia (New York, USA)**

Mono P HR 5/10 column, QAE-Sephadex A-50, Source 15S HR 10/10 column,  
Superdex 200 HR 16/60 column

**Phenomenex (Torrance, USA)**

C18(2) Luna column

**Pierce (Rockford, USA)**

Casein Blocker, FDAA, HRP-conjugated goat anti-mouse secondary antibody,  
Nitrocellulose Membrane Sheet, SuperSignal West Dura Extended Duration Substrate

**P-Lab (Prague, Czech Republic)**

Pasteur pipettes, scintillation vials

**Promega (Madison, USA)**

Pfu polymerase

**Qiagen (Germantown, USA)**

Plasmid Midi Kit

**Sarstedt (Numbrecht, Germany)**

tissue culture plastics

**Serva (Heidelberg, Germany)**

ammonium peroxodisulfate, bromphenol blue, Coomassie Brilliant Blue G250, lysozyme,  
Triton X100

**Sigma (St. Louis, USA)**

L-alanine, (S)-2-aminobutanoic acid, calcium chloride, chloroform, cupric sulphate,  
EDTA, glycine, L-glutamic acid, hemacytometer, HEPES (N-2-hydroxyethylpiperazine-  
N'-2-ethanesulfonic acid), LB agar, LB medium, Lentil Lectin-Sepharose, manganese  
chloride, L-methionine, mercaptoethanol, methyl- $\alpha$ -D-mannopyranoside, MOPS (3-[N-  
morpholino] propanesulfonic acid), NAAG, L-norleucine, L-norvaline,  
o-phthaldialdehyde, phenol, Ponceau S, sodium chloride, Trypan Blue

**Spectra/Por (Rancho Dominguez, USA)**

membrane tubing

**Top-Bio (Prague, Czech Republic)**

DNA Lego kit, dNTP's

**USB (Cleveland, USA)**

boric acid, ethidium bromide, sodium tetraborate, Tween 20,  
TRIS (tris(hydroxymethyl)aminomethane)

**Waters (Milford, USA)**

AccQ Fluor Reagent kit

**4.1.2. Instruments**

ABI Prism 310 Genetic Analyzer (The Perkin-Elmer Corporation, Foster City, USA)

AKTAEplorer FPLC system (Pharmacia, New York, USA)

BSB4A laminar flow-box (Gelaire, Sydney, Australia)

BT120 biological thermostat (Laboratorní přístroje, Prague, Czech Republic)

Centrifuges: Beckman J2-MI (Beckman, Fullerton, USA)

Megafuge 2.0R (Heraeus Instruments, Germany)

Beckman Avanti J-30I (Beckman, Fullerton, USA)

Biofuge pico (Heraeus Instruments, Germany)

Horizon 58 horizontal electrophoresis apparatus (Life Technologies, Grand Island, USA)

Innova 4300 incubator shaker (New Brunswick Scientific, Edison, USA)

LAS-1000 CCD camera (Fujifilm, Tokyo, Japan)

Microscope Nikon TMS (Tokyo, Japan)

Mini Protean II vertical electrophoresis apparatus (Bio-Rad, California, USA)

SemiPhor semidry transfer unit (Hoefer Scientific Instruments, San Francisco, USA)

Thermal cycler GeneAmp PCR System 2400 (Perkin-Elmer, Foster City, USA)

Thermal cycler T Gradient (Biometra, Göttingen, Germany)

Unicam Helios  $\alpha$  spectrophotometer (Waltham, USA)

Unicam 9450 pH meter (Waltham, USA)

UV transilluminator UVT-20 SML (Herolab, Wiesloch, Germany)

Waters 2795 Alliance HPLC system (Waters, Milford, USA)

Waters 2475 Multi  $\lambda$  Fluorescence Detector (Waters, Milford, USA)

Waters 2487 Dual  $\lambda$  Absorbance Detector (Waters, Milford, USA)

## 4.2. Methods

### 4.2.1. Site-Directed Mutagenesis

Site-directed mutagenesis was carried out according to the QuikChange Site-Directed Mutagenesis Kit Instruction Manual (Stratagene, La Jolla, USA). The pMTNAEXST plasmid (Fig. 11, page 49), prepared by Cyril Bařinka in our laboratory, was used as a template. This plasmid was derived from the pMT/Bip/V5-His A plasmid (Invitrogen, San Diego, USA) into which the DNA encoding the extracellular part of human GCPII (amino acids 44-750) was cloned. The main features of the plasmid are the *Drosophila* metallothionein promoter, which enables inducible heterologous expression in *Drosophila* S2 cells, and the Bip secretion signal, which targets the extracellular portion of GCPII for secretion into the culture medium.

Two complementary oligonucleotide primers harbouring the desired mutation were used to introduce the mutation into the pMTNAEXST plasmid. Sequences of the primers used for individual amino acid changes are shown in Table I (page 28).

The reaction mixture contained:

pMTNAEXST	30 ng
two complementary primers	125 ng of each
dNTP mix (10 mM)	1 $\mu$ l
Pfu DNA polymerase (2.5 U/ $\mu$ l)	1 $\mu$ l
10x reaction buffer	5 $\mu$ l
distilled water to the final volume of 50 $\mu$ l.	

The following temperature-cycling parameters were used for the synthesis of mutated plasmids:

initial denaturation:	94°C	5 min
16 cycles of amplification:	95°C	30 s
	55°C	1 min
	68°C	12 min
final extension:	68°C	10 min.



**Table I. Nucleotide sequences of primers used for site-directed mutagenesis.**

Mutation	Primer Designation	Nucleotide Sequence (5' → 3')
<b>E424A</b>	FNAE424A	GCTGGGATGCAGCTGAATTTGGTCTTCTTGG
	RNAE424A	CCAAGAAGACCAAATTCAGCTGCATCCCAGC
<b>K699S</b>	FNAK699S	CAAGCAGCCACAACCTCATATGCAGGGGAGTC
	RNAK699S	GACTCCCCTGCATATGAGTTGTGGCTGCTTG
<b>N257D</b>	FNAN257D	GTCCAGCGTGGAGATATCCTAAATCTGAATGG
	RNAN257D	CCATTCAGATTTAGGATATCTCCACGCTGGAC
<b>N519D</b>	FNAN519D	GCAAATTGGGATCCGGAGACGATTTTGAGG
	RNAN519D	CCTCAAATCGTCTCCGGATCCCAATTTGC
<b>R210A</b>	FNAR210A	GGGAAAGTTTTTCGCGGGAAATAAGGTTAAAAATG
	RNAR210A	CATTTTTAACCTTATTTCCCGCGAAAACCTTCCC
<b>R210K</b>	FNAR210K	GGGAAAGTTTTCAAGGGAAATAAGGTTAAAAATGC
	RNAR210K	GCATTTTTAACCTTATTTCCCTTGAAAACCTTCCC
<b>Y700F</b>	FNAY700F	GCAGCCACAACAAGTTCGCAGGGGAGTCATTCC
	RNAY700F	GGAATGACTCCCCTGCGAACTTGTTGTGGCTGC

Nucleotides substituted by site-directed mutagenesis are shown in red, while codons encoding mutated amino acid residues are shaded in gray.

The reaction mixture was then cooled on ice. Following the addition of 1  $\mu$ l of DpnI endonuclease (20 U/ $\mu$ l), the reaction was incubated at 37°C for 1 hour to digest the methylated (i.e., the template) DNA. The obtained mutated plasmid was subsequently transformed into competent DH5 $\alpha$  *E. coli* cells, plasmid DNA was isolated and the presence of the desired mutation was verified by sequencing.

#### 4.2.2. Transformation of *E. coli* Cells

Plasmid DNA (1-5  $\mu$ l) was added to competent DH5 $\alpha$  *E. coli* cells, which were prepared using the calcium chloride protocol [111]. Following 30-minute incubation on ice, heat-shock was performed at 42°C for 1.5 min and subsequently, the cells were cooled on ice for 1 min. 0.5 ml of sterile LB medium was added and the cells were incubated at

37°C for 45-60 min. 100-300 µl of the cell suspension were then spread on ampicillin agar plates (with ampicillin concentration of 100 µg/ml), which were pre-incubated at 37°C. The plates with the transformed cells were then incubated at 37°C overnight.

#### **4.2.3. Midipreparation of Plasmid DNA (Midiprep)**

Solution I: 50 mM glucose, 25 mM Tris-HCl (pH 8.0), 10 mM EDTA (pH 8.0)

Solution II: 0.2 M NaOH, 1% SDS

Solution III: 3 M CH<sub>3</sub>COOK, 2 M CH<sub>3</sub>COOH

12 ml of sterile LB medium with ampicillin (100 µg/ml) were inoculated with one colony from the agar plate and incubated at 37°C overnight with shaking at 220-230 rpm. The bacterial culture was then centrifuged at 3360 g for 10 min and the pellet was resuspended in 200 µl of Solution I. 30 µl of lysozyme (10 mg/ml) and 6 µl of RNase (10 mg/ml) were added and the mixture was incubated on ice for 30 min. Subsequently, 400 µl of Solution II were added, the sample was gently mixed and left on ice for 6 min. Finally, 300 µl of Solution III were added, the sample was again gently mixed, incubated on ice for 6 min and then centrifuged at 16,000 g for 7 min. 850 µl of supernatant were aspirated and added to 1200 µl of the DNA binding buffer (DNA Lego kit, Top-Bio, Prague, Czech Republic) and the mixture was briefly vortexed. 200 µl of the binding particles (DNA Lego kit) were loaded into a minicolumn and the mixture of DNA with the DNA binding buffer was sucked through the binding particles using a vacuum pump. The particles were then washed twice with 1 ml of the washing buffer (DNA Lego kit) and the residual washing buffer was removed by centrifuging the minicolumn in an Eppendorf tube at 16,000 g for 1 min. To elute the bound DNA, 100 µl of water were added and after one-minute incubation, the minicolumn was placed into a new Eppendorf tube and centrifuged at 16,000 g for 1 min. This procedure was repeated once more and then 100 µl of water, 33 µl of 3 M sodium acetate and 660 µl of chilled 95% ethanol were added to precipitate the eluted DNA. Following the incubation at -70°C for 15 min, the sample was centrifuged at 16,000 g for 8 min and the pellet of plasmid DNA was washed with 70% ethanol and dissolved in 20 µl of water.

#### 4.2.4. Determination of DNA Concentration

Concentration of DNA was determined by measuring the absorbance of the sample at 260 nm. Typically, 5  $\mu$ l of the DNA sample were dissolved in water to the final volume of 1 ml and the absorbance was measured at 260 and 280 nm. The purity of the isolated DNA was estimated using the ratio of the absorbance at 260 nm to the absorbance at 280 nm, which should be 1.8 for pure double-stranded DNA.

#### 4.2.5. DNA Sequencing

Sequencing of plasmid DNA was carried out using ABI Prism BigDye Terminator Cycle Sequencing Ready Reaction Kit (The Perkin-Elmer Corporation, Foster City, USA). Five sequencing primers were used for sequencing the DNA encoding the extracellular portion of GCPII. The sequences of the primers are shown in Table II.

**Table II. Nucleotide sequences of sequencing primers.**

<b>Primer Designation</b>	<b>Nucleotide Sequence (5' → 3')</b>
MT forward	CATCTCAGTGCAACTAAA
SECNA1	ACGGGACATGAAAATCAATTG
SECNA2	AAAAGTCAAGATGCACATCC
SECNA3	GTTTCATAGAAATACTGTAG
BGH reverse	TAGAAGGCACAGTCGAGG

The reaction mixture contained:

Terminator Ready Reaction Mix	2 $\mu$ l
sequencing buffer 5x	4 $\mu$ l
plasmid DNA	1 $\mu$ g
sequencing primer	10 pmol
distilled water to the final volume of 20 $\mu$ l.	

A PCR tube with the reaction mixture was placed into a thermal cycler and following parameters were set up:

initial denaturation:	95°C	30 s
25 cycles:	95°C	10 s
	50°C	5 s
	60°C	4 min
final extension:	60°C	7 min.
storage:	4°C	

The reaction mixture was then pipetted into a 1.5 ml microcentrifuge tube, 50 µl of chilled 95% ethanol were added and the sample was left on ice for 15 min. Subsequently, the tube was placed into a microcentrifuge, its orientation was marked and it was centrifuged at 16,000 g for 15 min. The supernatant was carefully aspirated, 250 µl of 70% ethanol were added into the tube and the sample was briefly vortexed. The tube was placed into a microcentrifuge in the same orientation as previously and centrifuged at 16,000 g for 5 min. The supernatant was again aspirated, 250 µl of 70% ethanol were added, the tube was briefly vortexed and centrifuged at 16,000 g for 5 min. Subsequently, the supernatant was aspirated and the sample was dried in a heating block at 95°C for 2 min. The pellet was resuspended in 30 µl of Template Suppression Reagent (The Perkin-Elmer Corporation), heated at 95°C for 5 min and then cooled on ice for 5 min.

Electrophoresis of samples was carried out on the ABI PRISM 310 Genetic Analyzer (The Perkin-Elmer Corporation) at the Institute of Molecular Genetics, Prague, Czech Republic.

#### **4.2.6. Maxipreparation of Plasmid DNA (Maxiprep)**

Solution I: 50 mM glucose, 25 mM Tris-HCl (pH 8.0), 10 mM EDTA (pH 8.0)

Solution II: 0.2 M NaOH, 1% SDS

Solution III: 3 M CH<sub>3</sub>COOK, 2 M CH<sub>3</sub>COOH

TE buffer: 10 mM Tris-HCl, 1 mM EDTA, pH 8.0

2 ml of sterile LB medium with ampicillin (100 µg/ml) were inoculated with one colony from the agar plate and incubated at 37°C for 8-10 hours with shaking at 220-230 rpm. The bacterial culture was then transferred into 0.5 l of sterile LB medium with ampicillin (100 µg/ml) and incubated at 37°C overnight with shaking at 220-230 rpm. The grown culture was centrifuged at 22,000 g for 10 min at 4°C and the pellet of cells was resuspended in 20 ml of Solution I. 1 ml of lysozyme (25 mg/ml) was added and the suspension was stirred at room temperature for 20 min. Subsequently, 40 ml of Solution II were added, the sample was mixed and left at room temperature for 10 min. Finally, 30 ml of Solution III were added, the sample was again mixed and incubated at room temperature for 5 min. After centrifugation at 15,000 g for 10 min at 4°C, the supernatant was filtered through folded gauze into a new cuvette. 60 ml of isopropanol were added and the sample was left at room temperature for 10 min prior to centrifugation at 15,000 g for 10 min at 25°C. The pellet was resuspended in 4.5 ml of TE buffer and transferred into a 15 ml Falcon tube. 300 µl of 1 M Tris-HCl, pH 8.0 and 1.5 ml of 10 M LiCl were added and the mixture was incubated on ice for 40 min. The sample was then centrifuged at 3360 g for 10 min at 4°C and the supernatant was transferred into a new Falcon tube. 6 ml of isopropanol were added, the mixture was left for 10 min at room temperature and then centrifuged at 3360 g for 10 min at 25°C. The pellet was resuspended in 0.5 ml of TE buffer, 10 µl of RNase (10 mg/ml) were added and the reaction mixture was incubated at 37°C for 1 hour. Following the addition of equal volume of 13% PEG 8,000 (w/v, in 1.6 M NaCl), the mixture was centrifuged at 16,000 g for 8 min at 25°C and the pellet was dissolved in 0.5 ml of TE buffer. Subsequently, an extraction with equal volume of fenol was performed followed by centrifugation at 16,000 g for 1 min. The upper water phase was transferred into a new Eppendorf tube and the extraction was repeated with equal volume of fenol/chloroform mixture (1:1). The upper phase was again transferred into a new tube and the extraction with fenol/chloroform was repeated once more, followed by two extractions with equal volume of chloroform. The upper phase was again transferred into a new tube, 3 M sodium acetate (1/10 of the volume of the sample) and 95% ethanol (twice the volume of the sample) were added and the mixture was incubated at room temperature for 10 min. The sample was then centrifuged at 16,000 g for 10 min, ethanol was aspirated and the pellet was washed with 70% ethanol and dissolved in 300 µl of sterile water.

#### 4.2.7. Purification of Plasmid DNA with QIAGEN Plasmid Midi Kit

QBT buffer: 750 mM NaCl, 50 mM MOPS (pH 7.0), 15% isopropanol

QC buffer: 1 M NaCl, 50 mM MOPS (pH 7.0), 15% isopropanol

QF buffer: 1.25 mM NaCl, 50 mM Tris-HCl (pH 8.5)

Prior to the transfection of insect cells, plasmid DNA isolated according to the maxiprep protocol was further purified using the QIAGEN Plasmid Midi Kit (Qiagen, Germantown, USA). 100 µg of plasmid DNA were mixed with 4 ml of QBT buffer and loaded onto QIAGEN-tip 100 column equilibrated in QBT buffer. The column was washed twice with 10 ml of QC buffer and plasmid DNA was eluted by the addition of 5 ml of QF buffer. Subsequently, the DNA was precipitated by 3.5 ml of isopropanol, followed by centrifugation at 3360 g for 30 min at 4°C. The pellet was washed with 1 ml of 95% ethanol and centrifuged at 3360 g for 10 min. The pellet was again washed, this time with 2 ml of 70% ethanol and centrifuged at 3360 g for 10 min. Ethanol was carefully aspirated and the pellet was dried on air for 10 min and then dissolved in 50 µl of sterile water for tissue cultures.

#### 4.2.8. Agarose Gel Electrophoresis

Solutions:

TAE buffer 50x: 242 g Tris, 57.1 ml 99% CH<sub>3</sub>COOH, 100 ml 0.5 M EDTA  
(pH 8.0), water added to the final volume of 1 l, pH 8.0

sample buffer: 40% sucrose (w/v), 0.1% (w/v) bromphenol blue, 0.02% NaN<sub>3</sub>

DNA molecules were resolved in 1% agarose gel in TAE buffer supplemented with ethidium bromide (with final concentration of 0.5 µg/ml) using the horizontal gel electrophoresis apparatus (Life Technologies, Grand Island, USA). Typically, the electrophoresis was run at 120V for 20-30 min. Bacteriophage λ DNA digested with BstE II restriction endonuclease was used as a molecular weight marker. DNA molecules were visualized using UV transilluminator (Herolab, Wiesloch, Germany) at 302 nm and photographed with digital camera (Kodak, USA).

#### 4.2.9. Stable Transfection of *Drosophila* S2 Cells Using Calcium Phosphate

Solution A: 2 M CaCl<sub>2</sub> 36 µl  
recombinant DNA 19 µg  
pCoHYGRO 1 µg  
tissue culture sterile water to the final volume of 300 µl

Solution B: 300 µl of 2x HEPES-Buffered Saline (HBS)

2x HEPES-Buffered Saline (HBS): 50 mM HEPES, 1.5 mM Na<sub>2</sub>HPO<sub>4</sub>,  
280 mM NaCl, pH 7.14

*Drosophila* Schneider's S2 cells (Invitrogen, San Diego, USA) were cultured in a 35 mm plate in SF900II medium (Gibco, Rockville, USA) supplemented with 10% fetal bovine serum (Gibco) at 22-24°C until they reached a density of 2 to 4 x 10<sup>6</sup> cells/ml. Solution A was added dropwise to Solution B with continuous vortexing and the final mixture was incubated at room temperature for 40 min. Subsequently, the solution was mixed and added dropwise to the cells. The cells were then incubated for 16-24 hours at 22-24°C. The transfected cells were then transferred into a 15 ml sterile Falcon tube and centrifuged at 500 g for 2 min. The medium was aspirated, 3 ml of fresh SF900II medium with 10% fetal bovine serum (complete medium) were added and the cells were replated into the same plate. After one-day incubation at 22-24°C, the medium was carefully aspirated and 3 ml of fresh complete medium containing hygromycin-B (300 µg/ml) were added. The selective medium was replaced every 4-5 days until resistant cells started growing out (usually 3-4 weeks).

#### **4.2.10. Trypan Blue Exclusion Assay of Cell Viability**

Trypan Blue: 0.4% solution of Trypan Blue in PBS, pH 7.4, filtered through 0.22  $\mu\text{m}$  filter

PBS: 137 mM NaCl, 2.7 mM KCl, 10 mM  $\text{Na}_2\text{HPO}_4$ , 1.8 mM  $\text{KH}_2\text{PO}_4$ , pH 7.4

Trypan Blue Exclusion Assay is used for distinguishing between living and dead cells. Dead cells take up the Trypan Blue dye and stain blue, while living cells are capable of excluding the dye.

Typically, 20  $\mu\text{l}$  of the cell suspension were mixed with 880  $\mu\text{l}$  of PBS and 100  $\mu\text{l}$  of the Trypan Blue solution were added. The mixture was left to stand for 5 min at room temperature, then mixed thoroughly and 13  $\mu\text{l}$  of the solution were pipetted under a hemacytometer (Sigma, St. Louis, USA) cover-slip. The cells were observed under a microscope at 100x magnification, the number of viable as well as dead cells were counted and the cell concentration was calculated.

#### **4.2.11. Expression of Mutant Forms of Recombinant GCPII**

Transfected S2 cells resistant to hygromycin-B were transferred into a spinner flask (Bellco, Vineland, USA) with SF900II medium (without hygromycin-B). Final cell density was approximately  $2 \times 10^6$  cells/ml. For smaller production of recombinant protein, 250 ml spinner flask was used and the volume of the cell culture was 120-150 ml. For larger production, 1 litre spinner flask was used and the cell culture volume didn't exceed 600 ml. Defined Lipid Concentrate (1/100 of the cell culture volume) and Yeastolate Ultrafiltrate (1/50 of the cell culture volume) were then added and the culture was incubated at 22-24°C with constant stirring at 100-120 rpm. When the cell density reached  $8 \times 10^6$  cells/ml, the production of the recombinant protein was induced by the addition of 100 mM  $\text{CuSO}_4$  to final concentration of 1 mM. 20% D-(+)-glucose (1/100 of the cell culture volume) and 200 mM L-glutamine (1/200 of the cell culture volume) were added on the third day after the induction. Cell density, viability and recombinant protein production was checked daily. Typically, the cells were harvested on the fifth day after the induction when the protein production reached a plateau. The cell culture was then centrifuged at 500 g for



3 min and the medium containing the recombinant protein was further centrifuged at 3360 g for 30 min at 4°C.

#### **4.2.12. Purification of Mutant Forms of Recombinant GCPII**

Purification of mutant forms of recombinant GCPII was carried out basically according to the protocol used in our laboratory for the purification of wild-type GCPII [99]. This protocol consists of initial dialysis and three chromatographic steps, i.e. QAE-Sephadex chromatography, Source 15S chromatography and affinity chromatography using lentil lectin. Minor changes, mainly in the composition of buffers used during purification, were made in the purification protocol for some of the mutant forms and these are summarized in Table III (page 37). Purification of mutant proteins N519D, R210A, R210K and Y700F was finished after lentil lectin chromatography, whereas gel permeation chromatography was performed as a next purification step for mutants E424A, K699S and N257D. Mutant protein E424A, which was intended for crystallization experiments, was further purified by chromatofocusing.

##### **4.2.12.1. Dialysis**

Culture medium containing recombinant GCPII was dialyzed against minimum ten-fold volume excess of Buffer A (Table III, page 37) for three days at 8°C with constant stirring. The dialyzing buffer was changed at least twice.

##### **4.2.12.2. QAE-Sephadex Batch Chromatography**

QAE-Sephadex A50 (Pharmacia, New York, USA) was swollen in Buffer A (typically, more than 200 ml of Buffer A were used per gram of the resin). 6 g of the resin were used per 1 litre of the culture medium. The resin was let to settle and the supernatant was decanted. This procedure was repeated at least four times and the swollen resin was then left at 8°C overnight.

The equilibrated resin was collected by filtration through a sintered-glass filter funnel mounted on a side-arm flask while applying suction. The resin was then added to the dialyzed medium in a beaker and the slurry was gently mixed every 10 min.

**Table III. Composition of buffers used for purification of individual mutant forms of recombinant GCPII.**

<b>Mutation</b>	<b>Buffer A</b>	<b>Buffer B</b>	<b>Buffer C</b>	<b>Buffer D</b>	<b>Buffer E</b>	<b>Buffer F</b>	<b>Buffer G</b>
<b>E424A</b>	20 mM Tris-HCl, pH 6.7	20 mM Tris-HCl, 1M NaCl, pH 6.7	100 mM Tris-HCl, 0.8 M NaCl, 2 mM CaCl <sub>2</sub> , 2 mM MnCl <sub>2</sub> , pH 7.4	20 mM Tris-HCl, 0.5 M NaCl, 1 mM CaCl <sub>2</sub> , 1 mM MnCl <sub>2</sub> , pH 7.4	20 mM Tris-HCl, 0.5 M NaCl, 0.3 M Met- $\alpha$ -D-Man, pH 7.4	20 mM MOPS, 300 mM NaCl, pH 7.4	-
	20 mM Tris-HCl, pH 6.7	20 mM Tris-HCl, 1M NaCl, pH 6.7	100 mM Tris-HCl, 0.8 M NaCl, 2 mM CaCl <sub>2</sub> , 2 mM MnCl <sub>2</sub> , pH 7.4	20 mM Tris-HCl, 0.5 M NaCl, 1 mM CaCl <sub>2</sub> , 1 mM MnCl <sub>2</sub> , pH 7.4	20 mM Tris-HCl, 0.5 M NaCl, 0.3 M Met- $\alpha$ -D-Man, pH 7.4	20 mM MOPS, pH 7.4	-
<b>N257D</b>	20 mM Tris-HCl, pH 6.7	20 mM Tris-HCl, 1M NaCl, pH 6.7	100 mM Tris-HCl, 0.8 M NaCl, 2 mM CaCl <sub>2</sub> , 2 mM MnCl <sub>2</sub> , pH 7.4	20 mM Tris-HCl, 0.5 M NaCl, 1 mM CaCl <sub>2</sub> , 1 mM MnCl <sub>2</sub> , pH 7.4	20 mM Tris-HCl, 0.5 M NaCl, 0.3 M Met- $\alpha$ -D-Man, pH 7.4	20 mM MOPS, 300 mM NaCl, pH 7.4	-
	20 mM Tris-HCl, pH 6.7	20 mM Tris-HCl, 1M NaCl, pH 6.7	100 mM Tris-HCl, 0.8 M NaCl, 2 mM CaCl <sub>2</sub> , 2 mM MnCl <sub>2</sub> , pH 7.4	20 mM Tris-HCl, 0.5 M NaCl, 1 mM CaCl <sub>2</sub> , 1 mM MnCl <sub>2</sub> , pH 7.4	20 mM Tris-HCl, 0.5 M NaCl, 0.3 M Met- $\alpha$ -D-Man, pH 7.4	20 mM MOPS, 20 mM MOPS, 20 mM NaCl, pH7.4	20 mM MOPS, 20 mM NaCl, pH7.4
<b>R210A</b>	20 mM MOPS, 20 mM NaCl, pH 7.0	20 mM MOPS, 1 mM NaCl, pH 7.0	100 mM MOPS, 0.8 M NaCl, 2 mM CaCl <sub>2</sub> , 2 mM MnCl <sub>2</sub> , pH 7.4	20 mM MOPS, 0.5 M NaCl, 1 mM CaCl <sub>2</sub> , 1 mM MnCl <sub>2</sub> , pH 7.4	20 mM MOPS, 0.5 M NaCl, 0.3 M Met- $\alpha$ -D-Man, pH 7.4	-	20 mM MOPS, pH7.4
	20 mM Tris-HCl, pH 6.7	20 mM Tris-HCl, 1M NaCl, pH 6.7	100 mM MOPS, 0.8 M NaCl, 2 mM CaCl <sub>2</sub> , 2 mM MnCl <sub>2</sub> , pH 7.4	20 mM MOPS, 0.5 M NaCl, 1 mM CaCl <sub>2</sub> , 1 mM MnCl <sub>2</sub> , pH 7.4	20 mM MOPS, 0.5 M NaCl, 0.3 M Met- $\alpha$ -D-Man, pH 7.4	-	20 mM MOPS, 20 mM NaCl, pH7.4
<b>R210K</b>	20 mM MOPS, 20 mM NaCl, pH 6.5	20 mM MOPS, 1 mM NaCl, pH 6.5	100 mM MOPS, 0.8 M NaCl, 2 mM CaCl <sub>2</sub> , 2 mM MnCl <sub>2</sub> , pH 7.4	20 mM MOPS, 0.5 M NaCl, 1 mM CaCl <sub>2</sub> , 1 mM MnCl <sub>2</sub> , pH 7.4	20 mM MOPS, 0.5 M NaCl, 0.3 M Met- $\alpha$ -D-Man, pH 7.4	-	20 mM MOPS, 20 mM NaCl, pH7.4
	20 mM Tris-HCl, pH 6.7	20 mM Tris-HCl, 1M NaCl, pH 6.7	100 mM MOPS, 0.8 M NaCl, 2 mM CaCl <sub>2</sub> , 2 mM MnCl <sub>2</sub> , pH 7.4	20 mM MOPS, 0.5 M NaCl, 1 mM CaCl <sub>2</sub> , 1 mM MnCl <sub>2</sub> , pH 7.4	20 mM MOPS, 0.5 M NaCl, 0.3 M Met- $\alpha$ -D-Man, pH 7.4	-	20 mM MOPS, 20 mM NaCl, pH7.4
<b>Y700F</b>	20 mM MOPS, 20 mM NaCl, pH 6.5	20 mM MOPS, 1 mM NaCl, pH 6.5	100 mM MOPS, 0.8 M NaCl, 2 mM CaCl <sub>2</sub> , 2 mM MnCl <sub>2</sub> , pH 7.4	20 mM MOPS, 0.5 M NaCl, 1 mM CaCl <sub>2</sub> , 1 mM MnCl <sub>2</sub> , pH 7.4	20 mM MOPS, 0.5 M NaCl, 0.3 M Met- $\alpha$ -D-Man, pH 7.4	-	20 mM MOPS, 20 mM NaCl, pH7.4
	20 mM Tris-HCl, pH 6.7	20 mM Tris-HCl, 1M NaCl, pH 6.7	100 mM MOPS, 0.8 M NaCl, 2 mM CaCl <sub>2</sub> , 2 mM MnCl <sub>2</sub> , pH 7.4	20 mM MOPS, 0.5 M NaCl, 1 mM CaCl <sub>2</sub> , 1 mM MnCl <sub>2</sub> , pH 7.4	20 mM MOPS, 0.5 M NaCl, 0.3 M Met- $\alpha$ -D-Man, pH 7.4	-	20 mM MOPS, 20 mM NaCl, pH7.4

After 40 min, the slurry was filtered through a sintered-glass filter funnel mounted on a side-arm flask and filtrate was collected. The resin was washed with 100 ml of Buffer A, filtered through a sintered-glass filter funnel and the filtrate was collected. The filtrates were then pooled and filtered through a 0.22  $\mu\text{m}$  filter (Millipore, Billerica, USA).

#### **4.2.12.3. Source 15S Column Chromatography**

The filtered solution was applied onto a Source 15S column (HR 10/10, Pharmacia) pre-equilibrated in Buffer A at room temperature. The column was washed with 50 ml of Buffer A and the bound proteins were eluted with a linear gradient of 0 - 50% Buffer B (flow rate: 2 ml/min, total volume of 50 ml). The absorbance was monitored at 220 and 280 nm and individual fractions were collected.

#### **4.2.12.4. Lentil Lectin Chromatography**

Fractions from Source 15S chromatography were analyzed using SDS-PAGE and the fractions containing the recombinant GCPII were pooled and mixed with equal volume of Buffer C. The sample was applied onto Lentil Lectin-Sepharose (Sigma, St. Louis, USA) column pre-equilibrated in Buffer D. The column was then washed with Buffer D (flow rate: 1 ml/min) until the absorbance at 280 nm reached the baseline. Bound recombinant GCPII was eluted with Buffer E (flow rate: 1 ml/min).

Lentil lectin chromatography was the last step of purification of mutant proteins N519D, R210A, R210K and Y700F. The fraction containing the mutant form of recombinant GCPII was then dialyzed against 100-fold volume excess of Buffer G for one day at 8°C with constant stirring, the dialyzing buffer was changed at least once. Finally, the sample was concentrated using Centriprep YM-50 (Millipore, Billerica, USA), aliquoted into Eppendorf tubes and stored at -80°C until further use.

#### **4.2.12.5. Gel Permeation Chromatography**

Gel permeation chromatography was performed as a next purification step for mutants E424A, K699S and N257D. The fraction from lentil lectin chromatography containing the mutant form of recombinant GCPII was concentrated to the volume of 3 ml

using Centriprep YM-50 (Millipore) and applied onto a Superdex HR200 column (16/60, Pharmacia, New York, USA) pre-equilibrated in Buffer F. Proteins were separated at a flow rate of 1 ml/min and absorbance was monitored at 220 and 280 nm. For mutants K699S and N257D, the fraction containing the recombinant GCPII was concentrated, aliquoted and stored at  $-80^{\circ}\text{C}$  until further use.

Mutant protein E424A was further purified by chromatofocusing. For the purpose of buffer exchange, the fraction containing mutant E424A was concentrated and applied onto a Superdex HR200 column pre-equilibrated in 20 mM Tris-HCl, pH 8.5. Absorbance was monitored at 220 and 280 nm and flow rate was set at 1 ml/min. The fraction containing mutant protein E424A was concentrated and subjected to chromatofocusing.

#### **4.2.12.6. Chromatofocusing**

Sample was applied onto Mono P column (HR 5/10, Pharmacia) pre-equilibrated in 20 mM Tris-HCl, pH 8.5 and the column was washed with 30 ml of the starting buffer. Proteins were eluted with Polybuffer 96 (Pharmacia) adjusted to pH 6.0 with 1 M HCl (flow rate: 1 ml/min). Fractions containing pure mutant protein E424A were pooled, dialyzed against 20 mM MOPS, 20 mM NaCl, pH 7.4 and concentrated to 6 mg/ml using Microcon YM-10 (Millipore, Billerica, USA).

#### **4.2.13. Determination of Protein Concentration**

The protein concentration in a sample was determined using Bio-Rad Protein Assay (Bio-Rad, Hercules, USA). The sample was diluted by distilled water to the final volume of 800  $\mu\text{l}$ , 200  $\mu\text{l}$  of dye reagent concentrate were added and the mixture was vortexed. Following five-minute incubation at room temperature, the absorbance was measured at 595 nm. Protein concentration was determined from a calibration curve constructed using bovine serum albumin as a standard.

#### **4.2.14. Sodium Dodecyl Sulfate-Polyacrylamide Gel Electrophoresis (SDS-PAGE)**

Solutions:

Separating gel (10% acrylamide): 2.5 ml 1.5 M Tris-HCl (pH 8.8), 2.3 ml 44% acrylamide mixture (42.8 g acrylamide, 1.2 g N,N'-bisacrylamide, water to the final volume of 100 ml), 100  $\mu$ l 10% (w/v) SDS, 100  $\mu$ l 10% (w/v) ammonium persulfate (APS), 10  $\mu$ l TEMED, water to the final volume of 10 ml

Stacking gel (5% acrylamide): 1.25 ml 1 M Tris-HCl (pH 6.8), 0.75 ml 44% acrylamide mixture, 50  $\mu$ l 10% SDS, 50  $\mu$ l 10% APS, 10  $\mu$ l TEMED, water to the final volume of 5 ml

Running buffer (5x): 15.1 g Tris, 94 g glycine, 5 g SDS, 900 ml water, pH 8.8 (not adjusted)

Sample buffer (6x): 3.5 ml 1 M Tris (pH 6.8), 3 ml glycerol, 1 g SDS, 600  $\mu$ l 2-mercaptoethanol, 1.2 mg bromphenol blue, water to the final volume of 10 ml

Proteins in the sample were resolved by denaturing discontinuous polyacrylamide gel electrophoresis (SDS-PAGE). Gels were prepared, let to polymerize and then placed into a vertical electrophoresis apparatus. The upper and lower reservoirs of the apparatus were filled with the running buffer. Prior to the loading onto gel, the sample was mixed with the sample buffer (6x) and boiled for 2-3 min. Electrophoresis was run at 150 V until the bromphenol blue dye reached the bottom of the running gel. Proteins in the gel were then either visualized by silver staining or subjected to Western blotting.

#### **4.2.15. Silver Staining**

Solutions:

Solution 1: 12% (v/v) acetic acid, 50% (v/v) methanol, 0.5 ml 37% formaldehyd, water to the final volume of 1 litre

Solution 2: 50% methanol

Solution 3:  $\text{Na}_2\text{S}_2\text{O}_3 \cdot 5\text{H}_2\text{O}$  (0.2 g/l)

Solution 4: 2 g  $\text{AgNO}_3$ , 0.5 ml 37% formaldehyd, water to the final volume of 1 litre

Solution 5: 60 g  $\text{Na}_2\text{CO}_3$ , 4 mg  $\text{Na}_2\text{S}_2\text{O}_3$ , 0.5 ml 37% formaldehyd, water to the final volume of 1 litre

Solution 6: 12% (v/v) acetic acid, 50% (v/v) methanol

Proteins resolved by SDS-PAGE were visualized by silver staining. After the electrophoresis, the gel was incubated for at least 30 min in Solution 1 and then washed in Solution 2 for 8 min three times. Subsequently, the gel was incubated in Solution 3 for 1 min, washed with water three times and incubated in Solution 4 for 20 min. The gel was then rinsed with water three times and the silver staining was developed by addition of Solution 5. When the protein bands were clearly visible, the gel was washed with water three times and the developing process was stopped by addition of Solution 6. The gel was then stored in Solution 2.

Stained gels were equilibrated in 25% (v/v) ethanol and 3% (v/v) glycerol for 20 min, placed between two cellophane sheets and dried at room temperature.

#### **4.2.16. Western Blotting**

Solutions:

Blotting concentrate: 72.1 g glycine, 15.1 g Tris, water to the final volume of 500 ml

Blotting buffer: 10 ml blotting concentrate, 10 ml methanol, 1 ml 10% (w/v) SDS, 80 ml water

Ponceau S (10x): 2 g Ponceau S, 30 g trichloroacetic acid, 30 g sulfosalicylic acid, water to the final volume of 100 ml

After electrophoretic separation of proteins, the gel and a nitrocellulose membrane (7.5 x 5 cm) were equilibrated in the blotting buffer for 5 min. Two sheets of filter paper, pre-wetted in the blotting buffer, were placed onto the anode of the transfer apparatus and the nitrocellulose membrane was placed on the top. The gel was then placed on top of the

membrane and covered with two pre-wetted sheets of filter paper. A test tube was rolled over the area of the stack to eliminate air bubbles. The transfer apparatus was then assembled and connected to power supply. Proteins were electroblotted at 50 mA per blot for 1 hour. The nitrocellulose membrane was then stained with Ponceau S solution for 2 min, rinsed with water and the position of molecular weight markers was marked. The membrane was then rinsed several times in PBS and nonspecific sites were blocked with Casein Blocker (Pierce, Rockford, USA) for at least 1 hour at room temperature with agitating. 1  $\mu$ l of anti-GCPII 04 murine monoclonal antibody (1 mg/ml) was added to 5 ml of Casein Blocker and the membrane was incubated with the solution of the primary antibody at room temperature overnight with agitating. Subsequently, the membrane was washed in PBS + 0.05% Tween 20 for 5 min with agitating. The washing buffer was replaced at least three times. 1:25,000 dilution of secondary antibody (goat anti-mouse antibody conjugated with horseradish peroxidase, Pierce) in Casein Blocker was prepared and the membrane was incubated with the solution of the secondary antibody at room temperature for 1 hour with agitating. To remove the unbound secondary antibody, the blot was washed in PBS + 0.05% Tween 20 for 5 min with agitating, the washing buffer was replaced at least three times. 0.4 ml of the Stable Peroxide Solution was mixed with 0.4 ml of the Luminol/Enhancer Solution (SuperSignal West Dura Chemiluminiscence Substrate, Pierce) and the blot was incubated with the mixture for 5 min. The membrane was then dried between two sheets of filter paper and placed in transparent plastic foil. The chemiluminiscent signal was detected using either film (Foma, Hradec Králové, Czech Republic) or CCD camera (LAS-1000, Fujifilm, Tokyo, Japan).

#### **4.2.16.1. Protein Quantification from Western Blot**

For protein quantification, the chemiluminiscent signal intensities were recorded by CCD camera (LAS-1000, Fujifilm) and the image was analyzed using ImageQuant software (GE Healthcare, Little Chalfont, UK). Concentration of GCPII in a sample was determined by comparing the signal intensity of the sample with calibration curve constructed using purified recombinant GCPII of known concentration as a standard.

#### **4.2.17. Hanging Drop Vapour Diffusion Crystallization**

Crystallization solution: 3g PEG 1550, 1 g PEG 400, 2 ml 1 M NaCl,  
10 ml 200 mM HEPES-Na (pH 7.4), 4 ml H<sub>2</sub>O

Stock solution of mutant protein E424A (6mg/ml) was mixed with either 10 mM N-Ac-Asp-Met or 20 mM N-Ac-Asp-Glu (1/10 of the volume of protein solution) and 1 µl of the mixture was pipetted onto a hanging-drop support. Equal volume of the crystallization solution was then added to the droplet and the hanging-drop support was screwed to the crystallization plate's well filled with 1 ml of the crystallization solution. Crystallization plates (Nextal Biotechnologies, Montreal, Canada) were stored at 19°C and the hanging drops were observed under a microscope.

#### **4.2.18. GCPII Enzymatic Activity Assays**

##### **4.2.18.1. Radiometric Measurement of NAAG-hydrolyzing Activity**

Solutions:

<sup>3</sup>H-NAAG substrate: 50 nM <sup>3</sup>H-NAAG, 950 nM NAAG

Reaction buffer: 50 mM Tris-HCl, 20 mM NaCl, pH 7.4

Resin: AG 1-X8 Resin, formate form (Bio-Rad, Hercules, USA)

Reaction buffer was mixed with the sample in the total volume of 180 µl and the mixture was incubated for 5 min at 37°C. The reaction was started by addition of 20 µl of <sup>3</sup>H-NAAG substrate and stopped by 200 µl of ice-cold 200 mM potassium phosphate, pH 7.4. The resin was mixed with water in 1:1 (w/w) ratio and columns were prepared by pipetting 2 ml of the resin mixture into a Pasteur pipette with a glass bead. After the resin had settled down, the columns were washed once with water. 200 µl of the reaction mixture were loaded onto a column and the sample was left to drain. The columns were then placed over 20 ml scintillation vials and bound glutamate was eluted with 2 ml of 1 M formic acid. 5 ml of the scintillation cocktail were added into a vial and the vial was shaken vigorously. Radioactivity of the samples was measured at the Department of Radioisotopes, IOCB.



#### 4.2.18.2. HPLC Assay of GCPII Enzymatic Activities

Solutions:

Reaction buffer: 20 mM MOPS, 20 mM NaCl, pH 7.4

Stopping buffer: 14 ml 100 mM sodium borate (pH 9.0), 7 ml 100 mM EDTA  
(pH 9.2), 33.6  $\mu$ l 10 mM L-arginine

AccQ Fluor reagent (Waters, Milford, USA): vial content dissolved in 4 ml of  
acetonitrile

Eluant A (5x concentrate): 700 mM sodium acetate, 85 mM triethanolamine,  
pH 5.05

Eluant B: 60% (v/v) acetonitrile, 40% eluant A

Reaction mixture was prepared in the total volume of 120  $\mu$ l and following incubation at 37°C, the reaction was stopped with 60  $\mu$ l of stopping buffer. Released amino acids were derivatized by addition of 20  $\mu$ l of AccQ Fluor reagent and the sample was briefly vortexed. 30  $\mu$ l of the sample were then injected onto a C-18(2) Luna HPLC column (4.6 x 250 mm, particle size 5  $\mu$ m, Phenomenex) and fluorescence was monitored at  $\lambda_{EX}/\lambda_{EM} = 250/395$  nm. Hydrolysis of several substrates of GCPII was analyzed using HPLC, therefore for different amino acid products, different gradients were run. The parameters of the gradients used for individual amino acids are shown in Tables IV - IX. The flow rate was set at 1 ml/min for all the gradients.

**Table IV. L-Glutamate and L-alanine.**

HPLC gradient used for resolving L-Glu and L-Ala derivatized with  
AccQ Fluor reagent.

Elution time of L-Glu: approximately 5.2 min

Elution time of L-Ala: approximately 8.1 min

Elution time of L-Arg (internal standard): approximately 7.0 min

Time (min)	% Eluant A	% Eluant B
0	80	20
9	65	35
100	0	100
17	0	100
18	80	20
21	80	20

**Table V. L-Methionine.**

HPLC gradient used for resolving L-Met derivatized with AccQ Fluor reagent.

Elution time of L-Met: approximately 4.7 min

Elution time of L-Arg (internal standard): approximately 3.7 min

Time (min)	% Eluant A	% Eluant B
0	60	40
10	38.6	61.4
11	0	100
16	0	100
17	60	40
20	60	40

**Table VI. L-Aminobutyric acid (L-Abu).**

HPLC gradient used for resolving L-Abu derivatized with AccQ Fluor reagent.

Elution time of L-Abu: approximately 4.4 min

Elution time of L-Arg (internal standard): approximately 3.8 min

Time (min)	% Eluant A	% Eluant B
0	65	35
10	55	45
11	0	100
17	0	100
18	65	35
21	65	35

**Table VII. L-Norvaline (L-norVal).**

HPLC gradient used for resolving L-norVal derivatized with AccQ Fluor reagent.

Elution time of L-norVal: approximately 12.4 min

Elution time of L-Arg (internal standard): approximately 8.8 min

Time (min)	% Eluant A	% Eluant B
0	90	10
14	40	60
15	0	100
20	0	100
21	90	10
23	90	10

**Table VIII. L-Norleucine (L-norLeu).**

HPLC gradient used for resolving L-norLeu derivatized with AccQ Fluor reagent.

Elution time of L-norLeu: approximately 11.9 min

Elution time of L-Arg (internal standard): approximately 6.3 min

Time (min)	% Eluant A	% Eluant B
0	80	20
13.5	35	65
14.5	0	100
19	0	100
20	80	20
23	80	20

**Table IX. 2-Aminoheptanoic acid (Ahp), 2-aminooctanoic acid (Aoc) and 2-aminononanoic acid (Ano).**

HPLC gradient used for resolving Ahp, Aoc and Ano derivatized with AccQ Fluor reagent.

Elution time of Ahp: approximately 10.3 min

Elution time of Aoc: approximately 11.8 min

Elution time of Ano: approximately 13.6 min

Elution time of L-Arg (internal standard): approximately 3.9 min

Time (min)	% Eluant A	% Eluant B
0	70	30
14	20	80
15	0	100
21	0	100
22	70	30
25	70	30

#### 4.2.18.2.1. Derivatization Reaction with FDAA

For distinguishing D- and L-amino acids, the reaction mixture was derivatized using 1-fluoro-2,4-dinitrophenyl-5-L-alanine amide (FDAA). 20 µl of the reaction mixture was mixed with 10 µl of 1 M KHCO<sub>3</sub> and 50 µl of FDAA solution in acetone (10 mg/ml) were added. Following 45-minute incubation at 45°C, the derivatization reaction was stopped by the addition of 10 µl of 2 M HCl and diluted 2 times with 50% acetonitrile. 50 µl of the mixture were then applied onto a C-18(2) Luna HPLC column (Phenomenex) and absorbance was monitored at 340 nm.

## 5. Results

The aim of the work reported here was to study the active site of GCPII on molecular level. The crystal structure of GCPII in complex with L-glutamate (i.e., the product of the cleavage of the naturally occurring substrate NAAG), solved by Cyril Bařinka and Jeroen Mesters in the laboratory of Rolf Hilgenfeld, revealed amino acid residues interacting with the bound glutamate, as well as showed residues located nearby the glutamate and presumably interacting with the N-acetyl-aspartyl portion of NAAG [66]. Hence, one of our objectives was to assess the influence of these residues on substrate binding and cleavage. To accomplish this task, we used site-directed mutagenesis approach to introduce amino acid changes into the sequence of recombinant human GCPII (rhGCPII). The mutants of rhGCPII were then expressed in insect cells, purified and kinetically characterized. The results of the mutagenesis studies of the GCPII active site are summarized in the first part of this chapter.

Substrate specificity studies, carried out in our laboratory, showed that, in addition to the substrates harbouring glutamate as the C-terminal amino acid residue, substrates with C-terminal methionine were also efficiently cleaved by rhGCPII [99]. As methionine has a hydrophobic side chain, hydrophobic interactions might also play a role in positioning the C-terminal residue of the substrate in the GCPII active site. We therefore decided to study these interactions in more detail using a series of potential dipeptidic substrates harbouring non-naturally occurring amino acids with aliphatic side chains in the C-terminal position of the substrate. The results of the characterization of novel dipeptidic substrates of GCPII constitute the second part of this chapter.

### 5.1. Active-site Mutants

As mentioned above, amino acid residues mutated in this study were chosen based on the crystal structure of GCPII in complex with glutamate [66]. The position of these residues in the GCPII active site is schematically depicted in Fig. 10 (page 48), while the mutations performed are listed in Table X (page 49). All the residues targeted for mutagenesis, except for Asn519, interact with the bound glutamate. While Tyr700 and Arg210 bind the  $\alpha$ -carboxylate group of the glutamate, the glutamate side chain is

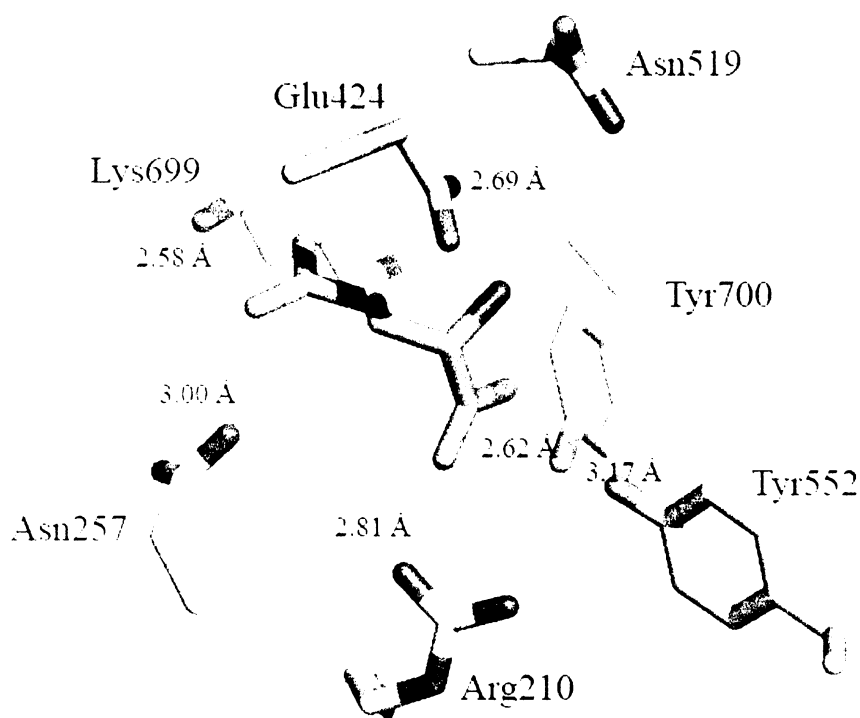


**Fig. 10 View of the GCPII active site with bound L-glutamate.**

L-glutamate, one of the products of the cleavage reaction (shown in green), is positioned in the GCPII active site via interactions of its  $\alpha$ -carboxylate group with Tyr700 (hydrogen-bonding distance 2.62 Å), Tyr552 (3.17 Å) and Arg210 (2.81 Å). The glutamate  $\gamma$ -carboxylate group accepts a hydrogen bond from Asn257 (3.00 Å) and forms a salt bridge with the  $\epsilon$ -amino group of Lys699 (2.58 Å). The free amino group of the bound glutamate interacts with the  $\gamma$ -carboxylate group of Glu424 (2.69 Å), the proposed catalytic amino acid residue.

The picture (from the crystal structure of the GCPII-glutamate complex [66], PDB code 2C6G) was generated using PyMOL [98].

positioned via interactions of its  $\gamma$ -carboxylate group with Lys699 and Asn257. Glu424, which was proposed to function as a proton shuttle during hydrolysis of a peptide bond, interacts with the water molecule bridging the two active site zinc ions, as well as with the free amino group of the bound glutamate. Asn519 is situated in the vicinity of the bound glutamate and is likely to interact with the N-acetyl-aspartyl portion of NAAG [66].

### 5.1.1. Site-directed Mutagenesis

Site-directed mutagenesis, as described in Method 4.2.1., was carried out to introduce the desired mutations into the sequence of recombinant human GCPII (rhGCPII). The pMTNAEXST plasmid (Fig. 11), prepared by Cyril Bařinka in our laboratory, was used as a template for the PCR reactions. This plasmid contains DNA sequence encoding

**Table X. List of the mutations performed.**

Wild-type amino acid residue	Mutated to	Mutation designation	Plasmid designation	Protein designation*
Arg210	Ala	R210A	pMTNAEXST_R210A	rhGCPII_R210A (R210A)
Arg210	Lys	R210K	pMTNAEXST_R210K	rhGCPII_R210K (R210K)
Asn257	Asp	N257D	pMTNAEXST_N257D	rhGCPII_N257D (N257D)
Glu424	Ala	E424A	pMTNAEXST_E424A	rhGCPII_E424A (E424A)
Asn519	Asp	N519D	pMTNAEXST_N519D	rhGCPII_N519D (N519D)
Lys699	Ser	K699S	pMTNAEXST_K699S	rhGCPII_K699S (K699S)
Tyr700	Phe	Y700F	pMTNAEXST_Y700F	rhGCPII_Y700F (Y700F)

\* Throughout the text, only the name of the respective mutation is used for designation of individual mutant proteins (i.e., R210K is used instead of rhGCPII\_R210K).

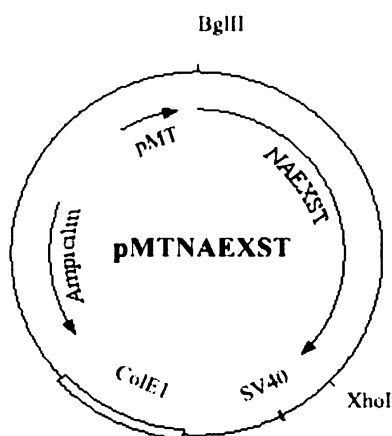


**Fig. 11 Map of pMTNAEXST plasmid.**

**pMT**, metallothionein promoter; **NAEXST**, extracellular domain of GCPII (amino acids 44-750); **SV40**, late polyadenylation signal; **ColE1**, origin of replication; **Ampicillin**, ampicillin resistance gene encoding  $\beta$ -lactamase.

the extracellular part of GCPII (amino acids 44-750), cloned in frame with the *Drosophila* BiP secretion signal and under the control of the *Drosophila* metallothionein promoter. The pMTNAEXST plasmid thus allows inducible expression of the extracellular portion of GCPII (herein, referred to as the wild-type rhGCPII) in *Drosophila* Schneider's S2 cells. Two complementary oligonucleotide primers harbouring the desired mutation were used to introduce the nucleotide changes

into the pMTNAEXST plasmid. Mutated plasmid DNA was synthesized using Pfu DNA polymerase in 16 PCR cycles. DpnI endonuclease was then added to digest methylated DNA. Since the mutated DNA was prepared *in vitro* and consequently was not methylated, only the template DNA, isolated from *E. coli* cells, was cleaved by DpnI.

Individual constructs were then transformed into the competent DH5 $\alpha$  *E. coli* cells and plasmid DNA was isolated as described in Method 4.2.3. To facilitate the identification of mutated plasmid DNA, new restriction sites for endonucleases BamHI and EcoRV were introduced into the constructs pMTNAEXST\_N519D and pMTNAEXST\_N257D, respectively. The isolated DNA for these constructs was therefore digested with respective endonucleases and the cleavage products were resolved by agarose gel electrophoresis (Fig. 12). The presence of the desired mutation in all the mutated plasmids was eventually verified by DNA sequencing.

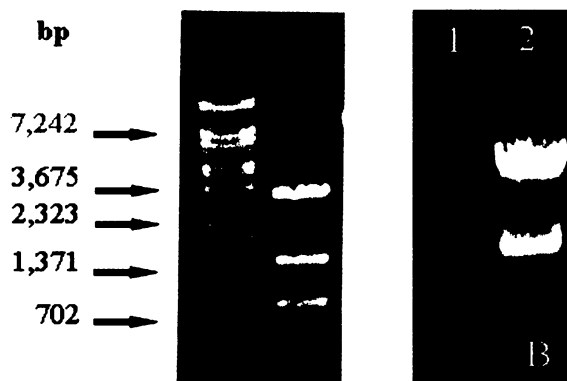


**Fig. 12 Identification of mutated plasmid DNA with new restriction site.**

To facilitate the identification of mutated plasmid DNA, new restriction sites for endonucleases BamHI and EcoRV were introduced into the constructs pMTNAEXST\_N519D (panel A) and pMTNAEXST\_N257D (panel B), respectively. Following digestion with respective endonucleases, reaction products were resolved on 1% agarose gel. Lane 1:  $\lambda$  DNA digested with BstEII. Panel A, lane 2: pMTNAEXST\_N519D digested with BamHI (expected size of products: 3335 bp, 1491 bp and 875 bp). Panel B, lane 2: pMTNAEXST\_N257D digested with EcoRV and XhoI (expected size of products: 4215 bp and 1486 bp).

For subsequent transfection of *Drosophila* Schneider's S2 cells, large-scale preparation of plasmid DNA (maxiprep) was performed and the isolated DNA was further purified using QIAGEN Plasmid Midi Kit (Qiagen, Germantown, USA). Whole DNA sequence encoding rhGCPII was then sequenced as described in Method 4.2.5. to confirm that the desired mutation was present and that no other mutation appeared in the course of DNA manipulations.

### 5.1.2. Expression of Mutant Forms of rhGCPII in *Drosophila* S2 Cells

Individual mutant constructs and pCoHygro selection vector were cotransfected into *Drosophila* Schneider's S2 cells using the calcium phosphate protocol as described in Method 4.2.9. The pCoHygro selection vector contains hygromycin resistance gene and therefore SF900II medium with 10% fetal bovine serum supplemented with hygromycin-B (300 µg/ml) was used for generation of stable cell lines. The selective medium was replaced every 4-5 days for 3-4 weeks, until cells resistant to hygromycin started growing out.

### 5.1.3. Expression and Activity Testing

To test for the production and activity of individual mutants, the hygromycin resistant cells were plated into 35 mm culture plate in SF900II medium with 10% fetal bovine serum. When cells reached the density of  $8 \times 10^6$  cells/ml, the production of recombinant protein was induced by the addition of copper sulphate to final concentration of 500 µM. Since recombinant GCPII was cloned in frame with the BiP secretion signal, the protein should be secreted into the culture medium. Cells were harvested on the third day after the induction and separated from the culture medium by centrifugation at 500 x g for 3 min. Expression of all the mutant proteins into the culture medium was confirmed by immunoblot analysis (Fig. 13). Culture medium was then dialyzed overnight against 20 mM Tris, pH 7.4 and NAAG-hydrolyzing activity was measured by radioenzymatic assay (see Method 4.2.18.1.) using  $^3\text{H}$ -NAAG radioactively labeled on glutamate. Glutamate, as a reaction product, was separated from noncleaved NAAG using ion exchange chromatography and radioactivity of the released  $^3\text{H}$ -Glu was measured at the Department of Radioisotopes, IOCB.



**Fig. 13 Immunoblot analysis of expression of mutant protein R210K.**

S2 cells were cotransfected with pMTNAEXST\_R210K and pCoHygro plasmids and following generation of a stable cell line, protein expression was induced with 500 µM CuSO<sub>4</sub>. Culture medium was harvested by centrifugation on the third day after the induction. Proteins were resolved on 10% SDS-PAGE gel, electroblotted onto a nitrocellulose membrane and immunostained as described in Method 4.2.16. The membrane was then exposed to film to visualize protein bands. Lane 1: 750 pg of purified wild-type rhGCPII; lane 2: mutant protein R210K (20 µl of culture medium).



All the mutants showed either very low or no activity in these preliminary experiments (data not shown), even though all of them were expressed as determined by immunoblot analysis. Therefore, we decided to produce larger quantities of the mutant proteins and concentrate the culture media to find out whether all of the mutants had low, yet detectable activity, or whether some of them were completely devoid of NAAG-hydrolyzing activity. Transfected cells resistant to hygromycin were thus grown in SF900II medium in two 100 mm culture plates, recombinant protein expression was induced with 500  $\mu$ M CuSO<sub>4</sub> and culture media were harvested on the third day post-induction. The media were then extensively dialyzed against 20 mM Tris, 20 mM NaCl, pH 7.4, concentrated 28-times using Centriprep YM-50 (Millipore, Billerica, USA), aliquoted and stored at  $-20^{\circ}$ C until further use. To compare the expression and activity of individual mutants with wild-type rhGCPII (wt rhGCPII), S2 cells transfected with pMTNAEXST and expressing wt rhGCPII were included in this experiment.

Both NAAG-hydrolyzing activities and expression levels of individual mutants were determined and compared with wild-type rhGCPII and the results are summarized in

**Table XI. Expression levels of individual mutant proteins in comparison to wild-type rhGCPII.**

Concentration of wild-type (WT) and individual mutants of rhGCPII in the culture medium was determined by Western blotting (see Method 4.2.16.). Chemiluminiscent signal intensities were recorded by CCD camera and concentration of wild-type/mutated rhGCPII in a sample was determined by comparing the signal intensity of the sample with calibration curve constructed using purified rhGCPII of known concentration as a standard.

<b>Mutation</b>	<b>Expression in culture medium [<math>\mu</math>g/ml]</b>
<b>WT</b>	6.0 $\pm$ 1.0
<b>E424A</b>	0.8 $\pm$ 0.1
<b>K699S</b>	1.7 $\pm$ 0.5
<b>N257D</b>	1.2 $\pm$ 0.1
<b>N519D</b>	1.2 $\pm$ 0.1
<b>R210A</b>	1.0 $\pm$ 0.2
<b>Y700F</b>	0.8 $\pm$ 0.1

Fig. 14 (page 53) and Table XI. All the mutants showed NAAG-hydrolyzing activity in this experimental setup, however, the specific activities were dramatically lower than that of wild-type rhGCPII, with the least active mutant, R210A, having the specific activity by five orders of magnitude lower than the wild-type protein. Expression levels of individual mutants and wild-type rhGCPII were determined by Western blotting and quantified using purified rhGCPII as a standard. As shown in Table XI, the expression of all the mutants was four to eight-fold lower than the expression of the wild-type. The epitope of the anti-GCPII 04 murine monoclonal antibody used in

this experiment was mapped in our laboratory and was found to be located between amino acid residues 100 – 104 [Šácha et al., submitted]. Since none of the mutant proteins has mutation in this region we assume that the antibody has the same affinity for the mutant proteins as for wild-type rhGCPII.

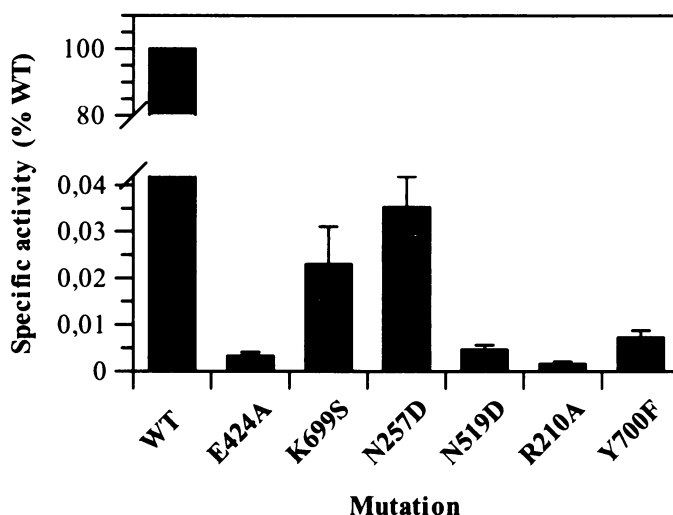


**Fig. 14 Specific activities of individual mutant proteins in comparison to wild-type rhGCPII.**

S2 cells expressing wild-type (WT) and individual mutants of rhGCPII were grown in SF900II medium and protein expression was induced with 500  $\mu\text{M}$   $\text{CuSO}_4$ . Culture media, harvested on the third day post-induction, were extensively dialyzed against 20 mM Tris, 20 mM NaCl, pH 7.4 and concentrated 28-times. Concentration of wild-type/mutated rhGCPII in the medium was determined by Western blotting (see Method 4.2.16.) and NAAG-hydrolyzing activities were measured by radioenzymatic assay (Method 4.2.18.1.), using following reaction setup: 30  $\mu\text{l}$  of concentrated medium were reacted with 100 nM NAAG in 50 mM Tris, 20 mM NaCl, pH 7.4 in total volume of 200  $\mu\text{l}$  and the reaction was allowed to proceed for 1 hour at 37°C. 200  $\mu\text{l}$  of 200 mM potassium phosphate were then added and reaction products were separated using ion exchange chromatography. Product formation was quantified by liquid scintillation and specific activities (in  $\text{s}^{-1}$ ) were calculated. Specific activities of individual mutants are expressed as percentage of specific activity of the wild-type protein.

Mutant protein R210K was due to technical problems during site-directed mutagenesis and transfection of S2 cells prepared later and therefore was omitted from these experiments.

#### 5.1.4. Large Scale Production and Purification

For the large scale production of mutant forms of rhGCPII, S2 cells transfected with individual constructs were transferred into a spinner flask with serum free SF900II

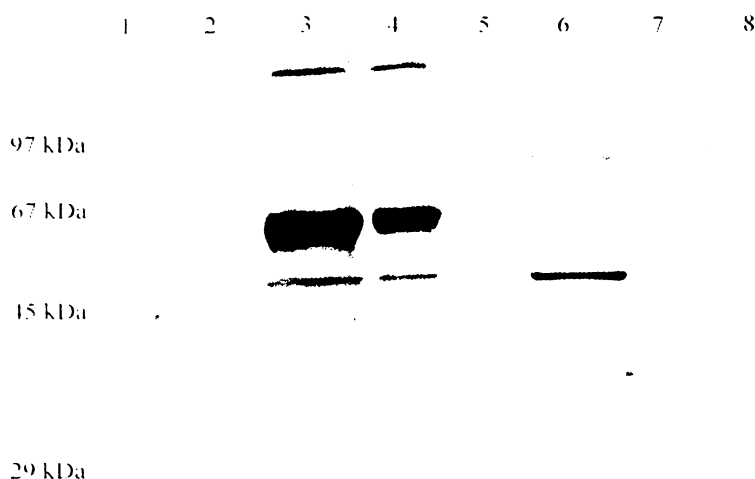


**Fig. 15 SDS-PAGE gel documenting the course of purification of mutant protein N519D.**

Lane 1: molecular weight marker; lane 2: purified wild-type rhGCPII (60 ng); lane 3: culture medium (15  $\mu$ l); lane 4: medium after dialysis (15  $\mu$ l); lane 5: pooled fractions from QAE Sephadex A50 batch chromatography (15  $\mu$ l); lane 6: pooled fractions containing mutant N519D from Source 15S chromatography (15  $\mu$ l); lane 7: a fraction containing mutant protein N519D from lentil lectin affinity chromatography (15  $\mu$ l); lane 8: purified, concentrated mutant protein N519D (2.5  $\mu$ l).

Proteins were resolved on 12% SDS-PAGE gel and visualized by silver staining.

medium and the recombinant protein production was induced with 1 mM CuSO<sub>4</sub> when the cell density reached  $8 \times 10^6$  cells/ml. Expression of mutant proteins was monitored by SDS electrophoresis and typically, the cells were harvested on the fifth day post-induction, when the production reached a plateau. The culture medium was then separated from cells by centrifugation and stored at  $-70^\circ\text{C}$  until purification.

Purification of individual mutants was performed basically according to the protocol used in our laboratory for the purification of wild-type rhGCPII. This protocol consists of initial dialysis of the culture medium, followed by ion exchange chromatography on QAE-Sephadex A50 (Pharmacia, New York, USA) in a batch procedure. In this step, most of the *Drosophila* proteins bound to the resin, whereas rhGCPII was detected in the flow-through fraction. To improve the recovery of individual mutants, salt concentration and pH of the buffer used in this step was varied slightly (for details on the composition of buffers used during purification of individual mutants, see Table III on page 37). The flow-through fraction was then loaded onto Source 15S column (HR 10/10, Pharmacia) and bound proteins were eluted with linear gradient of 0-0.5 M NaCl. Fractions containing rhGCPII were then pooled and applied onto Lentil

Lectin-Sepharose column. rhGCPII has ten potential N-glycosylation sites, all of which were shown to be occupied by oligosaccharide moieties [95], lectin affinity chromatography thus exploits the fact that rhGCPII is heavily glycosylated. Proteins bound to Lentil Lectin-Sepharose were eluted with 0.3 M methyl- $\alpha$ -D-mannopyranoside in 20 mM MOPS (or 20 mM Tris), 0.5 M NaCl, pH 7.4.

Purity of mutant proteins N519D, R210A, and Y700F after lentil lectin chromatography was more than 90% as estimated from SDS-PAGE gel and no further purification steps were performed. Purity of mutant R210K was only ~25%. However, since the purification yield was low (only ~ 70  $\mu$ g), no further purification of this mutant was attempted as additional chromatographic steps were likely not to yield enough protein for kinetic characterization. Gel permeation chromatography was carried out as the last purification step for mutant proteins N257D and K699S and the final purity was estimated to be more than 75% and 90%, respectively. The course of purification of mutant N519D is illustrated in Fig. 15 (page 54) and the purity of obtained mutant proteins is demonstrated by SDS-PAGE gel in Fig. 16.

Mutant protein E424A was intended for crystallization experiments and therefore was further purified by gel permeation chromatography and chromatofocusing. Even though the final purity was more than 95%, as estimated from SDS-PAGE gel (see Fig. 17, page 56), the final yield was only ~ 40  $\mu$ g of mutant rhGCPII and therefore the purification can hardly be called a success.

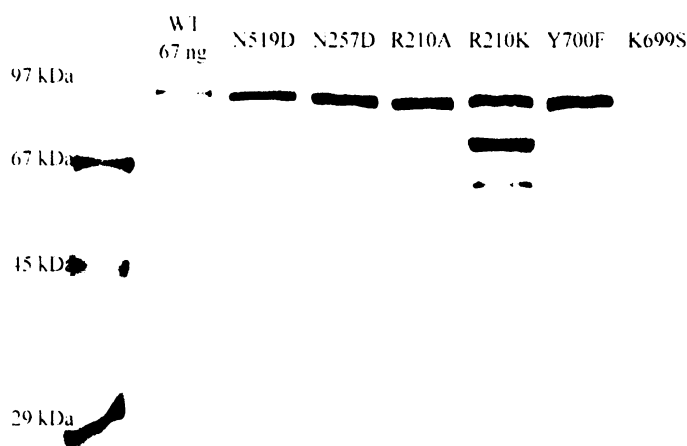


**Fig. 16 SDS-PAGE analysis of purified mutants of rhGCPII.**

Lane 1: molecular weight marker; lane 2: wild-type rhGCPII (67 ng), lanes 3 - 8: individual purified mutants of rhGCPII. Proteins were resolved on 12% SDS-PAGE gel and visualized by silver staining.

### 5.1.5. Crystallization Experiments with Mutant E424A

As mentioned above, glutamic acid residue in the position 424 was proposed to function as the general acid/base during catalytic hydrolysis of a peptide bond. We therefore decided to prepare inactive mutant of rhGCPII by mutating this catalytically important residue to alanine. Since only one of the reaction products, glutamate, is bound in the active site of GCPII cocrystallized with its substrate NAAG, crystal structure of

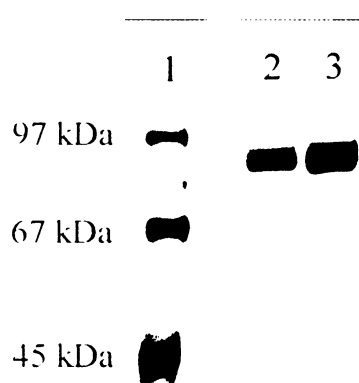


**Fig. 17 SDS-PAGE analysis of purified mutant protein E424A.**

Lane 1: molecular weight marker; lanes 2 and 3: the two purest fractions from chromatofocusing (17  $\mu$ l). Proteins were resolved on 12% SDS-PAGE gel and visualized by silver staining.

catalytically inactive mutant with NAAG might show the binding mode of noncleaved substrate in the GCPII active site. Applying this approach, we encountered two main obstacles. Firstly, the mutant protein E424A is not completely devoid of enzymatic activity (see Fig. 14, page 53) and secondly, the yield of the purification was very low, thus no large screens of crystallization conditions could be performed. We nevertheless tried to cocrystallize the mutant E424A with Ac-Asp-Glu (NAAG) and Ac-Asp-Met (i.e., two rhGCPII substrates) in the conditions used in our laboratory for crystallizing wild-type rhGCPII (see Method 4.2.17.). Up to now, we however obtained no diffracting crystals, just precipitate.

### 5.1.6. Kinetic Characterization of Mutant Proteins

Following purification, kinetic parameters of NAAG hydrolysis were determined for all the mutant proteins, except for E424A, the purification yield of which was very low. Since preliminary measurements indicated dramatic increase in Michaelis constant ( $K_M$ ) values for all the mutants, we decided to use HPLC assay as described in Method 4.2.18.2., instead of radioenzymatic assay (see Method 4.2.18.1.) used for determination of kinetic parameters for wild-type rhGCPII.

The HPLC assay is based on the derivatization of released L-glutamate, one of the reaction products, with AccQ Fluor reagent (Waters, Milford, USA) and subsequent reversed phase HPLC separation with fluorimetric detection of the derivative. AccQ Fluor reagent (6-aminoquinolyl-N-hydroxysuccinimidyl carbamate) is a highly reactive compound, which reacts with primary and secondary amino groups, yielding stable derivatives that fluoresce at 395 nm. In a slower reaction, excess reagent hydrolyzes to produce 6-aminoquinoline, which fluoresces weakly at 395 nm [112] (Fig. 18). Using this method, 0.1  $\mu\text{M}$  L-Glu could be detected and quantified in the reaction mixture, which corresponds to 1.8 pmol of respective derivative injected onto a column. The method can therefore be used for assaying kinetic parameters with  $K_M$  values in micromolar range,

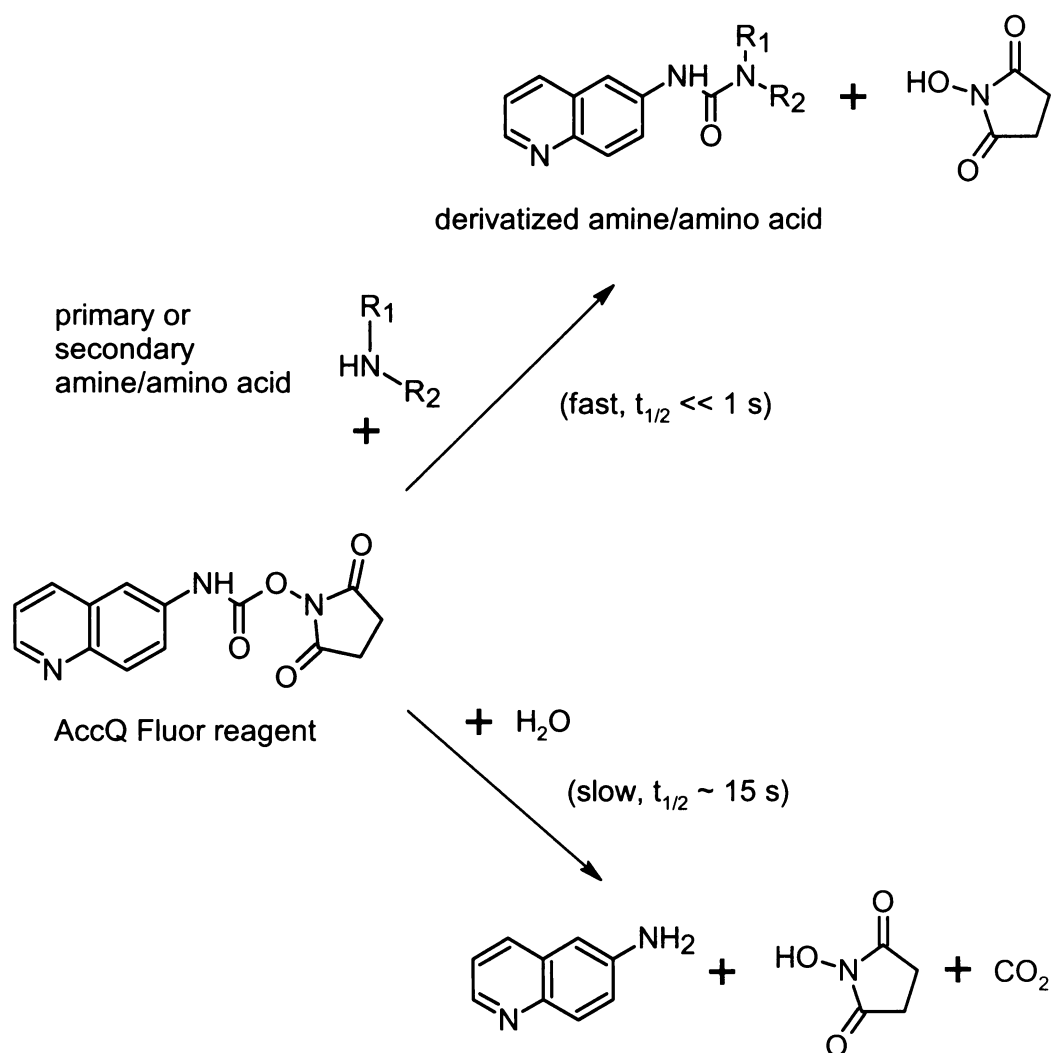


**Fig. 18 Derivatization reaction with AccQ Fluor reagent.**

AccQ Fluor reagent (6-aminoquinolyl-N-hydroxysuccinimidyl carbamate) reacts rapidly with primary and secondary amino groups, yielding stable ureas that fluoresce at 395 nm. In a slower reaction, excess reagent hydrolyzes to produce 6-aminoquinoline, N-hydroxysuccinimide and carbon dioxide. Adapted from [112].

however, the quantification limit is quite high for reliable determination of kinetic parameters of NAAG hydrolysis by wild-type rhGCPII ( $K_M \sim 1 \mu\text{M}$ ). Linearity of response for L-glutamate is demonstrated in Fig. 19.

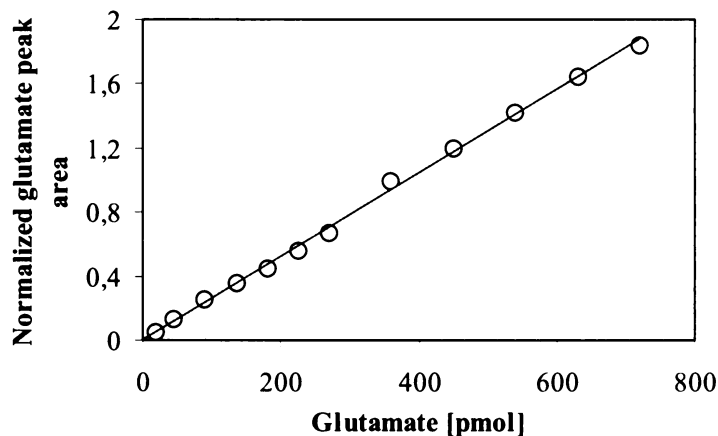


**Fig. 19 Linearity of response for L-glutamate derivatized with AccQ Fluor reagent.**

120  $\mu\text{l}$  of solution of L-glutamate (1 – 40  $\mu\text{M}$ ) were derivatized with AccQ Fluor reagent as described in Method 4.2.18.2. 30  $\mu\text{l}$  of the final solution were applied onto a C-18(2) Luna HPLC column (Phenomenex, Torrance, USA) and fluorescence was monitored at  $\lambda_{\text{EX}}/\lambda_{\text{EM}} = 250/395 \text{ nm}$ . Peak areas of glutamate derivative were normalized to the internal standard.

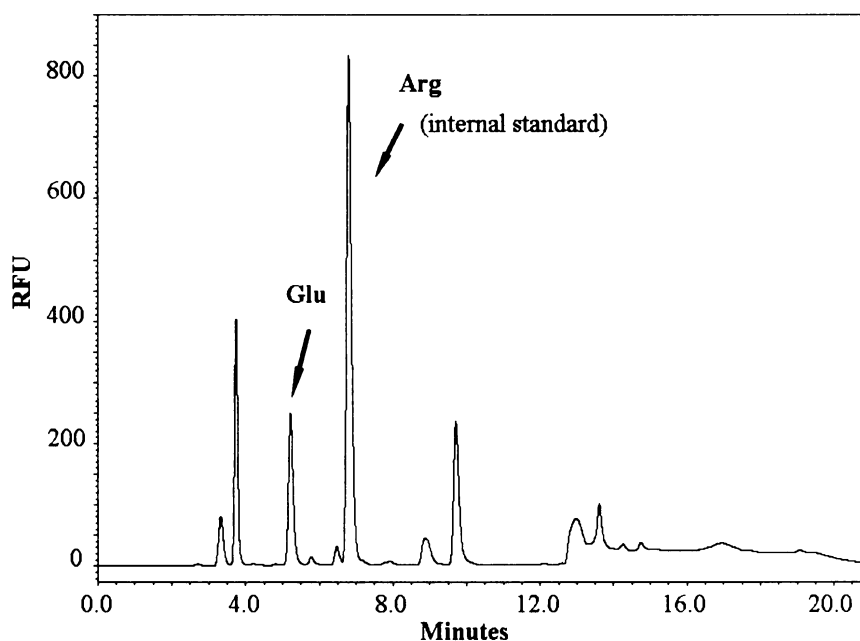


**Fig. 20 Chromatogram of L-glutamate derivatized with AccQ Fluor reagent.**

120  $\mu\text{l}$  of 5  $\mu\text{M}$  L-Glu solution were derivatized with AccQ Fluor reagent as described in Method 4.2.18.2. 30  $\mu\text{l}$  of the final solution were then applied onto a C-18(2) Luna HPLC column and fluorescence was monitored at  $\lambda_{\text{EX}}/\lambda_{\text{EM}} = 250/395 \text{ nm}$ . Derivatized L-glutamate and L-arginine (internal standard) eluted at approximately 5.2 and 7.0 min, respectively.

Measurements were carried out as described in Method 4.2.18.2. Typically, the substrate concentration was varied to cover the range of 0.3  $K_M$  to 6  $K_M$  and the reaction was allowed to proceed for 15 to 30 min at 37°C. Following derivatization with AccQ Fluor reagent, 30  $\mu$ l of the mixture were applied onto a C-18(2) Luna HPLC column (Phenomenex, Torrance, USA) and fluorescence was monitored at  $\lambda_{EX}/\lambda_{EM} = 250/395$  nm. Derivatized L-glutamate and L-arginine (internal standard, added into the stopping buffer) eluted with retention time of 5.2 and 7.0 min, respectively (Fig. 20, page 58).

**Table XII. Kinetic parameters of NAAG hydrolysis for wild-type (WT) and mutant forms of rhGCPII.**

Michaelis-Menten kinetic parameters of NAAG hydrolysis were determined using HPLC assay as described in Method 4.2.18.2. Released glutamate (*i.e.* one of the reaction products) was derivatized with AccQ Fluor reagent and quantified using reversed phase HPLC with fluorimetric detection. Concentration of mutant proteins, used for calculation of  $k_{cat}$  value, was determined by quantification from Western blot (see Method 4.2.16.1.)

<b>Mutation</b>	<b><math>K_M</math> [<math>\mu</math>M]</b>	<b><math>k_{cat}</math> [<math>s^{-1}</math>]</b>	<b><math>k_{cat} / K_M</math> [<math>l \cdot mmol^{-1} \cdot s^{-1}</math>]</b>
<b>WT</b>	1.15 $\pm$ 0.57*	1.1 $\pm$ 0.2*	957*
<b>K699S</b>	40.5 $\pm$ 22.7	0.27 $\pm$ 0.06	6.67
<b>N257D</b>	68.1 $\pm$ 19.7	0.32 $\pm$ 0.08	4.70
<b>N519D</b>	27.6 $\pm$ 0.3	0.078 $\pm$ 0.005	2.83
<b>R210A</b>	294 $\pm$ 15	0.023 $\pm$ 0.001	0.08
<b>R210K</b>	801 $\pm$ 123	0.13 $\pm$ 0.02	0.16
<b>Y700F</b>	45.7 $\pm$ 6.6	0.075 $\pm$ 0.003	1.64

\* Kinetic parameters for wild-type rhGCPII have been previously measured in our laboratory using radioenzymatic assay as described in Method 4.2.18.1. and are included herein for the purpose of comparison.

Kinetic parameters of cleavage of NAAG by the mutant proteins, assayed as described above, are summarized in Table XII and two examples of experimental data are shown in Fig. 21 (page 60). When compared to wild-type rhGCPII, all the mutant proteins showed dramatic increase in Michaelis constant ( $K_M$ ) value, ranging from  $\sim$  24-fold rise for mutant protein N519D to almost 700-fold increase for mutant R210K. Catalytic constants ( $k_{cat}$ ) were also affected by the amino acid substitutions introduced, however, the influence on  $k_{cat}$  value was less substantial than that on  $K_M$  value for all the mutants. While  $k_{cat}$  value for the most affected mutant, R210A, is  $\sim$  50-times lower than that of the



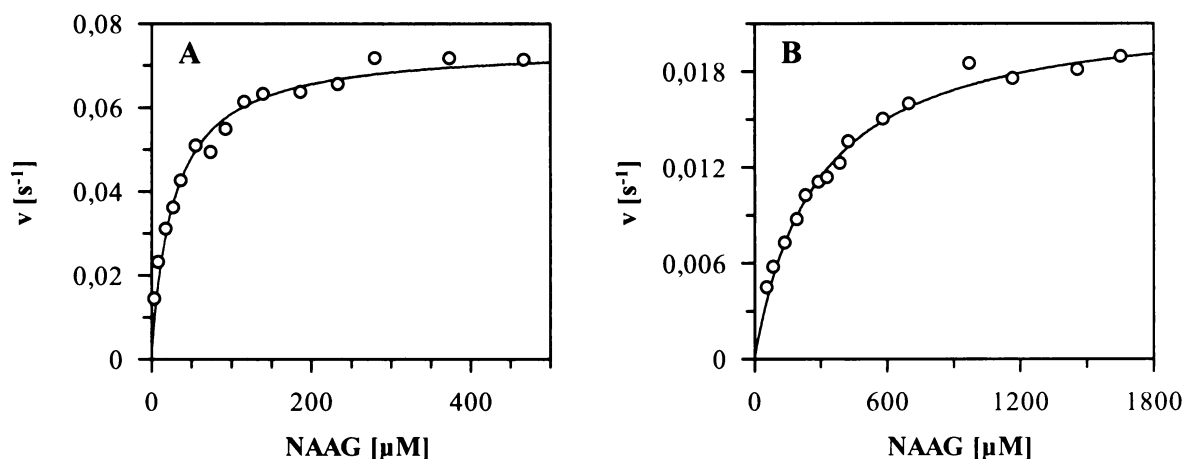


**Fig. 21 Michaelis-Menten plots for mutant proteins N519D (panel A) and R210A (panel B).**

The blue line drawn through the experimental data points represents non-linear least-squares fit to the Michaelis-Menten equation, generated using GraFit software (Erithacus Software Ltd., Horley, U.K.).

wild-type protein,  $K_M$  value for this mutant increased approximately 250-times. Catalytic constants for mutant proteins N257D and K699S were the least influenced by the respective mutation, differing approximately 4-times from wild-type rhGCPII. As a result of mainly large increase in  $K_M$  values, catalytic efficiencies of all the mutant proteins dropped by 2-4 orders of magnitude in comparison to the wild-type protein. Taken together, these data indicate that the mutations introduced into the rhGCPII sequence affected primarily the enzyme's ability to effectively bind the substrate.

### 5.1.7. Inhibition by 2-PMPA

Inhibition constants for 2-(phosphonomethyl)pentanedioic acid (2-PMPA), a potent competitive GCPII inhibitor [113], were, so far, determined for two of the mutant proteins, N519D and Y700F. Measurements were carried out with varying concentrations of the inhibitor while keeping the enzyme concentration fixed. Enzyme was preincubated with the inhibitor in 20 mM MOPS, 20 mM NaCl, pH 7.4 for 10 min at 37°C and then the reaction was started by the addition of NAAG (with final concentration of 60 and 100  $\mu\text{M}$  for mutants N519D and Y700F, respectively). Following 20 to 30-minute incubation at 37°C, the reaction mixture was derivatized with AccQ Fluor reagent and product formation was quantified by HPLC with fluorimetric detection as described in Method 4.2.18.2. The ratio of reaction rates of inhibited reaction to uninhibited reaction ( $v_i/v_0$ ) was plotted

against inhibitor concentration and apparent inhibition constant ( $K_{i(app)}$ ) was determined from non-linear fit to the Morrison equation for tight-binding inhibitors [114], using GraFit software (Erithacus Software Ltd., Horley, U.K.). Inhibition constant ( $K_i$ ) was then calculated using equation (1), which assumes competitive type of inhibition. However, the mode of inhibition was determined for neither of the mutant proteins since it was assumed that the inhibition type was not changed by the mutations introduced.

$$K_i = \frac{K_{i(app)}}{1 + \frac{[S]}{K_M}} \quad (1)$$

**Table XIII. Inhibition constant ( $K_i$ ) values for 2-PMPA.**

$K_i$  values for 2-PMPA were determined using HPLC assay as described in Method 4.2.18.2. Inhibitor concentration was varied, while enzyme and substrate concentrations were kept fixed. 60  $\mu$ M and 100  $\mu$ M NAAG was used as a substrate for mutants N519D and Y700F, respectively. For the wild-type protein (WT), 100  $\mu$ M Ac-Asp-Met was used as a substrate.

Mutation	$K_i$ [nM]
WT	$0.9 \pm 0.2$
N519D	$5.6 \pm 0.4$
Y700F	$49.5 \pm 2.5$

The results of inhibition constants determination are summarized in Table XIII and an example of experimental data is shown in Fig. 22. Inhibition constants for both the mutant proteins were affected by the amino acid substitution introduced, however, the influence of Y700F mutation (55-fold increase in  $K_i$  value in comparison to wild-type rhGCPII) was more substantial than that of N519D mutation (6-fold increase).

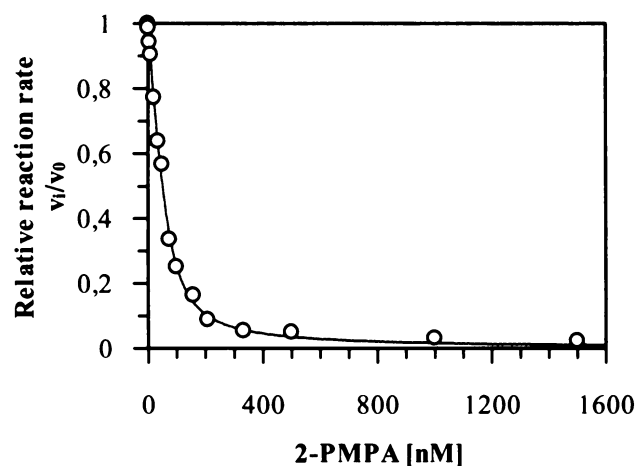


**Fig. 22 Plot of relative reaction rate as a function of 2-PMPA concentration for mutant protein N519D.**

The blue line drawn through the experimental data points represents non-linear least-squares fit to the Morrison equation, generated using GraFit software (Erithacus Software Ltd., Horley, U.K.).

## 5.2. Novel Dipeptidic Substrates

All the known naturally occurring substrates of GCPII harbour glutamate residue in the C-terminal position of the substrate. However, studies of substrate specificity of rhGCPII, carried out in our laboratory using dipeptidic libraries of general formulas Ac-X-Glu and Ac-Asp-X (where X stands for any naturally occurring amino acid), revealed that methionine was also tolerated in the C-terminal position (or P1' position) of the substrate [99]. Methionine, unlike glutamate, the side chain of which is negatively charged in physiological pH, has hydrophobic side chain. Hydrophobic interactions must therefore also play a role in positioning the side chain of the C-terminal amino acid residue in the GCPII active site.

The crystal structure of rhGCPII in complex with L-methionine, solved by Cyril Bařinka from our laboratory, shows that, quite surprisingly, L-methionine binds in a similar way as L-glutamate in the GCPII active site (Bařinka et al, manuscript in preparation). Even the side chains of Asn257 and Lys699, which bind the  $\gamma$ -carboxylate group of glutamate in the complex of rhGCPII with glutamate, retain very similar positions in the rhGCPII-methionine complex (Fig. 23). The  $\epsilon$ -amino group of Lys699 is thus

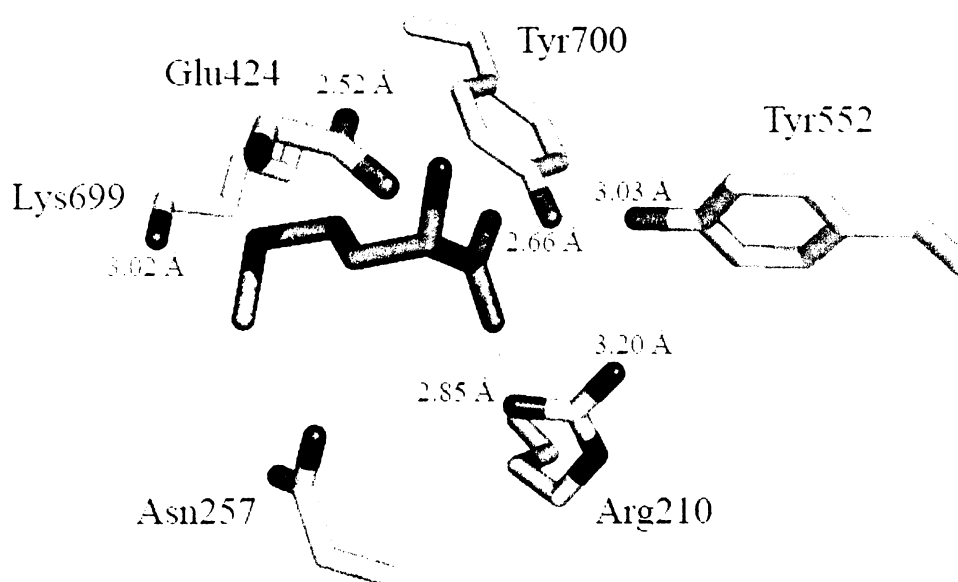


**Fig. 23 The GCPII active site with bound L-methionine.**

Binding mode of L-methionine in the GCPII active site is very similar to that of L-glutamate (compare to Fig. 10, page 48). The methionine  $\alpha$ -carboxylate group interacts with Tyr700 (2.66 Å), Tyr552 (3.03 Å) and Arg210 (2.85 and 3.20 Å), while the free amino group is hydrogen-bonded to Glu424. The side chain thioether group comes to close proximity of the  $\epsilon$ -amino group of Lys699 (3.02 Å). The figure was generated using PyMOL [98].

located near the thioether group of methionine. The small distance (3.02 Å) observed between these two groups suggests that the possible polar contact might contribute to the binding of methionine in the GCPII active site. To test this hypothesis, we substituted methionine in Ac-Asp-Met by norleucine (norLeu). The only difference between the side chains of methionine and norleucine is that the thioether group of methionine is replaced by a methylene group in the case of norleucine. Ac-Asp-norLeu showed to be efficiently cleaved by rhGCPII (see below) and further re-screening of Ac-Asp-X library using higher enzyme concentration revealed that Ac-Asp-Ala was also hydrolyzed by rhGCPII. As both these dipeptides harbour unbranched aliphatic side chain in the P1' position of the substrate, we decided to study the influence of the length of the aliphatic side chain on substrate binding/cleavage in more detail.

A novel series of Ac-Asp-X dipeptides, harbouring 2-aminoalkanoic acids with progressively longer unbranched side chains in the P1' position, was synthesized by L. Lepša (Fig. 24). The length of the C-terminal amino acid side chain ranged from one carbon atom in the case of alanine (Ala) to seven carbon atoms of 2-aminononanoic acid (Ano). The structure of the rhGCPII-methionine complex showed hydrophobic cavities adjacent to methionine binding site, into which longer aliphatic side chains than is that of methionine/norleucine might fit. Therefore, potential dipeptidic substrates with up to seven carbon atoms in the P1' side chain were included into this study.

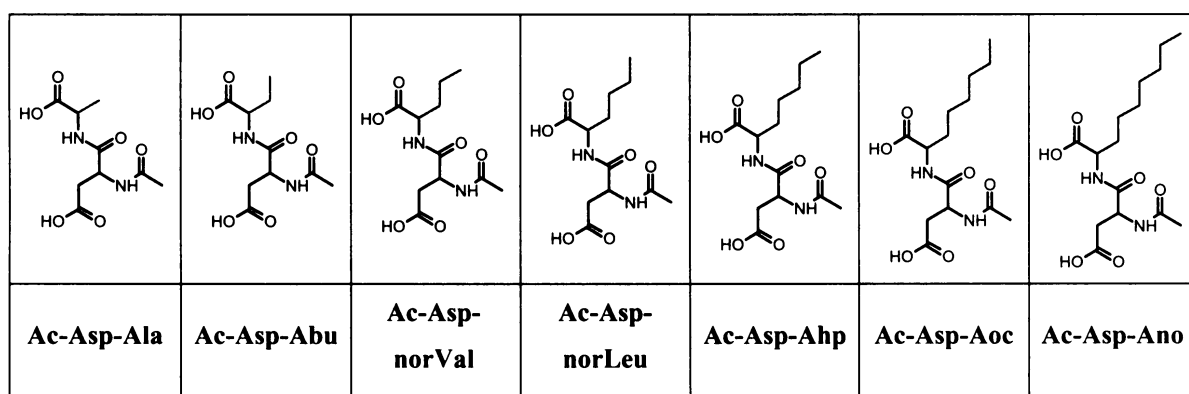


**Fig. 24 A series of novel dipeptidic substrates of rhGCPII harbouring 2-aminoalkanoic acids with progressively longer side chains in the P1' position of the substrate.**

Alkyl side chains in the P1' position of the substrate are shown in blue.

The potential dipeptidic substrates were dissolved in HPLC-grade water and the exact concentration of the stock solution was determined by amino acid analysis. Since all of these N-terminally protected dipeptides were found to be efficiently cleaved by rhGCPII

in preliminary experiments, we decided to measure the kinetic parameters of the cleavage for all the dipeptides in the series.

### 5.2.1. Kinetic Characterization of Novel Dipeptidic Substrates

Kinetic parameters of the cleavage of dipeptidic substrates harbouring 2-aminoalkanoic acids in the P1' position of the substrate were measured using HPLC assay as described in Method 4.2.18.2. Typically, 1-2  $\mu\text{g/ml}$  of wild-type rhGCPII were reacted with varying concentrations of respective dipeptidic substrates in 20 mM MOPS,

20 mM NaCl, pH 7.4. The reaction mixture was incubated for 15-30 min at 37°C. Released 2-aminoalkanoic acids were then derivatized with AccQ Fluor reagent and quantified using HPLC with fluorimetric detection.

2-aminohepatanoic acid (Ahp), 2-aminooctanoic acid (Aoc) and 2-aminononanoic acid (Ano) were purchased as racemic mixtures and the respective dipeptidic substrates synthesized from them are therefore likely to be equimolar mixtures of two diastereomeric forms. The method used for product quantification (i.e., derivatization with AccQ Fluor reagent and subsequent HPLC separation on C-18 column) cannot distinguish D- and L-amino acids and hence is

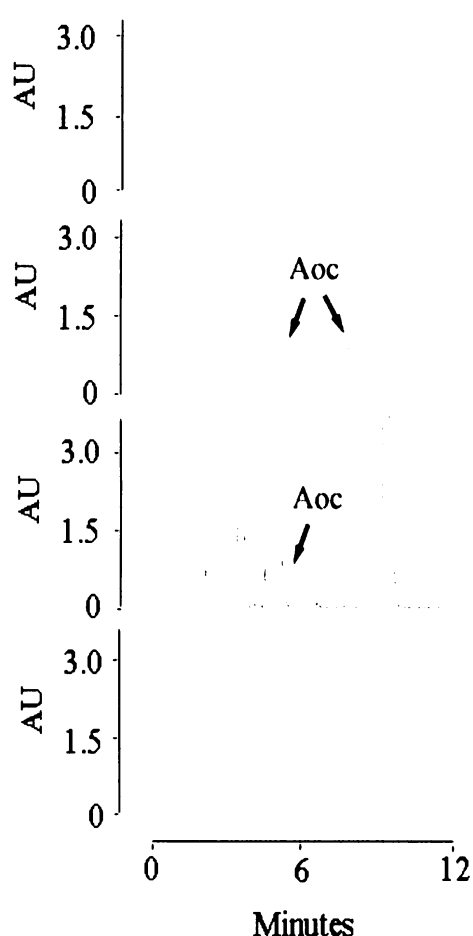


**Fig. 25 HPLC analysis of Ac-Asp-Aoc hydrolysis by rhGCPII using derivatization with FDAA reagent.**

Orange chromatogram, buffer (20 mM MOPS, 20 mM NaCl, pH 7.4) derivatized with FDAA reagent as described in Method 4.2.18.2.1.; green chromatogram, 2 mM D,L-Aoc derivatized with FDAA reagent; dark blue chromatogram, 1.9 mM Ac-Asp-Aoc reacted with 6.3  $\mu\text{g/ml}$  of rhGCPII for 24 hours at 37°C and subsequently derivatized with FDAA reagent; light blue chromatogram, 1.9 mM Ac-Asp-Aoc derivatized with FDAA reagent.

Following derivatization with FDAA reagent, 50  $\mu\text{l}$  of the final solution were applied onto a C-18(2) Luna HPLC column and absorbance was monitored at 340 nm.

not applicable for testing whether both the diastereomers are substrates of rhGCPII. Since previously reported data suggested that GCPII is inactive towards D-amino acids [1], we assumed that only the diastereomers containing L-aminoalkanoic acids served as substrates of rhGCPII. To test this hypothesis, we reacted respective dipeptides (1-3 mM) with 6.3 µg/ml of rhGCPII in 20 mM MOPS, 20 mM NaCl, pH 7.4 for 24 hours at 37°C to accomplish total cleavage of the substrate. The reaction mixture was then derivatized with FDAA, a chiral reagent used for distinguishing D- and L-amino acids, as described in Method 4.2.18.2.1. and analyzed using HPLC with UV detection at 340 nm. In all cases, only a peak of one (presumably an L-enantiomer) of the enantiomeric forms of the respective 2-aminoalkanoic acids was detected as a reaction product in the chromatogram (Fig. 25, page 64). Experimentally determined  $K_M$  values for Ac-Asp-Ahp, Ac-Asp-Aoc and Ac-Asp-Ano dipeptides were therefore halved to reflect the fact that only one of the two diastereomers serves as a substrate of rhGCPII.

The results of kinetic parameters determination are summarized in Table XIV and Fig. 26 (page 66). All the dipeptides in the series were efficiently hydrolyzed by rhGCPII with  $K_M$  values in low micromolar range and  $k_{cat}$  values of  $\sim 0.2 - 0.6 \text{ s}^{-1}$ . Progressive lengthening of the aliphatic side chain in the P1' position of the substrate resulted in moderate decrease in  $K_M$  values and slight rise in  $k_{cat}$  values. Overall catalytic efficiency thus increased with the lengthening of the side chain, which can be illustrated by the fact

**Table XIV. Kinetic parameters of wild-type rhGCPII dipeptidic substrates harbouring 2-aminoalkanoic acids with progressively longer side chains in the P1' position of the substrate.**

Michaelis-Menten kinetic parameters were determined using HPLC assay as described in Method 4.2.18.2. Reaction products (*i.e.* released C-terminal amino acids) were derivatized with AccQ Fluor reagent and quantified using reversed phase HPLC with fluorimetric detection.

Substrate	The side chain in the P1' position	$K_M$ [µM]	$k_{cat}$ [ $\text{s}^{-1}$ ]	$k_{cat} / K_M$ [ $\text{l}\cdot\text{mmol}^{-1}\cdot\text{s}^{-1}$ ]
<b>Ac-Asp-Ala</b>	methyl	$85 \pm 21$	$0.23 \pm 0.05$	2.7
<b>Ac-Asp-Abu</b>	ethyl	$29 \pm 8$	$0.25 \pm 0.03$	8.6
<b>Ac-Asp-norVal</b>	propyl	$31 \pm 12$	$0.42 \pm 0.05$	13.5
<b>Ac-Asp-norLeu</b>	butyl	$19 \pm 4$	$0.24 \pm 0.01$	12.6
<b>Ac-Asp-Ahp</b>	pentyl	$12 \pm 1$	$0.44 \pm 0.04$	36.7
<b>Ac-Asp-Aoc</b>	hexyl	$8 \pm 2$	$0.60 \pm 0.03$	75.0
<b>Ac-Asp-Ano</b>	heptyl	$10 \pm 2$	$0.62 \pm 0.10$	62.0

that Ac-Asp-Ala, the substrate with the shortest side chain, is about 20-fold worse substrate of rhGCPII than Ac-Asp-Ano, the dipeptide with the longest C-terminal side chain. When compared with Ac-Asp-Glu (or NAAG), the naturally occurring substrate of GCPII, the most efficient substrates in the series (i.e., Ac-Asp-Aoc and Ac-Asp-Ano) have comparable catalytic constants as Ac-Asp-Glu ( $k_{\text{cat}} = 1.1 \text{ s}^{-1}$ , see Table XII, page 59), while their  $K_{\text{M}}$  values are  $\sim 7$  to 9-fold higher than that of Ac-Asp-Glu ( $K_{\text{M}} = 1.15 \mu\text{M}$ ). This fact illustrates the preference of the GCPII active site for binding of substrates harbouring glutamate as the C-terminal residue.

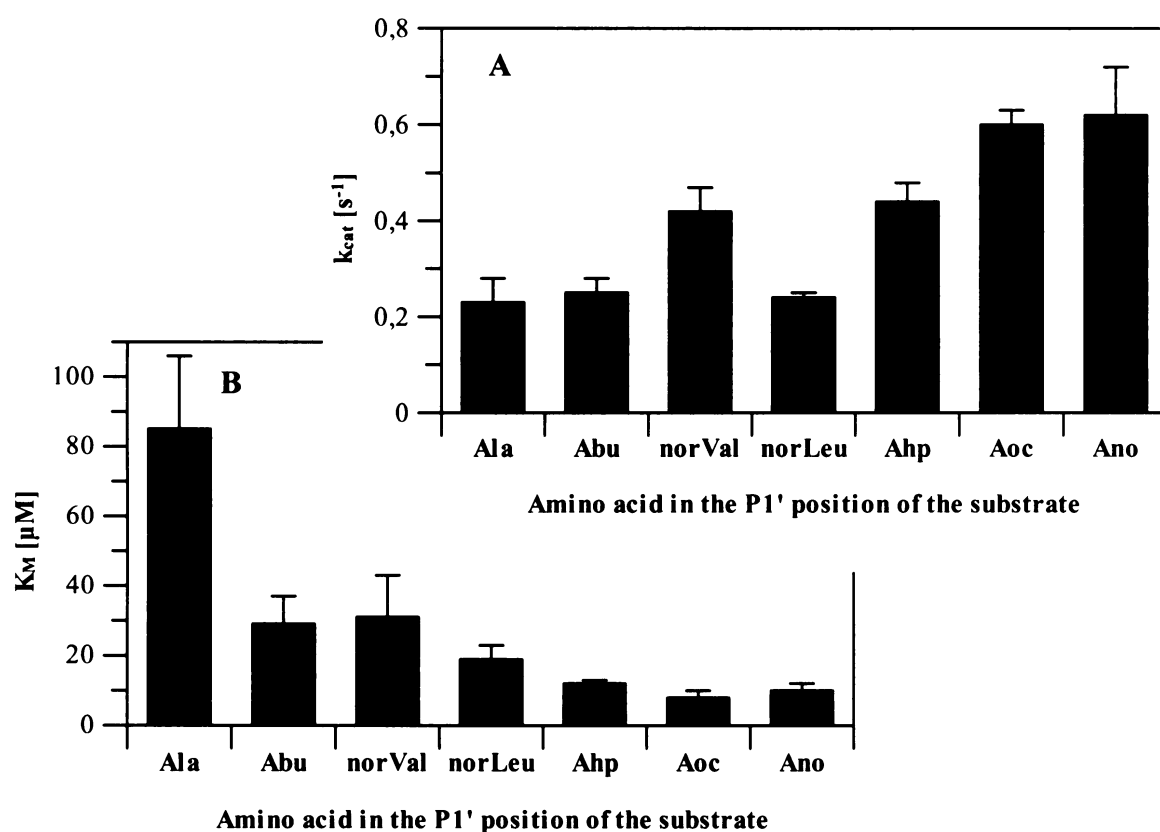


**Fig. 26** Influence of progressive lengthening of the P1' aliphatic side chain on  $k_{\text{cat}}$  (panel A) and  $K_{\text{M}}$  (panel B) values of dipeptidic substrates harbouring 2-aminoalkanoic acids in the P1' position of the substrate.

## 5.2.2. The Role of Lys699 in the GCPII Specificity for Glutamate-containing Substrates

As mentioned above, GCPII strongly prefers glutamate in the P1' position of the substrate. The crystal structure of GCPII with bound glutamate showed that the  $\gamma$ -carboxylate group of glutamate interacts with two residues, Lys699 and Asn257. Lys699 also interacts with thioether group of methionine in the GCPII-methionine complex. Mutation of this lysine residue to serine leads to  $\sim 35$ -fold increase in  $K_M$  value for Ac-Asp-Glu, while  $k_{cat}$  is less affected (see Table XV). To determine the influence of the K699S mutation on binding/cleavage of substrates harbouring methionine/2-aminoalkanoic acid in the P1' position, we also measured kinetic parameters of the cleavage of Ac-Asp-Met and Ac-Asp-Ano by mutant protein K699S, using HPLC assay as described above. The results, summarized in Table XV, show that, in comparison to the wild-type protein, Michaelis constants for Ac-Asp-Met and Ac-Asp-Ano hydrolysis are slightly (approximately 3-fold) improved for mutant K699S. Taken together, these data indicate that Lys699 is critical for the GCPII specificity for substrates with glutamate at the C-terminus. However, it does not play substantial role in binding substrates with methionine/2-aminoalkanoic acid in the P1' position.

**Table XV. Comparison of kinetic parameters of cleavage of Ac-Asp-Glu (NAAG), Ac-Asp-Met and Ac-Asp-Ano for wild-type (WT) rhGCPII and for mutant K699S.**

Michaelis-Menten kinetic parameters were determined using HPLC assay as described in Method 4.2.18.2. Reaction products (*i.e.* released C-terminal amino acids) were derivatized with AccQ Fluor reagent and quantified using reversed phase HPLC with fluorimetric detection.

Substrate	$K_M$ [ $\mu$ M]		$k_{cat}$ [ $s^{-1}$ ]		$k_{cat} / K_M$ [ $l \cdot mmol^{-1} \cdot s^{-1}$ ]	
	WT	K699S	WT	K699S	WT	K699S
Ac-Asp-Glu	$1.15 \pm 0.57^*$	$40.5 \pm 22.7$	$1.1 \pm 0.2^*$	$0.27 \pm 0.06$	957*	6.7
Ac-Asp-Met	$7.5 \pm 1.6$	$2.6 \pm 1.1$	$0.32 \pm 0.07$	$0.19 \pm 0.03$	42.7	73.1
Ac-Asp-Ano	$10.4 \pm 2.5$	$2.9 \pm 0.7$	$0.62 \pm 0.10$	$0.29 \pm 0.04$	59.6	100.0

\* Kinetic parameters of cleavage of Ac-Asp-Glu for wild-type rhGCPII have been previously measured in our laboratory using radioenzymatic assay as described in Method 4.2.18.1. and are included herein for the purpose of comparison.



## 6. Discussion

### 6.1. Active-site Mutants

In this study, we used site-directed mutagenesis to assess the influence of individual active site amino acid residues of rhGCPII on substrate binding and cleavage. The mutated residues were chosen based on the crystal structure of rhGCPII in complex with glutamate [66], the product of the cleavage of naturally occurring substrate NAAG, and most of them are located in the close proximity of the bound product (see Fig. 10, page 48).

All the mutants of rhGCPII were prepared by site-directed mutagenesis using QuikChange Site-Directed Mutagenesis Kit (Stratagene, La Jolla, USA) and expressed in *Drosophila* Schneider's S2 cells, the expression system used in our laboratory for wild-type rhGCPII [99]. All the mutant proteins were expressed, as demonstrated by immunoblot analysis. However, when quantified by Western blotting, the expression level of the mutants showed to be lower (approximately 4 to 8-fold) than that of wild-type rhGCPII (see Table XI, page 52). Since the epitope of the anti-GCPII antibody used for the quantification of the expression is in the N-terminal region of rhGCPII [Šácha et al., submitted] where none of the mutations was situated, we assume that the differences in the expression level of the mutants and the wild-type protein observed are not caused by lower affinity of the antibody for the mutant proteins. Lower expression of the mutants into the culture medium might be brought about by their lower stability caused by the introduced mutation. Furthermore, the transfection and expression protocol was not optimized for the mutant forms of rhGCPII.

Preliminary measurements of NAAG-hydrolyzing activity in the culture medium of S2 cells transfected with cDNA for individual mutants revealed that specific activities of all the mutant proteins were dramatically lower than that of the wild-type (see Fig. 14, page 53). We therefore decided to measure kinetic parameters of NAAG hydrolysis for purified mutants to determine whether observed drop in specific activities could be attributed to defect in substrate binding (as expressed in  $K_M$  value) or catalytic turnover (as expressed in  $k_{cat}$ ).

The mutant forms of rhGCPII were purified using very similar purification protocol as is used for purification of wild-type rhGCPII in our laboratory [99]. For some of the mutant proteins, the composition and pH of the buffer used in the first chromatographic

step, i.e. QAE-Sephadex batch chromatography, were optimized to increase the yield. However, no optimization of further purification steps was performed. Upscaling the expression to a spinner flask increased expression level of mutant proteins to approximately 3–4  $\mu\text{g/ml}$  (data not shown) and typical yield of the purification was  $\sim 1 \mu\text{g}$  of mutant rhGCPII from 1 ml of the culture medium.

One of the aims of this study was to prepare inactive mutant of rhGCPII and cocrystallize it with the naturally occurring substrate NAAG. We therefore mutated glutamate residue in the position 424, which was assigned an important role of the general acid/base in the proposed catalytic mechanism [66;107], to alanine, an amino acid residue that is unable to transfer protons. Surprisingly, the mutant protein E424A showed some residual NAAG-hydrolyzing activity, although the specific activity was more than 30,000-fold lower than that of wild-type rhGCPII (see Fig. 14, page 53). In a similar study, Speno et al. mutated the same amino acid residue to glutamine and observed slight increase in  $K_M$  value ( $\sim 2$ -fold) and approximately 7-fold decrease in  $V_{\text{max}}$  value in comparison to wild-type GCPII [107]. Due to low purification yield and very low activity of the mutant E424A, we were not able to measure its kinetic parameters. We therefore cannot determine whether the observed drop in specific activity is caused by increase in  $K_M$  value or decrease in  $k_{\text{cat}}$  value, or both. Crystallization experiments with the mutant E424A were not successful either, presumably due to the low number of crystallization conditions tested. The question of the exact role of Glu424 in the GCPII catalytic mechanism thus remains unanswered. For further studies of the mutant E424A, the purification protocol needs to be modified. Reduction of purification steps would be particularly desirable as the high number of chromatographic steps employed is probably the main reason of the low purification yield of the mutant E424A.

All the mutant proteins, except for E424A, were kinetically characterized using the HPLC assay as described in the Methods. Most of the activity measurements for wild-type rhGCPII are carried out in our laboratory using the radioenzymatic assay (for details, see Method 4.2.18.1.). This assay is also widely used by other groups studying GCPII [1]. We nevertheless decided to use the HPLC assay for the mutant proteins as the quantification limit of the method (approximately 0.1  $\mu\text{M}$  product in the reaction mixture) is sufficient for reliable determination of kinetic parameters with  $K_M$  value in micromolar range, which is the case of all the mutants. Furthermore, we avoided handling of radioactivity. In addition,

the assay can be easily adapted for other (potential) peptidic substrates of GCPII, and therefore the method is also suitable for substrate specificity studies (see below).

Kinetic characterization of NAAG-hydrolyzing activity revealed dramatic increase in  $K_M$  value in comparison to wild-type rhGCPII for all the mutant proteins (see Table XII, page 59). Mutations that affected the enzyme's affinity for the substrate most showed to be those of Arg210. We substituted this arginine residue to alanine and lysine, which resulted in approximately 250- and 700-fold increase in  $K_M$  value, respectively. Mutation to alanine, unlike the substitution to lysine, does not preserve the positive charge of arginine residue. Surprisingly, the mutant protein R210A has approximately 3-fold lower  $K_M$  value than the mutant R210K. Mutations R210A and R210K also affected  $k_{cat}$  value, however, the influence was less substantial (only ~ 50- and 8-fold decrease, respectively).

The guanidinium group of Arg210 forms a salt bridge with the  $\alpha$ -carboxylate group of bound glutamate in the rhGCPII-glutamate complex [66] (see Fig. 10, page 48). The same interaction was also observed with methionine in the rhGCPII-methionine complex [Bařinka et al., manuscript in preparation]. In addition, the  $\alpha$ -carboxylate group of the bound product is also hydrogen-bonded to the hydroxyl group of Tyr700, which was mutated to phenylalanine in this study. Removal of this interaction resulted in 40-fold rise in  $K_M$  value and ~ 15-fold decrease in  $k_{cat}$ . The data presented here thus supports the crucial role of the C-terminal  $\alpha$ -carboxylate group of the GCPII substrates for substrate binding and subsequent cleavage. Interaction of this group with Arg210 is clearly critical for substrate binding, while hydrogen-bonding with Tyr700 also substantially contributes to the enzyme's affinity for the substrate.

The side chain  $\gamma$ -carboxylate group of the bound glutamate is positioned in the GCPII active site via interactions with Lys699 and Asn257, which were mutated to serine and aspartate, respectively. Both these amino acid substitutions lead to comparable kinetic parameters:  $K_M$  value for both the mutants is more than one order of magnitude higher than that of the wild-type protein, while  $k_{cat}$  is approximately 4-times lower. The data indicate that these two residues are important for efficient substrate binding. Moreover, via specific interactions with the glutamate side chain, they most probably account for the GCPII strong preference for substrates with glutamate at the C-terminus. We experimentally confirmed this role of Lys699, mutation of which resulted in slightly improved kinetic parameters for hydrolysis of dipeptides with hydrophobic C-terminal side chains (see Table XV, page 67). This is presumably caused by release of steric crowding imposed by

the long side chain of Lys699 and maybe due to removal of the positive charge of the lysine residue.

Asn519 is located in the vicinity of the bound glutamate in the rhGCPII-glutamate complex and consequently, it was proposed to interact with the N-acetyl-aspartyl portion of NAAG [66]. To test this hypothesis, we mutated Asn519 to aspartate. The kinetic parameters of NAAG-hydrolysis determined for the mutant N519D (~ 24-fold increase in  $K_M$  value and ~ 14-fold decrease in  $k_{cat}$  value in comparison to wild-type rhGCPII) indeed suggest important role of this residue in NAAG binding and hydrolysis. The same mutation was also performed in Speno's study [107], however, very little activity was measured for the mutant N519D and therefore the kinetic parameters were not determined. Considering the low substrate concentration used in this study for activity testing (30 nM, i.e. 1000-times lower than the  $K_M$  value determined in our study), these results are consistent with our findings that the mutation N519D leads to ~ 340-fold drop in catalytic efficiency in comparison to the wild-type protein.

Taken together, the data presented here confirm the assignment of the above-mentioned active site residues as highly important for substrate binding.

## 6.2. Novel Dipeptidic Substrates

GCPII, as its name suggests, is a carboxypeptidase with a strong preference for glutamate residue in the C-terminal position of the substrate. However, dipeptides harbouring methionine as the C-terminal residue were recently also identified as efficient substrates of GCPII [99]. Consequently, the crystal structure of rhGCPII in complex with L-methionine was solved in our laboratory [Bařinka et al., manuscript in preparation]. The binding mode of L-methionine in the GCPII active site suggested: 1) possible polar contact between the thioether group of the methionine and the  $\epsilon$ -amino group of Lys699 and 2) existence of hydrophobic cavities adjacent to the methionine binding site that might accommodate amino acids with longer alkyl side chains.

To test the hypothesis that the possible polar contact between the sulphur of methionine and the side chain of Lys699 might be important for binding of substrates with C-terminal methionine in the GCPII active site, we substituted methionine in the dipeptidic substrate Ac-Asp-Met by norleucine (norLeu). The side chain of norleucine contains a methylene group in place of the thioether group of methionine and consequently cannot

participate in polar interactions. Comparison of kinetic parameters of hydrolysis of Ac-Asp-Met and Ac-Asp-norLeu by rhGCPII revealed that  $K_M$  value for Ac-Asp-norLeu is slightly ( $\sim 2.5$ -times) higher than that for Ac-Asp-Met (compare Table XIV and Table XV, page 65 and 67, respectively). However, the differences observed between the two dipeptidic substrates are not pronounced and the kinetic parameters are well comparable. We therefore conclude that the interaction between Lys699 and the thioether group of methionine does not play substantial role in binding of methionine in the GCPII active site. This finding is also supported by our mutational studies of the rhGCPII active site as the mutant K699S has approximately 3-fold lower  $K_M$  value for Ac-Asp-Met hydrolysis than wild-type rhGCPII (Table XV, page 67).

The structure of the rhGCPII-methionine complex showed hydrophobic cavities adjacent to the methionine binding site, into which longer aliphatic side chains than is that of methionine/norleucine might fit. To study the hydrophobic interactions in the GCPII active site, a series of potential dipeptidic substrates, harbouring 2-aminoalkanoic acids with progressively longer aliphatic side chains in the C-terminal position, was synthesized and tested for hydrolysis by rhGCPII using the HPLC assay as described in the Methods. Surprisingly, all the dipeptides in the series showed to be efficiently cleaved by rhGCPII and the progressive lengthening of the C-terminal aliphatic side chain resulted in moderate increase in overall catalytic efficiency (see Table XIV, page 65). The interaction of the C-terminal side chain with the GCPII active site seems to be necessary for substrate binding and hydrolysis as dipeptide Ac-Asp-Gly, which has no side chain in the C-terminal position, is not cleaved by rhGCPII [99]. Dipeptides harbouring naturally occurring amino acids with aliphatic but branched side chain at the C-terminus (i.e., valine, leucine and isoleucine) or bulky side chain (phenylalanine, tyrosine) are not efficiently hydrolyzed by rhGCPII, either [99], suggesting the GCPII binding cleft is too narrow to accommodate bulkier C-terminal side chains.

GCPII is viewed as a promising target for treatment of various neurological disorders [21] and consequently a number of potent GCPII inhibitors have been reported [101-103]. However, most of these compounds are analogs of glutamate or glutarate and therefore are highly polar, which causes their poor pharmacokinetic properties. Studies of hydrophobic interactions in the GCPII active site thus might be useful for design of specific GCPII inhibitors with improved pharmacokinetic properties.

## 7. Conclusions

- Seven active site mutants of recombinant human GCPII (rhGCPII) were prepared, expressed in *Drosophila* S2 cells and purified.
- Dipeptidase activities of six of the mutant proteins were characterized.
- In comparison to wild-type rhGCPII, all the mutants showed dramatic increase in Michaelis constant ( $K_M$ ) value, while catalytic constants ( $k_{cat}$ ) were less affected by the mutations introduced.
- Residue R210 was identified as crucial for substrate binding via its interaction with the C-terminal  $\alpha$ -carboxylate group of substrates.
- Residue Lys699 was shown to be largely responsible for the GCPII preference for substrates harbouring glutamate as the C-terminal residue.
- All the residues selected for mutation were confirmed to play an important role in substrate binding and hydrolysis.
- An inactive mutant of rhGCPII was not prepared since the mutation of the proposed catalytic residue, Glu424, did not completely abolish enzymatic activity.
  
- Dipeptides of general formula Ac-Asp-X (where X stands for a 2-aminoalkanoic acid) were identified as novel substrates of rhGCPII with  $K_M$  values in low micromolar range and  $k_{cat}$  values of  $\sim 0.2 - 0.6 \text{ s}^{-1}$ .

## 8. List of Abbreviations

Abu	2-(S)-aminobutanoic acid
AccQ	6-aminoquinolyl-N-hydroxysuccinimidyl carbamate
Ahp	2-(R,S)-aminoheptanoic acid
ALS	amyotrophic lateral sclerosis
AMPA	$\alpha$ -amino-3-hydroxy-5-methyl-4-isoxasolepropionate
Ano	2-(R,S)-aminononanoic acid
Aoc	2-(R,S)-aminooctanoic acid
APS	ammonium persulfate
bp	base pair
cDNA	complementary DNA
Da	dalton
DMSO	dimethylsulfoxide
DNA	deoxyribonucleic acid
dNTP	deoxyribonucleoside triphosphate
EDTA	ethylenediaminetetraacetic acid
EGTA	ethyleneglycol-bis-(aminoethylether)-tetraacetic acid
FBS	fetal bovine serum
FDA	1-fluoro-2,4-dinitrophenyl-5-L-alanine amide
FPLC	fast protein liquid chromatography
GABA	$\gamma$ -aminobutyric acid
GCPII	glutamate carboxypeptidase II
GCPIII	glutamate carboxypeptidase III
GluR	glutamate receptor
GPI-18431	(S)-2-(4-iodobenzylphosphonomethyl)pentanedioic acid
GPI5232	2-[(pentafluorophenylmethyl)hydroxyphosphinyl]methyl)pentanedioic acid
HEPES	N-2-hydroxyethylpiperazine-N'-2-ethanesulfonic acid
HPLC	high performance liquid chromatography
HRP	horseradish peroxidase
iGluR	ionotropic glutamate receptor
IOCB	Institute of Organic Chemistry and Biochemistry
KA	kainate
$k_{cat}$	catalytic constant
kDa	1,000 daltons
$K_I$	inhibition constant
$K_{I(app)}$	apparent inhibition constant

K <sub>M</sub>	Michaelis constant
LB	Luria-Bertani medium
LNCaP	lymph node prostate cancer cell line
Met- $\alpha$ -D-Man	methyl- $\alpha$ -D-mannopyranoside
mGluR	metabotropic glutamate receptor
MOPS	3-[N-morpholino]propanesulfonic acid
2-MPPA	2-(3-mercaptopropyl)pentanedioic acid
mRNA	messenger RNA
NAA	N-acetylaspartate
NAAG	N-acetyl-L-aspartyl-L-glutamate
$\beta$ -NAAG	N-acetyl- $\beta$ -L-aspartyl-L-glutamate
NAALADase	N-acetylated- $\alpha$ -linked acidic dipeptidase
NMDA	N-methyl-D-aspartate
norLeu	2-(S)-aminohexanoic acid
norVal	2-(S)-aminopentanoic acid
PAGE	polyacrylamide gel electrophoresis
PBS	phosphate buffered saline
PCR	polymerase chain reaction
PDB	Protein Data Bank
PEG	polyethylen glycol
2-PMPA	2-(phosphonomethyl)pentanedioic acid
PSMA	prostate-specific membrane antigen
rhGCPII	recombinant human glutamate carboxypeptidase II
RNA	ribonucleic acid
SDS	sodium dodecylsulfate
TAE	Tris-Acetate-EDTA
TEMED	N,N,N',N'-tetramethylethylenediamine
TGF- $\beta$	transforming growth factor $\beta$
Tris	tris(hydroxymethyl)aminomethane
WT	wild-type



## 9. References

- [1] Robinson,M.B., Blakely,R.D., Couto,R., & Coyle,J.T.: Hydrolysis of the brain dipeptide N-acetyl-L-aspartyl-L-glutamate. Identification and characterization of a novel N-acetylated alpha-linked acidic dipeptidase activity from rat brain. *J. Biol. Chem.* **262**, 14498-14506 (1987)
- [2] Horoszewicz,J.S., Kawinski,E., & Murphy,G.P.: Monoclonal antibodies to a new antigenic marker in epithelial prostatic cells and serum of prostatic cancer patients. *Anticancer Res.* **7**, 927-935 (1987)
- [3] Barrett,A.J.: Nomenclature Committee of the International Union of Biochemistry and Molecular Biology (NC-IUBMB). Enzyme Nomenclature. Recommendations 1992. Supplement 4: corrections and additions (1997). *Eur. J. Biochem.* **250**, 1-6 (1997)
- [4] Pinto,J.T., Suffoletto,B.P., Berzin,T.M., Qiao,C.H., Lin,S., Tong,W.P., May,F., Mukherjee,B., & Heston,W.D.: Prostate-specific membrane antigen: a novel folate hydrolase in human prostatic carcinoma cells. *Clin. Cancer Res.* **2**, 1445-1451 (1996)
- [5] Purves,D., Augustine,G.J., Fitzpatrick,D., Katz,L.C., LaMantia,A., McNamara,J.O., & Williams,S.M.: Neuroscience, edn 2<sup>nd</sup>. Sinauer Associates, Sunderland (2001)
- [6] Siegel,G.J., Agranoff,B.W., Albers,R.W., Fisher,S.K., & Uhler,M.D.: Basic Neurochemistry: Molecular, Cellular and Medical Aspects, edn 6<sup>th</sup>. Lippincott-Raven, Philadelphia (1999)
- [7] Carpenter,K.J. & Dickenson,A.H.: Amino acids are still as exciting as ever. *Curr. Opin. Pharmacol.* **1**, 57-61 (2001)
- [8] Kew,J.N. & Kemp,J.A.: Ionotropic and metabotropic glutamate receptor structure and pharmacology. *Psychopharmacology (Berl)* **179**, 4-29 (2005)
- [9] Ozawa,S., Kamiya,H., & Tsuzuki,K.: Glutamate receptors in the mammalian central nervous system. *Prog. Neurobiol.* **54**, 581-618 (1998)
- [10] Moldrich,R.X. & Beart,P.M.: Emerging signalling and protein interactions mediated via metabotropic glutamate receptors. *Curr. Drug Targets. CNS. Neurol. Disord.* **2**, 109-122 (2003)
- [11] Skerry,T.M. & Genever,P.G.: Glutamate signalling in non-neuronal tissues. *Trends Pharmacol. Sci.* **22**, 174-181 (2001)
- [12] Doble,A.: The role of excitotoxicity in neurodegenerative disease: implications for therapy. *Pharmacol. Ther.* **81**, 163-221 (1999)
- [13] Dodd,P.R.: Excited to death: different ways to lose your neurones. *Biogerontology.* **3**, 51-56 (2002)
- [14] McGeer,E.G. & McGeer,P.L.: Pharmacologic approaches to the treatment of amyotrophic lateral sclerosis. *BioDrugs.* **19**, 31-37 (2005)
- [15] Won,S.J., Kim,D.Y., & Gwag,B.J.: Cellular and molecular pathways of ischemic neuronal death. *J. Biochem. Mol. Biol.* **35**, 67-86 (2002)

- [16] Arundine, M. & Tymianski, M.: Molecular mechanisms of glutamate-dependent neurodegeneration in ischemia and traumatic brain injury. *Cell Mol. Life Sci.* **61**, 657-668 (2004)
- [17] Simon, R.P., Swan, J.H., Griffiths, T., & Meldrum, B.S.: Blockade of N-methyl-D-aspartate receptors may protect against ischemic damage in the brain. *Science* **226**, 850-852 (1984)
- [18] Dirnagl, U., Iadecola, C., & Moskowitz, M.A.: Pathobiology of ischaemic stroke: an integrated view. *Trends Neurosci.* **22**, 391-397 (1999)
- [19] Hoyte, L., Barber, P.A., Buchan, A.M., & Hill, M.D.: The rise and fall of NMDA antagonists for ischemic stroke. *Curr. Mol. Med.* **4**, 131-136 (2004)
- [20] Neale, J.H., Bzdega, T., & Wroblewska, B.: N-Acetylaspartylglutamate: the most abundant peptide neurotransmitter in the mammalian central nervous system. *J. Neurochem.* **75**, 443-452 (2000)
- [21] Neale, J.H., Olszewski, R.T., Gehl, L.M., Wroblewska, B., & Bzdega, T.: The neurotransmitter N-acetylaspartylglutamate in models of pain, ALS, diabetic neuropathy, CNS injury and schizophrenia. *Trends Pharmacol. Sci.* **26**, 477-484 (2005)
- [22] Forloni, G., Grzanna, R., Blakely, R.D., & Coyle, J.T.: Co-localization of N-acetyl-aspartyl-glutamate in central cholinergic, noradrenergic, and serotonergic neurons. *Synapse* **1**, 455-460 (1987)
- [23] Moffett, J.R. & Namboodiri, M.A.: Differential distribution of N-acetylaspartylglutamate and N-acetylaspartate immunoreactivities in rat forebrain. *J. Neurocytol.* **24**, 409-433 (1995)
- [24] Tsai, G., Slusher, B.S., Sim, L., & Coyle, J.T.: Immunocytochemical distribution of N-acetylaspartylglutamate in the rat forebrain and glutamatergic pathways. *J. Chem. Neuroanat.* **6**, 277-292 (1993)
- [25] Valivullah, H.M., Lancaster, J., Sweetnam, P.M., & Neale, J.H.: Interactions between N-acetylaspartylglutamate and AMPA, kainate, and NMDA binding sites. *J. Neurochem.* **63**, 1714-1719 (1994)
- [26] Trombley, P.Q. & Westbrook, G.L.: Excitatory synaptic transmission in cultures of rat olfactory bulb. *J. Neurophysiol.* **64**, 598-606 (1990)
- [27] Westbrook, G.L., Mayer, M.L., Namboodiri, M.A., & Neale, J.H.: High concentrations of N-acetylaspartylglutamate (NAAG) selectively activate NMDA receptors on mouse spinal cord neurons in cell culture. *J. Neurosci.* **6**, 3385-3392 (1986)
- [28] Jones, H.E. & Sillito, A.M.: The action of the putative neurotransmitters N-acetylaspartylglutamate and L-homocysteate in cat dorsal lateral geniculate nucleus. *J. Neurophysiol.* **68**, 663-672 (1992)
- [29] Puttfarcken, P.S., Handen, J.S., Montgomery, D.T., Coyle, J.T., & Werling, L.L.: N-acetyl-aspartylglutamate modulation of N-methyl-D-aspartate-stimulated [<sup>3</sup>H]norepinephrine release from rat hippocampal slices. *J. Pharmacol. Exp. Ther.* **266**, 796-803 (1993)
- [30] Greene, R.: Circuit analysis of NMDAR hypofunction in the hippocampus, in vitro, and psychosis of schizophrenia. *Hippocampus* **11**, 569-577 (2001)

- [31] Losi,G., Vicini,S., & Neale,J.: NAAG fails to antagonize synaptic and extrasynaptic NMDA receptors in cerebellar granule neurons. *Neuropharmacology* **46**, 490-496 (2004)
- [32] Bergeron,R., Coyle,J.T., Tsai,G., & Greene,R.W.: NAAG reduces NMDA receptor current in CA1 hippocampal pyramidal neurons of acute slices and dissociated neurons. *Neuropsychopharmacology* **30**, 7-16 (2005)
- [33] Ghose,S., Wroblewska,B., Corsi,L., Grayson,D.R., De Blas,A.L., Vicini,S., & Neale,J.H.: N-acetylaspartylglutamate stimulates metabotropic glutamate receptor 3 to regulate expression of the GABA(A) alpha6 subunit in cerebellar granule cells. *J. Neurochem.* **69**, 2326-2335 (1997)
- [34] Wroblewska,B., Wroblewski,J.T., Pshenichkin,S., Surin,A., Sullivan,S.E., & Neale,J.H.: N-acetylaspartylglutamate selectively activates mGluR3 receptors in transfected cells. *J. Neurochem.* **69**, 174-181 (1997)
- [35] Wroblewska,B., Santi,M.R., & Neale,J.H.: N-acetylaspartylglutamate activates cyclic AMP-coupled metabotropic glutamate receptors in cerebellar astrocytes. *Glia* **24**, 172-179 (1998)
- [36] Sanabria,E.R., Wozniak,K.M., Slusher,B.S., & Keller,A.: GCP II (NAALADase) inhibition suppresses mossy fiber-CA3 synaptic neurotransmission by a presynaptic mechanism. *J. Neurophysiol.* **91**, 182-193 (2004)
- [37] Zhao,J., Ramadan,E., Capiello,M., Wroblewska,B., Bzdega,T., & Neale,J.H.: NAAG inhibits KCl-induced [(3)H]-GABA release via mGluR3, cAMP, PKA and L-type calcium conductance. *Eur. J. Neurosci.* **13**, 340-346 (2001)
- [38] Bruno,V., Battaglia,G., Casabona,G., Copani,A., Caciagli,F., & Nicoletti,F.: Neuroprotection by glial metabotropic glutamate receptors is mediated by transforming growth factor-beta. *J. Neurosci.* **18**, 9594-9600 (1998)
- [39] Thomas,A.G., Liu,W., Olkowski,J.L., Tang,Z., Lin,Q., Lu,X.C., & Slusher,B.S.: Neuroprotection mediated by glutamate carboxypeptidase II (NAALADase) inhibition requires TGF-beta. *Eur. J. Pharmacol.* **430**, 33-40 (2001)
- [40] Berger,U.V., Luthi-Carter,R., Passani,L.A., Elkabes,S., Black,I., Konradi,C., & Coyle,J.T.: Glutamate carboxypeptidase II is expressed by astrocytes in the adult rat nervous system. *J. Comp Neurol.* **415**, 52-64 (1999)
- [41] Luthi-Carter,R., Berger,U.V., Barczak,A.K., Enna,M., & Coyle,J.T.: Isolation and expression of a rat brain cDNA encoding glutamate carboxypeptidase II. *Proc. Natl. Acad. Sci. U. S. A* **95**, 3215-3220 (1998)
- [42] Riveros,N. & Orrego,F.: A study of possible excitatory effects of N-acetylaspartylglutamate in different in vivo and in vitro brain preparations. *Brain Res.* **299**, 393-395 (1984)
- [43] Slusher,B.S., Robinson,M.B., Tsai,G., Simmons,M.L., Richards,S.S., & Coyle,J.T.: Rat brain N-acetylated alpha-linked acidic dipeptidase activity. Purification and immunologic characterization. *J. Biol. Chem.* **265**, 21297-21301 (1990)
- [44] Carter,R.E., Feldman,A.R., & Coyle,J.T.: Prostate-specific membrane antigen is a hydrolase with substrate and pharmacologic characteristics of a neuropeptidase. *Proc. Natl. Acad. Sci. U. S. A* **93**, 749-753 (1996)

- [45] Luthi-Carter,R., Barczak,A.K., Speno,H., & Coyle,J.T.: Molecular characterization of human brain N-acetylated alpha-linked acidic dipeptidase (NAALADase). *J. Pharmacol. Exp. Ther.* **286**, 1020-1025 (1998)
- [46] Pangalos,M.N., Neefs,J.M., Somers,M., Verhasselt,P., Bekkers,M., van der,H.L., Fraiponts,E., Ashton,D., & Gordon,R.D.: Isolation and expression of novel human glutamate carboxypeptidases with N-acetylated alpha-linked acidic dipeptidase and dipeptidyl peptidase IV activity. *J. Biol. Chem.* **274**, 8470-8483 (1999)
- [47] Bacich,D.J., Ramadan,E., O'Keefe,D.S., Bukhari,N., Wegorzewska,I., Ojeifo,O., Olszewski,R., Wrenn,C.C., Bzdega,T., Wroblewska,B., Heston,W.D., & Neale,J.H.: Deletion of the glutamate carboxypeptidase II gene in mice reveals a second enzyme activity that hydrolyzes N-acetylaspartylglutamate. *J. Neurochem.* **83**, 20-29 (2002)
- [48] Hlouchová,K.: Cloning, expression and biochemical characterization of glutamate carboxypeptidase III, a homolog of a metallopeptidase from the central nervous system: Diploma Thesis. Department of Biochemistry, Faculty of Science, Charles University, Prague (2005)
- [49] Slusher,B.S., Vornov,J.J., Thomas,A.G., Hum,P.D., Harukuni,I., Bhardwaj,A., Traystman,R.J., Robinson,M.B., Britton,P., Lu,X.C., Tortella,F.C., Wozniak,K.M., Yudkoff,M., Potter,B.M., & Jackson,P.F.: Selective inhibition of NAALADase, which converts NAAG to glutamate, reduces ischemic brain injury. *Nat. Med.* **5**, 1396-1402 (1999)
- [50] Tortella,F.C., Lin,Y., Ved,H., Slusher,B.S., & Dave,J.R.: Neuroprotection produced by the NAALADase inhibitor 2-PMPA in rat cerebellar neurons. *Eur. J. Pharmacol.* **402**, 31-37 (2000)
- [51] Williams,A.J., Lu,X.M., Slusher,B., & Tortella,F.C.: Electroencephalogram analysis and neuroprotective profile of the N-acetylated-alpha-linked acidic dipeptidase inhibitor, GPI5232, in normal and brain-injured rats. *J. Pharmacol. Exp. Ther.* **299**, 48-57 (2001)
- [52] Yamamoto,T., Nozaki-Taguchi,N., & Sakashita,Y.: Spinal N-acetyl-alpha-linked acidic dipeptidase (NAALADase) inhibition attenuates mechanical allodynia induced by paw carrageenan injection in the rat. *Brain Res.* **909**, 138-144 (2001)
- [53] Yamamoto,T., Nozaki-Taguchi,N., Sakashita,Y., & Inagaki,T.: Inhibition of spinal N-acetylated-alpha-linked acidic dipeptidase produces an antinociceptive effect in the rat formalin test. *Neuroscience* **102**, 473-479 (2001)
- [54] Yamamoto,T., Hirasawa,S., Wroblewska,B., Grajkowska,E., Zhou,J., Kozikowski,A., Wroblewski,J., & Neale,J.H.: Antinociceptive effects of N-acetylaspartylglutamate (NAAG) peptidase inhibitors ZJ-11, ZJ-17 and ZJ-43 in the rat formalin test and in the rat neuropathic pain model. *Eur. J. Neurosci.* **20**, 483-494 (2004)
- [55] Zhang,W., Slusher,B., Murakawa,Y., Wozniak,K.M., Tsukamoto,T., Jackson,P.F., & Sima,A.A.: GCPII (NAALADase) inhibition prevents long-term diabetic neuropathy in type 1 diabetic BB/Wor rats. *J. Neurol. Sci.* **194**, 21-28 (2002)
- [56] Berent-Spillson,A., Robinson,A.M., Golovoy,D., Slusher,B., Rojas,C., & Russell,J.W.: Protection against glucose-induced neuronal death by NAAG and GCP II inhibition is regulated by mGluR3. *J. Neurochem.* **89**, 90-99 (2004)

- [57] Ghadge,G.D., Slusher,B.S., Bodner,A., Canto,M.D., Wozniak,K., Thomas,A.G., Rojas,C., Tsukamoto,T., Majer,P., Miller,R.J., Monti,A.L., & Roos,R.P.: Glutamate carboxypeptidase II inhibition protects motor neurons from death in familial amyotrophic lateral sclerosis models. *Proc. Natl. Acad. Sci. U. S. A* **100**, 9554-9559 (2003)
- [58] Dumas,F., Gala,J.L., Berteau,P., Brasseur,F., Eschwege,P., Paradis,V., Lacour,B., Philippe,M., & Loric,S.: Molecular expression of PSMA mRNA and protein in primary renal tumors. *Int. J. Cancer* **80**, 799-803 (1999)
- [59] Israeli,R.S., Powell,C.T., Corr,J.G., Fair,W.R., & Heston,W.D.: Expression of the prostate-specific membrane antigen. *Cancer Res.* **54**, 1807-1811 (1994)
- [60] Renneberg,H., Friedetzky,A., Konrad,L., Kurek,R., Weingartner,K., Wennemuth,G., Tunn,U.W., & Aumuller,G.: Prostate specific membrane antigen (PSM) is expressed in various human tissues: implication for the use of PSM reverse transcription polymerase chain reaction to detect hematogenous prostate cancer spread. *Urol. Res.* **27**, 23-27 (1999)
- [61] Chang,S.S., Reuter,V.E., Heston,W.D., Bander,N.H., Grauer,L.S., & Gaudin,P.B.: Five different anti-prostate-specific membrane antigen (PSMA) antibodies confirm PSMA expression in tumor-associated neovasculature. *Cancer Res.* **59**, 3192-3198 (1999)
- [62] Silver,D.A., Pellicer,I., Fair,W.R., Heston,W.D., & Cordon-Cardo,C.: Prostate-specific membrane antigen expression in normal and malignant human tissues. *Clin. Cancer Res.* **3**, 81-85 (1997)
- [63] Troyer,J.K., Beckett,M.L., & Wright,G.L., Jr.: Detection and characterization of the prostate-specific membrane antigen (PSMA) in tissue extracts and body fluids. *Int. J. Cancer* **62**, 552-558 (1995)
- [64] Israeli,R.S., Powell,C.T., Fair,W.R., & Heston,W.D.: Molecular cloning of a complementary DNA encoding a prostate-specific membrane antigen. *Cancer Res.* **53**, 227-230 (1993)
- [65] Davis,M.I., Bennett,M.J., Thomas,L.M., & Bjorkman,P.J.: Crystal structure of prostate-specific membrane antigen, a tumor marker and peptidase. *Proc. Natl. Acad. Sci. U. S. A* **102**, 5981-5986 (2005)
- [66] Mesters,J.R., Barinka,C., Li,W., Tsukamoto,T., Majer,P., Slusher,B.S., Konvalinka,J., & Hilgenfeld,R.: Structure of glutamate carboxypeptidase II, a drug target in neuronal damage and prostate cancer. *EMBO J.* (2006)
- [67] Schulke,N., Varlamova,O.A., Donovan,G.P., Ma,D., Gardner,J.P., Morrissey,D.M., Arrigale,R.R., Zhan,C., Chodera,A.J., Surowitz,K.G., Maddon,P.J., Heston,W.D., & Olson,W.C.: The homodimer of prostate-specific membrane antigen is a functional target for cancer therapy. *Proc. Natl. Acad. Sci. U. S. A* **100**, 12590-12595 (2003)
- [68] Liu,H., Rajasekaran,A.K., Moy,P., Xia,Y., Kim,S., Navarro,V., Rahmati,R., & Bander,N.H.: Constitutive and antibody-induced internalization of prostate-specific membrane antigen. *Cancer Res.* **58**, 4055-4060 (1998)
- [69] Lawrence,C.M., Ray,S., Babyonyshev,M., Galluser,R., Borhani,D.W., & Harrison,S.C.: Crystal structure of the ectodomain of human transferrin receptor. *Science* **286**, 779-782 (1999)

- [70] Qian,Z.M., Li,H., Sun,H., & Ho,K.: Targeted drug delivery via the transferrin receptor-mediated endocytosis pathway. *Pharmacol. Rev.* **54**, 561-587 (2002)
- [71] Rajasekaran,S.A., Anilkumar,G., Oshima,E., Bowie,J.U., Liu,H., Heston,W., Bander,N.H., & Rajasekaran,A.K.: A novel cytoplasmic tail MXXXL motif mediates the internalization of prostate-specific membrane antigen. *Mol. Biol. Cell* **14**, 4835-4845 (2003)
- [72] Anilkumar,G., Rajasekaran,S.A., Wang,S., Hankinson,O., Bander,N.H., & Rajasekaran,A.K.: Prostate-specific membrane antigen association with filamin A modulates its internalization and NAALADase activity. *Cancer Res.* **63**, 2645-2648 (2003)
- [73] Ghosh,A. & Heston,W.D.: Tumor target prostate specific membrane antigen (PSMA) and its regulation in prostate cancer. *J. Cell Biochem.* **91**, 528-539 (2004)
- [74] Rajasekaran,A.K., Anilkumar,G., & Christiansen,J.J.: Is prostate-specific membrane antigen a multifunctional protein? *Am. J. Physiol Cell Physiol* **288**, C975-C981 (2005)
- [75] Bostwick,D.G., Pacelli,A., Blute,M., Roche,P., & Murphy,G.P.: Prostate specific membrane antigen expression in prostatic intraepithelial neoplasia and adenocarcinoma: a study of 184 cases. *Cancer* **82**, 2256-2261 (1998)
- [76] Ross,J.S., Sheehan,C.E., Fisher,H.A., Kaufman,R.P., Jr., Kaur,P., Gray,K., Webb,I., Gray,G.S., Mosher,R., & Kallakury,B.V.: Correlation of primary tumor prostate-specific membrane antigen expression with disease recurrence in prostate cancer. *Clin. Cancer Res.* **9**, 6357-6362 (2003)
- [77] Sweat,S.D., Pacelli,A., Murphy,G.P., & Bostwick,D.G.: Prostate-specific membrane antigen expression is greatest in prostate adenocarcinoma and lymph node metastases. *Urology* **52**, 637-640 (1998)
- [78] Wright,G.L., Jr., Grob,B.M., Haley,C., Grossman,K., Newhall,K., Petrylak,D., Troyer,J., Konchuba,A., Schellhammer,P.F., & Moriarty,R.: Upregulation of prostate-specific membrane antigen after androgen-deprivation therapy. *Urology* **48**, 326-334 (1996)
- [79] Lamb,H.M. & Faulds,D.: Capromab pendetide. A review of its use as an imaging agent in prostate cancer. *Drugs Aging* **12**, 293-304 (1998)
- [80] Lopes,A.D., Davis,W.L., Rosenstraus,M.J., Uveges,A.J., & Gilman,S.C.: Immunohistochemical and pharmacokinetic characterization of the site-specific immunoconjugate CYT-356 derived from antiprostata monoclonal antibody 7E11-C5. *Cancer Res.* **50**, 6423-6429 (1990)
- [81] Rosenthal,S.A., Haseman,M.K., & Polascik,T.J.: Utility of capromab pendetide (ProstaScint) imaging in the management of prostate cancer. *Tech. Urol.* **7**, 27-37 (2001)
- [82] Troyer,J.K., Feng,Q., Beckett,M.L., & Wright,G.L., Jr.: Biochemical characterization and mapping of the 7E11-C5.3 epitope of the prostate-specific membrane antigen. *Urol Oncol* **1**, 29-37 (1995)
- [83] Bander,N.H., Nanus,D.M., Milowsky,M.I., Kostakoglu,L., Vallabahajosula,S., & Goldsmith,S.J.: Targeted systemic therapy of prostate cancer with a monoclonal antibody to prostate-specific membrane antigen. *Semin. Oncol* **30**, 667-676 (2003)

- [84] Morris,M.J., Divgi,C.R., Pandit-Taskar,N., Batraki,M., Warren,N., Nacca,A., Smith-Jones,P., Schwartz,L., Kelly,W.K., Slovin,S., Solit,D., Halpern,J., Delacruz,A., Curley,T., Finn,R., O'donoghue,J.A., Livingston,P., Larson,S., & Scher,H.I.: Pilot trial of unlabeled and indium-111-labeled anti-prostate-specific membrane antigen antibody J591 for castrate metastatic prostate cancer. *Clin. Cancer Res.* **11**, 7454-7461 (2005)
- [85] Vallabhajosula,S., Goldsmith,S.J., Kostakoglu,L., Milowsky,M.I., Nanus,D.M., & Bander,N.H.: Radioimmunotherapy of prostate cancer using 90Y- and 177Lu-labeled J591 monoclonal antibodies: effect of multiple treatments on myelotoxicity. *Clin. Cancer Res.* **11**, 7195s-7200s (2005)
- [86] Salgaller,M.L., Tjoa,B.A., Lodge,P.A., Ragde,H., Kenny,G., Boynton,A., & Murphy,G.P.: Dendritic cell-based immunotherapy of prostate cancer. *Crit Rev. Immunol.* **18**, 109-119 (1998)
- [87] Tjoa,B., Boynton,A., Kenny,G., Ragde,H., Misrock,S.L., & Murphy,G.: Presentation of prostate tumor antigens by dendritic cells stimulates T-cell proliferation and cytotoxicity. *Prostate* **28**, 65-69 (1996)
- [88] Murphy,G.P., Tjoa,B.A., Simmons,S.J., Jarisch,J., Bowes,V.A., Ragde,H., Rogers,M., Elgamal,A., Kenny,G.M., Cobb,O.E., Ireton,R.C., Troychak,M.J., Salgaller,M.L., & Boynton,A.L.: Infusion of dendritic cells pulsed with HLA-A2-specific prostate-specific membrane antigen peptides: a phase II prostate cancer vaccine trial involving patients with hormone-refractory metastatic disease. *Prostate* **38**, 73-78 (1999)
- [89] Tjoa,B.A., Simmons,S.J., Elgamal,A., Rogers,M., Ragde,H., Kenny,G.M., Troychak,M.J., Boynton,A.L., & Murphy,G.P.: Follow-up evaluation of a phase II prostate cancer vaccine trial. *Prostate* **40**, 125-129 (1999)
- [90] Heston,W.D.: Characterization and glutamyl preferring carboxypeptidase function of prostate specific membrane antigen: a novel folate hydrolase. *Urology* **49**, 104-112 (1997)
- [91] Chang,S.S., O'Keefe,D.S., Bacich,D.J., Reuter,V.E., Heston,W.D., & Gaudin,P.B.: Prostate-specific membrane antigen is produced in tumor-associated neovasculature. *Clin. Cancer Res.* **5**, 2674-2681 (1999)
- [92] Liu,H., Moy,P., Kim,S., Xia,Y., Rajasekaran,A., Navarro,V., Knudsen,B., & Bander,N.H.: Monoclonal antibodies to the extracellular domain of prostate-specific membrane antigen also react with tumor vascular endothelium. *Cancer Res.* **57**, 3629-3634 (1997)
- [93] Sokoloff,R.L., Norton,K.C., Gasior,C.L., Marker,K.M., & Grauer,L.S.: A dual-monoclonal sandwich assay for prostate-specific membrane antigen: levels in tissues, seminal fluid and urine. *Prostate* **43**, 150-157 (2000)
- [94] Rawlings,N.D. & Barrett,A.J.: Structure of membrane glutamate carboxypeptidase. *Biochim. Biophys. Acta* **1339**, 247-252 (1997)
- [95] Barinka,C., Sacha,P., Sklenar,J., Man,P., Bezouska,K., Slusher,B.S., & Konvalinka,J.: Identification of the N-glycosylation sites on glutamate carboxypeptidase II necessary for proteolytic activity. *Protein Sci.* **13**, 1627-1635 (2004)
- [96] Ghosh,A. & Heston,W.D.: Effect of carbohydrate moieties on the folate hydrolysis activity of the prostate specific membrane antigen. *Prostate* **57**, 140-151 (2003)

- [97] Holz,R.C., Bzymek,K.P., & Swierczek,S.I.: Co-catalytic metallopeptidases as pharmaceutical targets. *Curr. Opin. Chem. Biol.* **7**, 197-206 (2003)
- [98] DeLano,W.L. The PyMOL Molecular Graphics System. DeLano Scientific, San Carlos, CA, USA (2002)
- [99] Barinka,C., Rinnova,M., Sacha,P., Rojas,C., Majer,P., Slusher,B.S., & Konvalinka,J.: Substrate specificity, inhibition and enzymological analysis of recombinant human glutamate carboxypeptidase II. *J. Neurochem.* **80**, 477-487 (2002)
- [100] Serval,V., Barbeito,L., Pittaluga,A., Cheramy,A., Lavielle,S., & Glowinski,J.: Competitive inhibition of N-acetylated-alpha-linked acidic dipeptidase activity by N-acetyl-L-aspartyl-beta-linked L-glutamate. *J. Neurochem.* **55**, 39-46 (1990)
- [101] Jackson,P.F., Cole,D.C., Slusher,B.S., Stetz,S.L., Ross,L.E., Donzanti,B.A., & Trainor,D.A.: Design, synthesis, and biological activity of a potent inhibitor of the neuropeptidase N-acetylated alpha-linked acidic dipeptidase. *J. Med. Chem.* **39**, 619-622 (1996)
- [102] Jackson,P.F., Tays,K.L., Maclin,K.M., Ko,Y.S., Li,W., Vitharana,D., Tsukamoto,T., Stoermer,D., Lu,X.C., Wozniak,K., & Slusher,B.S.: Design and pharmacological activity of phosphinic acid based NAALADase inhibitors. *J. Med. Chem.* **44**, 4170-4175 (2001)
- [103] Majer,P., Jackson,P.F., Delahanty,G., Grella,B.S., Ko,Y.S., Li,W., Liu,Q., Maclin,K.M., Polakova,J., Shaffer,K.A., Stoermer,D., Vitharana,D., Wang,E.Y., Zakrzewski,A., Rojas,C., Slusher,B.S., Wozniak,K.M., Burak,E., Limsakun,T., & Tsukamoto,T.: Synthesis and biological evaluation of thiol-based inhibitors of glutamate carboxypeptidase II: discovery of an orally active GCP II inhibitor. *J. Med. Chem.* **46**, 1989-1996 (2003)
- [104] Stoermer,D., Liu,Q., Hall,M.R., Flanary,J.M., Thomas,A.G., Rojas,C., Slusher,B.S., & Tsukamoto,T.: Synthesis and biological evaluation of hydroxamate-Based inhibitors of glutamate carboxypeptidase II. *Bioorg. Med. Chem. Lett.* **13**, 2097-2100 (2003)
- [105] Kozikowski,A.P., Nan,F., Conti,P., Zhang,J., Ramadan,E., Bzdega,T., Wroblewska,B., Neale,J.H., Pshenichkin,S., & Wroblewski,J.T.: Design of remarkably simple, yet potent urea-based inhibitors of glutamate carboxypeptidase II (NAALADase). *J. Med. Chem.* **44**, 298-301 (2001)
- [106] Kozikowski,A.P., Zhang,J., Nan,F., Petukhov,P.A., Grajkowska,E., Wroblewski,J.T., Yamamoto,T., Bzdega,T., Wroblewska,B., & Neale,J.H.: Synthesis of urea-based inhibitors as active site probes of glutamate carboxypeptidase II: efficacy as analgesic agents. *J. Med. Chem.* **47**, 1729-1738 (2004)
- [107] Speno,H.S., Luthi-Carter,R., Macias,W.L., Valentine,S.L., Joshi,A.R., & Coyle,J.T.: Site-directed mutagenesis of predicted active site residues in glutamate carboxypeptidase II. *Mol. Pharmacol.* **55**, 179-185 (1999)
- [108] Chevrier,B., Schalk,C., D'Orchymont,H., Rondeau,J.M., Moras,D., & Tarnus,C.: Crystal structure of *Aeromonas proteolytica* aminopeptidase: a prototypical member of the co-catalytic zinc enzyme family. *Structure.* **2**, 283-291 (1994)
- [109] Greenblatt,H.M., Almog,O., Maras,B., Spungin-Bialik,A., Barra,D., Blumberg,S., & Shoham,G.: *Streptomyces griseus* aminopeptidase: X-ray crystallographic structure at 1.75 Å resolution. *J. Mol. Biol.* **265**, 620-636 (1997)



- [110] Mlčochová,P.: Vztah mezi strukturou a aktivitou mutantů glutamát karboxypeptidasy II: Diploma Thesis. Department of Biochemistry, Faculty of Science, Charles University, Prague (2002)
- [111] Ausubel,F.M., Brent,R., Kingston,R.E., Moore,D.D., Seidman,J.G., Smith,J.A., & Struhl,K.: Current Protocols in Molecular Biology. John Wiley & Sons, Inc. (1994)
- [112] Cohen,S.A. & Michaud,D.P.: Synthesis of a fluorescent derivatizing reagent, 6-aminoquinolyl-N-hydroxysuccinimidyl carbamate, and its application for the analysis of hydrolysate amino acids via high-performance liquid chromatography. *Anal. Biochem.* **211**, 279-287 (1993)
- [113] Rojas,C., Frazier,S.T., Flanary,J., & Slusher,B.S.: Kinetics and inhibition of glutamate carboxypeptidase II using a microplate assay. *Anal. Biochem.* **310**, 50-54 (2002)
- [114] Morrison,J.F.: Kinetics of the reversible inhibition of enzyme-catalysed reactions by tight-binding inhibitors. *Biochim. Biophys. Acta* **185**, 269-286 (1969)

Svoluji k zapůjčení této práce pro studijní účely a prosím, aby byla řádně vedena evidence vypůjčovatelů.

Jméno a příjmení s adresou	Číslo OP	Datum vypůjčení	Poznámka